

Development of a Laser Scanning Thickness Measurement Inspection System

By

S. M. Mahfuzul Haque, B Eng

This thesis is submitted as the fulfilment of the requirement for the
award of degree of

Master of Engineering (M Eng)

By research from

School of Mechanical and Manufacturing Engineering
Dublin City University, Ireland

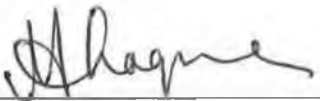
June 2004

Research Supervisors:

Dr. Dermot Brabazon
Professor Mohie El Baradie

Declaration

I hereby certify that this material, which I now submit for assessment on the programme of study leading to the award of Master of Engineering is entirely my own work and has not been taken from the work of others save and to the extent that such work has been cited and acknowledged within the text of my work.

Signed: 
(Candidate)

ID No.: 99145030

Date: 08/02/2005

Acknowledgement

I must acknowledge first the all out support of my initial supervisor, Professor Mohie El-Baradie, and would like to express my sincere thanks to him.

This work could not even be successful without the unthinkable help and valuable supervision of Dr. Dermot Brabazon. He provided me abundant time and energy to complete this work what was really incomparable, I feel.

I had received tremendous support throughout my time of research in this school from my research technician, Mr. Liam Domican.

I would like to take this opportunity to show my heartiest gratitude and special thanks to both of them.

I hereby highly appreciate and give my wholehearted thanks to Professor M. S. J. Hashmi, the Head of School, to offer me the position to pursue this research in the school.

I also very much thank to Dr. M. Iqbal and Mrs. S. Iqbal for their unforgettable contribution towards myself.

Finally I do recognise all the sufferings received by my family back home. I could not stand by them and share the feelings on many occasions whilst staying abroad. Their endless prayer brings my work successful today. This acknowledgement would not be complete without mentioning the love and care of my wife. My sons, Mustakim and Muhtarim, have made my life happier to live and easier to bear the loads of study with their heavenly smiles and lovely touches.

Dedication

To my parents, wife, and sons

Table of Contents

	Page No.
- Title	i
- Declaration	ii
- Acknowledgement	iii
- Dedication	iv
- Table of Contents	v
- List of Figures	x
- List of Tables	xiii
- Nomenclature	xv
- Abstract	xvii

Chapter One

1. Introduction	1
------------------------	----------

Chapter Two

2. Literature Survey	3
2.1 Laser	3
2.2 Types of laser systems	3
2.2.1 Solid-state lasers	3
2.2.2 Gas lasers	4
2.2.3 Semiconductor lasers	5
2.2.4 Other lasers	5
2.3 Properties of laser	5
2.4 Laser applications	8
2.4.1 Low power laser applications	8
2.4.2 High power laser applications	9
2.5 Laser safety	9
2.5.1 Laser safety class	9
2.5.2 Laser safety accessories	9

2.6	Scanning systems	10
2.6.1	Classification of scanning methods	10
2.6.2	Laser scanning systems	11
2.6.3	Data collection techniques in laser scanning systems	13
2.6.4	Speckle effects in laser scanning systems	14
2.7	Laser-optical triangulation systems	15
2.7.1	Characteristics of laser-optical triangulation systems	15
2.7.2	Construction of laser-optical triangulation systems	16
2.7.3	Types of laser-optical triangulation systems	16
2.7.4	Mechanism of laser-optical triangulation systems	16
2.7.5	Reflection factor of object surface in laser-optical triangulation systems	18
2.7.6	Analysis of main precision factors of a laser-optical triangulation system	19
2.7.7	Methods of increasing measurement precision in a laser-optical triangulation system	21
2.7.8	Limitations of laser-optical triangulation systems	22
2.7.9	Advantages of laser-optical triangulation systems	23
2.7.10	Disadvantages of laser-optical triangulation systems	24
2.7.11	Measurement errors in laser-optical triangulation systems	24
2.7.12	Requirements in laser-optical triangulation systems	27
2.7.13	Recent advancements of laser-optical triangulation systems	28
2.7.14	Applications of laser-optical triangulation systems	29
2.8	Surface inspection	30
2.8.1	Conventional method for surface inspection	31
2.8.2	Optical method for surface inspection	31
2.9	Distance measurement	32
2.9.1	Uncertainty limit in distance sensing	33
2.9.2	Displacement sensors	33

Chapter Three

3.	System Set-up and Result for Surface Profile Measurement	36
3.1	A system for study	36

3.2	System set-up	36
3.2.1	Laser displacement sensor, Micro-Epsilon optoNCDT 2000	37
3.3	Commissioning experiments	39
3.3.1	Safety measures	39
3.3.2	Experiment considerations	39
3.3.3	Experiment procedures	40
3.3.4	System parameters	41
3.4	Results and discussion	43
3.4.1	Scan of through holes area of brass plate	44
3.4.2	Scan of flat area of brass plate	46
3.4.3	Scan of blind holes area of brass plate	48
3.5	Characterisation of the system	50
3.5.1	Merits of the system	50
3.5.2	Demerits of the system	52
3.5.3	Displacement measurement error producing factors	53
3.6	Further development of the system	55
3.6.1	Experimental development	55
3.6.2	Hardware development	55
3.6.3	Software development	56

Chapter Four

4.	Experiment Set-up for Thickness Measurement	57
4.1	Laser scanning system components	57
4.2	Measuring principle of the laser sensor, Keyence LK-031	58
4.3	Laser scanning system calibration	59
4.4	Principle of thickness measurement	61
4.5	Thickness measurement of moving samples	65
4.5.1	Procedures for thickness measurement of moving samples	65
4.6	Kinetic system	66
4.6.1	Lead screw table	66
4.6.2	Stepper motor	66
4.6.3	Motor control unit	69
4.6.4	Motor power and frequency supply	69

4.7 Data acquisition and analysis (DAQ) system	69
4.7.1 Break-Out box	69
4.7.2 Data acquisition card	70
4.7.3 Communication software	70
4.7.4 Data analysing software	71

Chapter Five

5. Thickness Measurement System Results	75
5.1 System parameters	75
5.2 Calibration results and discussion	76
5.3 System performances	77
5.3.1 Laser scanning system	77
5.3.2 Kinetic system	78
5.3.3 Data acquisition and analysis (DAQ) system	79
5.4 Results from scans	81
5.4.1 Scan of aluminium taper block	82
5.4.2 Scan of aluminium block with various thickness	84
5.4.3 Scan of kinked thin aluminium plate	86
5.4.4 Scan of aluminium plate with a rectangular hole inside	87
5.4.5 Scan of double taper aluminium block	89
5.4.6 Scan of brass plate with 7 through holes	91
5.5 System accuracy	94
5.6 Characterisation of system errors	95
5.6.1 Set-up errors	96
5.6.2 External errors	100
5.6.3 Environmental error	102
5.7 Errors analysis	103

Chapter Six

6. Conclusion	106
6.1 Comparison between the two laser scanning systems	106
6.2 Recommendation for further work	109
6.2.1 Laser scanning system	109

6.2.2	Kinetic system	109
6.2.3	Data acquisition and analysis (DAQ) system	110
6.3	Conclusion	110
REFERENCES		112
Appendix A		116
Related information regarding laser safety class		
Appendix B		120
Related information regarding products used in Surface Profile Measurement System		
Appendix C		125
Related information regarding products used in Thickness Measurement System		
Appendix D		132
Experiment to determine mechanical vibration in Thickness Measurement System		
Appendix E		137
Drawings of the Thickness Measurement Rig assembly		
Appendix F		146
Drawings of the samples		

List of Figures

- Figure 2-1: Beam divergence and size
- Figure 2-2: Coherent and incoherent light waves
- Figure 2-3: Schematic giving the arrangement of a laser-optical triangulation measurement system
- Figure 2-4: The relation between the spatial point P and its image p
- Figure 2-5: Measuring error caused by system structure
- Figure 2-6: Measurement errors in LOTS
- Figure 2-7: Schematic of the measurement arrangement of a typical laser displacement sensor [13]
- Figure 2-8: Light quantity distribution on PSD and CCD
- Figure 3-1: Schematic diagram of system set-up
- Figure 3-2: Photograph of system set-up
- Figure 3-3: Measurement window of Micro-Epsilon ILD2000 Demo Version 3.1
- Figure 3-4: Picture of brass plate with 7 through holes (scan-1)
- Figure 3-5: Scan of through holes area of brass plate
- Figure 3-6: Scanning signal fluctuation on sharp edge area
- Figure 3-7: Picture of brass plate (scan-2)
- Figure 3-8: Scan of flat area of brass plate showing the vertical displacement of the plate (mm) versus the scanned points
- Figure 3-9: Picture of brass plate with 5 blind holes (scan-3)
- Figure 3-10: Scan of blind holes area of brass plate
- Figure 3-11: Scanning resolution
- Figure 3-12: Dimension of laser beam spot
- Figure 3-13: Measuring range of the laser scanner
- Figure 4-1: Measuring principle of the laser sensor
- Figure 4-2: Initial system set-up without sample translation
- Figure 4-3: Principle of thickness measurement
- Figure 4-4: Examples of thickness measurement

Figure 4-5: Schematic diagram of system set-up

Figure 4-6: Photograph of system set-up

Figure 4-7: Lead screw assembly and clamped sample

Figure 4-8: Interaction in Hyper Terminal program

Figure 4-9: Control panel (user interface) of the VI created in LabVIEW

Figure 4-10: Block diagram (program code) of the VI created in LabVIEW

Figure 5-1: Calibration graph

Figure 5-2: Signal recorded while holding the sample and the scanner head stationary

Figure 5-3: Relationship between sample travel speed and motor frequency

Figure 5-4: Relationship between data acquisition rate and data flow speed used
in the first LabVIEW program

Figure 5-5: Aluminium taper block (sample-1)

Figure 5-6: Scanning result of sample-1 in LabVIEW environment

Figure 5-7: Scanning result of sample-1 in Hyper Terminal environment

Figure 5-8: Aluminium block with various thickness (sample-2)

Figure 5-9: Scanning result of sample-2 in LabVIEW environment

Figure 5-10: Scanning result of sample-2 in Hyper Terminal environment

Figure 5-11: Kinked 1 mm thick Aluminium plate (sample-3)

Figure 5-12: Scanning result of sample-3 in Hyper Terminal environment

Figure 5-13: Aluminium plate with a rectangular hole inside (sample-4)

Figure 5-14: Scanning result of sample-4 in LabVIEW environment

Figure 5-15: Scanning result of sample-4 in Hyper Terminal environment

Figure 5-16: Double taper Aluminium block (sample-5)

Figure 5-17: Scanning result of sample-5 in Hyper Terminal environment

Figure 5-18: Brass plate with 7 through holes (sample-6)

Figure 5-19: Scanning result of sample-6 in LabVIEW environment

Figure 5-20: Scanning result of sample-6 in Hyper Terminal environment

Figure 5-21: Classification of system errors

Figure 5-22: Distant reference planes

Figure 5-23: Overlapped reference planes

Figure 5-24: Co-axial of laser beam spots

(a) accurate measurement and

(b) error rendering measurement

Figure 5-25: (a) Scope of error in tilting sample and
(b) close-up of measured region

Figure B-1: Starting window of Micro-Epsilon ILD2000 Demo Version 3.1

Figure C-1: Keyence LK-031

Figure C-2: Keyence RD-50RW

Figure C-3: Keyence LK-2001

Figure C-4: MINI-LAB 603B

Figure C-5: Data acquisition card

Figure C-6: Break-out box

Figure D-1: Set-up diagram of the experiment to determine mechanical vibration

Figure D-2: Acceleration signals at motor frequency of 700 Hz

Figure D-3: Vibration frequency at motor frequency of 700 Hz

Figure E-1: Laser displacement sensor

Figure E-2: Spacers for sensor heads

Figure E-3: Bracket and spacers

Figure E-4: Sample holders

Figure E-5: Micrometer stage

Figure E-6: Lead screw slide

Figure E-7: Lead screw table

Figure E-8: Stepper motor

Figure F-1: Brass plate with 7 through holes

Figure F-2: Brass plate with 5 blind holes

Figure F-3: Aluminium taper block

Figure F-4: Aluminium block with various thickness

Figure F-5: Kinked thin aluminium plate

Figure F-6: Aluminium plate with a rectangular hole inside

Figure F-7: Double taper aluminium block

List of Tables

- Table 2-1: Classification of scanning methods
- Table 3-1 (a): Relationship among system parameters when $S_p = 5$ mm/s
- Table 3-1 (b): Relationship among system parameters when $S_p = 20$ mm/s
- Table 3-2: Comparison in dimension on the scanned brass plate
- Table 3-3: Error of angle influences
- Table 4-1: Calculation of thickness measurement
- Table 5-1: Calibration data
- Table 5-2: Performance of kinetic system
- Table 5-3: Data acquisition rate in Hyper Terminal environment
- Table 5-4: Data acquisition rate in LabVIEW environment (with DFS control)
- Table 5-5: Data acquisition rate in LabVIEW environment (without DFS control)
- Table 5-6: Dimension of sample-2
- Table 5-7: Comparison in dimension on sample-2
- Table 5-8: Comparison in dimension on sample-4
- Table 5-9: Comparison in dimension on sample-5
- Table 5-10: Comparison in dimension on sample-6
- Table 5-11: System accuracy
- Table 5-12: Error in tilting sample
- Table 5-13: Maximum vertical displacement error from mechanical vibration
- Table 5.14: Estimation of expected errors in the system
- Table 6-1: Comparison between the two laser systems
- Table A-1: Accessible emission limit (AEL) for wavelength ≥ 400 nm to ≤ 700 nm
- Table A-2: Summary of manufacturing requirements for laser products
- Table B-1: Specifications of Micro-Epsilon optoNCDT 2000
- Table B-2: Specifications of Micro-Epsilon IFPS 2001
- Table B-3: Output value interpretation
- Table B-4: LED indicators with its corresponding serial interface output
- Table C-1: Specifications of Keyence LK series
- Table C-2: Specifications of Keyence RD-50RW

Table C-3: Specifications of Keyence KV-U6W

Table D-1: Measurement of maximum vibration acceleration

Table D-2: Measurement of vibration frequency

Table D-3: Measurement of displacement caused by mechanical vibration

Nomenclature

r	the radius of laser beam spot
D	the distance between the laser source and the centre of beam spot
δ	laser beam divergence
d	the horizontal distance between the imaging and focusing lens
b	the image distance
α	the viewing angle in a laser-optical triangulation measurement
A'	the vertical distance between a point A' and the imaging lens
BB'	the image spot displacement on the detector
x_w, y_w, z_w	the co-ordinates values of the spatial point P
x, y	the co-ordinates values of p , the image of the spatial point P
f_o	the focal length
$g(x, y)$	the filter function
$f(x, y)$	the image function
W	the size of filter window
S	the sampling cycle of laser sensor
N	the total number of scan data points
S_p	sample travel speed
t	the total time elapsed for a set of scan
S_r	scan resolution
A	the distance between the reference plane of sensor A and the top surface of the sample to be measured
B	the distance between the reference plane of sensor B and the bottom surface of the sample to be measured
T_h	the thickness of the sample to be measured
f_m	the frequency of motor
P	the path travelled by sample
L_s	the length of the sample to be measured
DAR	data acquisition rate
DFS	data flow speed
σ	standard deviation

μ	confidence interval
θ	the angle of tilt in sample alignment
E_{ref}	the error of reference plane
E_{tit}	the error due to titled alignment of sample to be measured
E_{cal}	the calibration error
$E_{hardware}$	the hardware error
E_{vib}	the error due to mechanical vibration
E_{temp}	the error due to temperature fluctuation
β	the co-efficient of linear expansion
T	the working temperature
ΔT	the change in working temperature
ΔL_s	the change in length of the sample to be measured
X	the displacement of the sample due to simple harmonic motion
X_o	the amplitude of displacement of the sample due to simple harmonic motion
X'	the velocity of the sample due to simple harmonic motion
X''	the acceleration of the sample due to simple harmonic motion
f	the linear frequency of simple harmonic motion
ω	the angular frequency of simple harmonic motion
E_r	the relative error
E_a	the absolute error

Abstract

Development of a Laser Scanning Thickness Measurement Inspection System

By

S. M. Mahfuzul Haque

The quality specifications for products and the materials used in them are becoming ever more demanding. The solution to the many visual inspection quality assurance (QA) problems is the use of automatic in-line surface inspection systems. These need to achieve uniform product quality at high throughput speeds. As a result, there is a need for systems that allow 100% in-line testing of materials and surfaces. To reach this goal laser technology integrated with computer control technology provides a useful solution. In this work, a high speed, low cost, and high accuracy non-contact laser scanning inspection system is developed. The system is capable of measuring the thickness of solid, non-transparent objects using the principle of laser-optical triangulation. Measurement accuracies and repeatabilities to the micrometer level are achieved with the developed system.

Chapter 1

Introduction

The rapid growth in science and technology has opened up new industrial vistas in micro-engineering and nano-technology. Ultra-precision engineering has left hardly any area untouched, from characterisation of materials in science to health care and bio-sciences [1]. In the modern computer-integrated material processing plant, statistical process control plays an increasingly important role. A corresponding need for rugged and non-invasive in-line sensors capable of reliable and unattended performance is becoming more and more urgent. Optical sensors are often being adopted for such tasks not only because of their non-contact nature, implying an easy adaptability to the automated inspection of continuously moving products at any temperature, but also in view of their high response speed, intrinsic resolution, and increasing ruggedness [2].

There are two such optical sensors systems used in the present work. The first one is built for surface profile measurement. This system can detect any change or variation in vertical displacement of the object surface surveyed. It is able to recognise surface defect with micrometer resolution. It is the background development work for the later system – the thickness measurement system. This system can measure the thickness of a moving solid object very precisely. It is the main project work where most of the research effort is offered.

This thesis is organised into six chapters. Chapter 2 presents the literature survey. It covers the literature review behind the present work including the basics of laser and its properties, an overview of laser scanning systems and a detailed discussion on laser-optical triangulation systems.

Chapter 3 describes the laser scanning system that was used for surface profile measurement. It includes system set-up, description, and experiment procedures. Results and discussion on these results are also worked out in this chapter.

Chapter 4 presents the laser scanning system for thickness measurement that was designed, developed and analysed in present work. It contains system organisation, description, principle of measurement, experiment set-up, procedures and calibration of the system.

Chapter 5 contains all the results of the experiments carried out using the thickness measurement system. It also discusses these results with the scope of errors. Finally system accuracy and error analysis are calculated in this chapter too.

Chapter 6 is the concluding chapter of this work and outlines the recommendations for further work. This chapter also draws the comparison between the two laser scanning systems used in present work – surface profile measurement system and thickness measurement system.

Chapter 2

Literature Survey

This chapter contains the literature survey behind the present work. It includes basics of laser and its properties, an overview of laser scanning systems, and a detailed discussion on laser-optical triangulation systems.

2.1 Laser

The laser sits near the top of any list of the greatest inventions of the last half of the twentieth century. Laser technology is both fascinating in itself and an important tool in fields from medicine to communication. The word *laser* is an acronym, which stands for *Light Amplification by the Stimulated Emission of Radiation*. What makes lasers worthwhile for enormous applications, however, is the narrow beam they produce [3].

Albert Einstein was the first to suggest the existence of stimulated emission in 1917. The first to succeed was Charles H. Townes. Instead of working with light, he worked with microwaves which have much longer wavelength. He built a device, called a “*maser*” (*Microwave Amplification by the Stimulated Emission of Radiation*) [4]. In 1960 the first laser beam was created by Theodore Maiman through pumping flashes of light into a small cube of ruby crystal [5].

2.2 Types of laser systems

Lasers can be classified according to the type of material used for the active (amplifying) medium and the temporal (time) characteristics of the output [6]. The three main groups of laser systems are solid-state lasers, gas lasers, and diode lasers.

2.2.1. Solid-state lasers

Solid-state lasers consist of a solid laser rod that is optically pumped with light from a lamp. Their operation may be either continuous or pulsed. In continuous operation

there is very little fluctuation or flicker in the output power level. In pulsed operation the laser output lasts for only a short period of time (usually less than 5 ms) during one cycle of operation.

Pulsed solid-state lasers are among the most numerous and important commercial laser systems. They are by far the most popular lasers for applications such as range finding and material processing. They are also used in many technical areas such as short-pulse holography and in research applications. The three most common types of pulsed solid-state lasers are ruby, Nd:YAG and Nd:glass. Ruby laser was the first solid-state laser demonstrated and also the first to be used for industrial applications. The Nd:YAG laser is widely used in many military applications and larger pulsed Nd:YAG lasers are the most common for material processing. The Nd:glass laser systems are employed in applications that require high-energy pulses that cannot be achieved with Nd:YAG or ruby. It has efficiencies as high as 2% compared to 0.5% for ruby.

2.2.2. Gas lasers

The family of gas lasers is large and has a wide variety of characteristics. Their output range is from deep in the ultraviolet through the visible and infrared to the borderland of millimetre waves and microwaves [4]. Below is a short description of different gas lasers.

(1) CO₂ laser – The carbon-dioxide (CO₂) laser is the most versatile gas laser that can operate in either pulsed or continuous mode, and is able to produce the highest continuous-wave power of any laser [7]. An important area of industrial application for CO₂ lasers has been in materials processing, including hole drilling in various substances, paper cutting and perforation, cloth cutting, scribing of semiconductor wafers and welding. In addition, CO₂ lasers are being used in laser-induced fusion studies, experimental optical communications, tracking systems, and in environmental testing and monitoring [6].

(2) Ion lasers – Ion lasers are gas lasers in which the stimulated emission process occurs between two energy states of an ion. Two types of ion lasers are in common use. One type uses helium as a buffer gas for achieving lasing of ionic metal vapours. The most common laser of this type is the helium-cadmium (He-Cd) laser,

which produces a few milli-watts at 441.6 nm and 325 nm. The other most common type of ion laser is the argon laser that operates in the blue-green region of the visible spectrum. The next most popular ion laser system is the krypton laser, which has output lines across the entire visible spectrum. These two are similar in construction and performance, with the argon system producing higher powers for longer [6].

(3) Helium-Neon lasers – The helium-neon gas laser is another common types of laser. Its low power red beam is used to read bar-codes at supermarket checkout counters, in surveying instruments at construction sites, and to demonstrate how lasers work in school laboratories [7].

2.2.3 Semiconductor lasers

A third group of lasers is diode lasers. These have a remarkably wide field of application in fibre-communication, detection of fire smoke, and robot-machines. Semiconductor laser technology has been growing explosively for the past several years. It is based on a combination of optical and semiconductor electronic technology that gives semiconductor lasers their own distinct properties. Initially able to provide only modest power, semiconductor lasers now are packaged in arrays that can deliver steady power of a watt or more. This is the type of laser that was used in the present work.

2.2.4 Other lasers

Not all lasers fit neatly into the three categories stated above. There are three important types that are categorised in themselves. They are the dye laser, the free-electron laser, and the X-ray laser.

2.3 Properties of laser

(1) Wavelength - It is a fundamental characteristic of visible light and other forms of electromagnetic radiation. The wavelength of a laser depends on the type of material that emits the laser light, the laser's optical system, and the way the laser is energised. Laser action can produce infrared, visible and ultraviolet light. Most lasers emit only one wavelength, but some can emit two or more wavelengths at once. This is called *multi-line operation*.

(2) Output power – This differs widely among lasers. Some lasers produce beams containing less than a milli-watt whereas others produce more than a kilowatt. The power is measured as the flow of light energy from the laser and is defined by the formula:

$$\text{Power} = d(\text{energy}) / d(\text{time}) \quad [2.1]$$

(3) Duration of emission – Although we see lasers as emitting a steady beam of light, in fact, the beam may be comprised of pulses that come in various duration and repetition rates. The length or duration of a pulse can range from milli-seconds to femto-seconds (10^{-15}).

There are important and fundamental relationships among pulse length, energy, repetition rate and power. A laser may have extremely high peak power during a short pulse, but because the pulse is short, it does not contain much energy. To make a simple approximation:

$$\text{Pulse Energy} = \text{Peak Power} \times \text{Pulse length} \quad [2.2]$$

As power varies with time during the pulse, so we have to take an integral to make the relationship exact:

$$\text{Energy} = \int \text{Power } d(\text{time}) \quad [2.3]$$

The average power in a pulsed laser beam is different from the peak power. It is a measure of the average energy flow per second. Thus it equals:

$$\text{Average Power} = \frac{\text{Number of Pulses} \times \text{Pulse Energy}}{\text{Time}} \quad [2.4]$$

If the number of pulses is measured as repetition rate and time is normalised to one second, the average power becomes:

$$\text{Average Power} = \text{Repetition Rate} \times \text{Pulse Energy} \quad [2.5]$$

(4) Beam divergence and size – The important laser property is its small beam divergence. Because of this property, the laser is a source of energy which can be

concentrated by a lens to achieve extremely high power density at a focal spot. Beam divergence typically is measured in milli-radians. Radians are used because the size of a small angle in radian is almost equal to its sine, making it simple to calculate the size of a laser beam. Thus,

$$\text{Radius} = D \times \sin \delta \quad [2.6]$$

Figure 2-1 indicates the calculation of the size of a laser beam spot from the beam divergence, δ , and the distance from the laser, D .

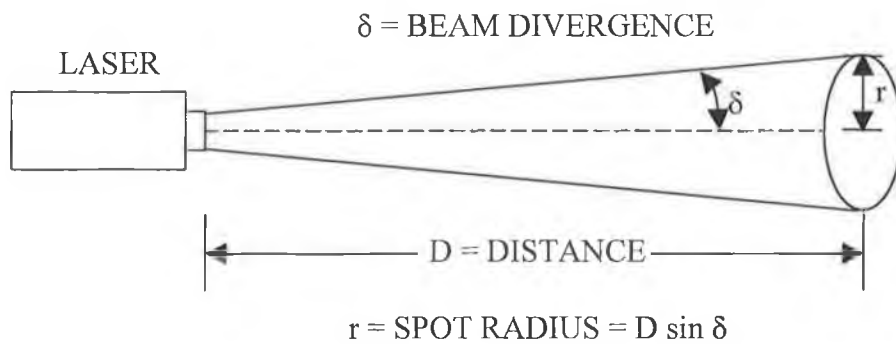


Figure 2-1: Beam divergence and size

(5) Coherence – Light waves are coherent if they are all in phase with one another - i.e. if their peaks and valleys are lined up at the same point. Figure 2-2 sets examples of coherent and incoherent light waves. To be coherent the light waves must start out having the same phase at the same position and their wavelength must be the same. Laser light is coherent because stimulated emission is coherent with the light wave or photon that stimulates it. The stimulated wave has the same phase and wavelength. It, in turn, can stimulate the emission of other photons, which are in phase and have the same wavelength both with it and the original wave.



Figure 2-2: Coherent and incoherent light waves

(6) Efficiency and power requirement – Lasers differ widely in how efficiently they convert input energy (usually in the form of electricity) into light. They are not

very efficient in generating light, with the best converting up to about 30% of input energy into light. However, efficiency becomes a more important consideration at higher output powers.

2.4 Laser applications

2.4.1 Low power laser applications

(1) Reading with lasers - Low power lasers are often used to read printed symbols, such as the striped Universal Product Code (UPC) symbols on food packages, or special type fonts in OCR's. A laser beam is used to illuminate the object being read and a light detector and electronic receiver decode the information.

(2) Holography – Wavefront reconstruction, or holography is a way to retrieve the likeness of a subject from a record of its unfocused diffraction pattern. Holography is widely used as a practical means for storing wavefronts in a record from which the wavefronts may later be reconstructed. The record, formed in photosensitive material, is called a hologram [8]. Virtually all holograms are made with lasers. Holography can be combined with interferometry to make sensitive measurements of how objects deform under stress. One of the important holographic interferometry is a non-destructive testing. It has proved its utility in aerodynamics, heat transfer, and plasma diagnostics [9].

(3) Art and entertainment - The most striking uses of low-power visible lasers are displays and light shows. The beams are generally scattered off moving mirrors. The mirrors scan the laser beams in patterns in the air or on a screen. The scanning patterns can be controlled by music, a computer program, or by someone operating the lasers.

2.4.2 High power laser applications

High power laser applications are used to cause major changes to the objects the laser beam strikes. They have applications in the following areas:

(1) Material working: soldering, cutting, milling, evaporating, punching, welding, piercing, engraving, scribing, drilling, hardening, marking, melting, sintering, and in forming.

(2) Medical treatment: laser surgery, laser eye treatment, laser dermatology, laser cancer treatment.

(3) Science: surveying, analysing, range finding, Photochemistry and isotope separation, laser-driven nuclear fusion.

2.5 Laser safety

Both visible and invisible laser light poses hazards to the eye. Invisible near-infrared and near-ultraviolet light can enter the eye and near-infrared light (in particular) can reach the retina without one sensing it [4]. Peak output power of a pulsed solid state laser is so high that direct viewing of the beam or its reflections is an eye hazard even at long distance. The diffuse reflection of a high powered beam from a roughened surface may also present a serious eye hazard. Output pulses from larger pulsed solid state lasers have sufficient energy to produce minor skin burns and focused beams can cause deep burns.

In a material processing application a respiratory hazard is presented by material vaporised by the focused laser beam. The vaporised material forms small particles, typically a micron in diameter, that are lodged in the lungs if inhaled. All vaporised material should be exhausted from the work area or trapped in fine filters [6].

2.5.1 Laser safety class

Based on the combination of output and wavelength of the accessible laser radiation over the full range of operational capability at any time after manufacturing, all lasers are classified into five categories: Laser class 1, Laser class 2, Laser class 3A, Laser class 3B, and Laser class 4 [10]. In relation to this classification, more information will be presented in Appendix A.

2.5.2 Laser safety accessories

Laser safety goggles are made to block the wavelengths emitted by specific lasers and transmit other light. For example, goggles made to block the 1.06 μm neodymium laser wavelength transmit only visible light. Goggles made to block the argon laser light block light with wavelengths of 488 and 514 nm but transmit red light [4].

2.6 Scanning systems

At a time of rapid development, introduction of new technologies, and increasing world-wide competition, the quality specifications for products and materials are becoming ever more demanding. As a result, there is a need for systems which allow 100% on-line testing of materials and surfaces.

In order to facilitate on-line inspection different scanning techniques and systems are developed in recent years. Further research is being undertaken to achieve optimal high speed, high accuracy and low cost as well as to promote the real-time full automation in industrial environment.

2.6.1 Classification of scanning methods

Based on the measurement techniques scanning methods can be divided into two main categories: contact and non-contact methods. Non-contact methods can be again sub-divided into optical and non-optical methods. For our present work we have limited ourselves to optical methods. Table 2-1 presents the classification of scanning methods.

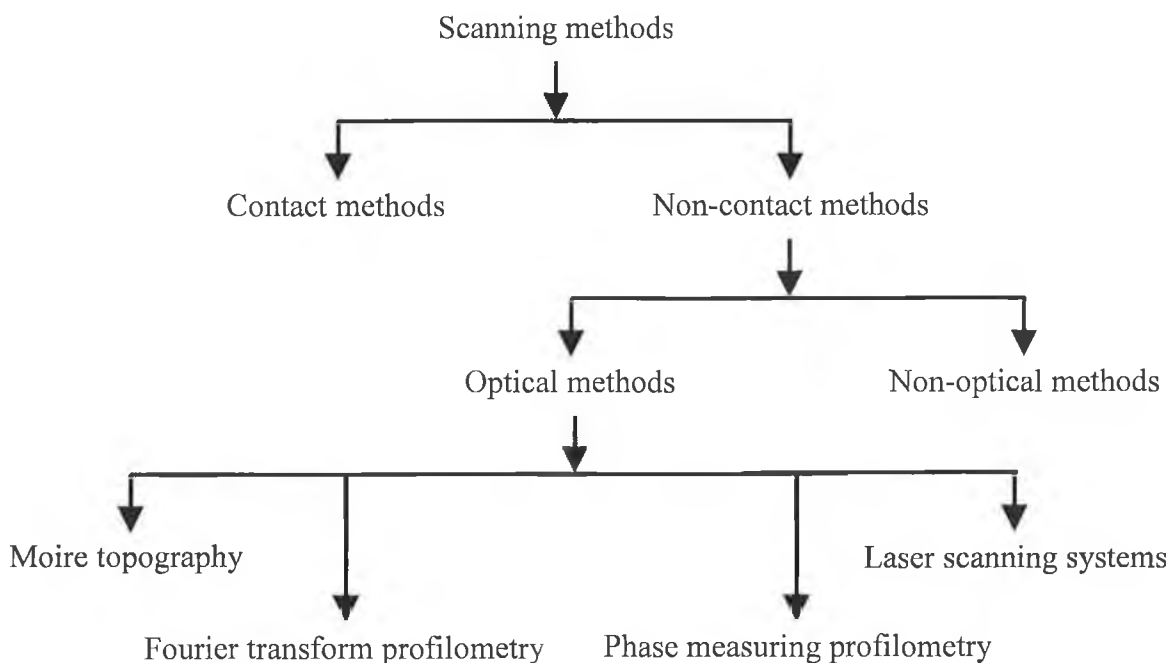


Table 2-1: Classification of scanning methods

In contact methods measurement is done by Co-ordinate Measurement Machine (CMM) which uses a touch probe. CMM generally collects data a point at a time. Such process is slow, and because it is a contact process, it is limited to measurement and calibration applications where accuracy, rather than speed, is paramount [11].

Better knowledge of a product's physical characteristics is essential if quality control is to improve in industrial companies. Several surface evaluation systems have been developed. Among these, systems based on non-contact optical methods have attracted well-deserved attention because of their particularly good adaptation to specific applications.

3-D profile measurement techniques based on structure light have been used widely in many domains, because these methods have the advantages of non-contact, high precision and easy control. Now-a-days, some techniques of 3-D profile measurement based on structure light such as Moire topography (MT), Fourier transform profilometry (FTP), phase measuring profilometry (PMP), and laser scanning triangulation have been presented. Among these techniques MT, FTP, and PMP are full-court measurements. The methods of 3-D profile measurement based on structure light use the analysis on the deformed light to gain the profile information of the surveyed object [12].

Full-court measurement is seldom used on a large-scale object. Because when the object is large, the measurement system is bulky and some special parts are needed. This makes the cost of measurement system much higher, whilst laser scanning triangulation measurement is an effective method due to its advantages of a simple structure, being a real-time process and enabling the quick measurement of the full-court with the use of laser scanning equipment. Presently, the study of this method stresses the increase of measuring precision [12].

2.6.2 Laser scanning systems

Optical inspection systems have found widespread acceptance in industrial manufacturing for increasing productivity, product quality, and process control. Typical systems consist of an optical laser scanner, a detection unit, and the data processing part, where the scanner represents an essential part of high accuracy

implementations. The most common principle of position measurement is laser-optical triangulation due to its simplicity and robustness. It also provides high accuracy and feasibility [13].

In the last decades, laser scanning systems have been adopted world-wide for the fully automatic testing of surfaces. Devices of this kind have been further developed in collaboration with a large number of materials manufacturers. Their optical systems and electronics have been optimised for various specific applications [14].

Widely varied material surfaces have been inspected with laser scanning systems. These include from metals of all types to paper, glass, plastics, films, as well as magnetic and optical discs [15]. The major advantages of a laser scanning system are higher resolution, faster scanning speed, and high contrast image acquisition.

Roughness measurements and micro-topographic inspection of rough surfaces have required measuring ranges from a few hundreds of micrometers to a few millimetres. Several profilers and micro-topographers have recently been reported. Methods and techniques (interferometric, scattering, triangulation, fringe projection, etc.) that have been known for a long time are being rediscovered and developed to meet new reliability requirements. Specially triangulation based methods are being used extensively in the range sensing, in three dimensional (3-D) shape inspection, in topographic evaluation, and even in the micro-inspection of rough surfaces.

Although area methods, such as fringe projection and moire, have proved useful in many situations and the inherent problems of heavy data processing seem no longer to be a major drawback, the point to point inspection approach has a clear advantage in simplicity and especially in flexibility.

The term *moire effect* refers to a geometrical interference formed when two transmitting screens of similar motif partly overlap. In other way, it denotes a fringe pattern formed by the superposition of two grid structures of similar period [16].

In laser scanning systems the surface being inspected usually is swept point to point by a laser light beam, which creates a bright spot on the surface. The measuring

range depends on the particular system's implementation. Ranges up to some tens of millimetres with resolutions in the micrometer are possible. The area to be analysed can be as large as desired with positioning resolutions in the sub-micrometer range permitted by precise X-Y positioning stages.

When a focused laser beam falls on a surface the amount of radiation scattered depends on the nature and structure of the surface. For total inspection of the surface of a material the focused laser beam must sample every point on the surface without leaving gaps. This is usually achieved by rapid scanning of the surface; for example, where the material is in the form of strip, the laser spot moves at a high speed perpendicular to the material movement direction.

The velocity of the laser spot in the scanning direction is essentially determined by the required scan width and the design of the laser scanner. Spot velocities of up to 8000 m/s are attainable in practice. The frequency limit depends ultimately on the type of detector, the light wavelength, the required detector area, and the intensity of light falling on the detector. The width of the laser spot intensity distribution in the scanning direction is restricted to a value which depends on the length of the scan path and the design of the laser scanner. The length of the laser spot along the direction of the material flow can, however, vary over a wide range [14].

2.6.3 Data collection techniques in laser scanning systems

Data collection technique in laser scanning systems can be divided into two classes of methods: flying spot scan method, and pattern projection method [11]. These are discussed below:

(1) Flying spot scan method – This is done by the projection of a single point of laser light which is viewed at an oblique angle. The offset of the point relative to a datum is measured and if calibrated correctly can be given as a co-ordinate. This method of data collection technique is implemented in our present work.

(2) Pattern projection method – This is by far the largest category of optical scanning methods. The two major techniques are laser line or grid projection and interferometric fringe techniques. The laser line (or grid) method is similar to the

flying spot technique but instead of the line (or grid) offset is measured. This allows more points to be measured at a time. Interferometric fringe techniques rely on the interference of two beams of light. A reference grid is projected onto the surface of an object. The object is then viewed through a grid with a similar pitch frequency and a series of dark and light contours are superimposed on an image of the surface. These lines correspond to a series of imaginary planes whose normals lies along the viewing axis of the instrument. The departure of a fringe from a straight line implies a change in surface height. Similarly a series of parallel fringes implies a flat surface. The resolution of the process is limited by the object depth or contour range divided by the number of fringes resolved by the viewing system. This type of process has the advantage of capturing the surface of the object in one go. The disadvantages are the relatively large amount of processing that is required to convert the image data to point data and the system is not view point independent or able to cope with a wide range of surface types [11].

2.6.4 Speckle effects in laser scanning systems

Lasers are recommended as illuminating sources, because of their monochromaticity, stability, high intensity, low cost, and user friendly characteristics. However, on inspection of optically rough surfaces the speckle effects can reduce the system resolution. Because when an object is illuminated by a laser, it appears to be covered with a very fine granular structure. All the points of the object illuminated by the laser are coherent, and the waves that they transmit to the eye are capable of interfering. The image from each object point produces on the retina a diffraction image that depends upon the imaging system of the eye. It is the interference between these diffraction images that is responsible for the granular structure known as speckle.

However, the formation of an image is not necessary to obtain speckle. A diffuse object illuminated by a laser produces a speckle pattern in the space surrounding causing a degradation of image quality [17]. Speckle reduction techniques, such as spatial averaging, may allow a better resolution limited by technical considerations such as mechanical noise and the physical and electrical characteristics of the observation system [7].

The speckle image noise, the precision of locating of the speckle centre and the accurate calibration of the measuring system are key factors that influence the measuring precision of the laser scanning measurement system. Using a combined filter of a recursive median filter and a Gaussian filter the speckle noise can be decreased efficiently. With the approximate method based on the physical characteristics of the intensity of the speckle image and the linear calibration of the measuring system parameter, the measuring precision can be increased remarkably [12].

2.7 Laser-optical triangulation systems

The principle of triangulation has been known since the time of the early Greek, and indeed optical triangulation has been used for hundreds of years in the field of surveying [18]. Recently, with the advent of low-cost, compact semiconductor diode lasers, lasers have been used in optical triangulation instruments. Early applications of a laser-optical triangulation device consisted principally of sensor controls for industrial processes such as web thickness monitors and position sensors.

At present, one of the most common principles of commercial three-dimensional displacement sensing is laser-optical triangulation because of its simplicity and robustness [19, 20]. It has been applied to both profiling and gaging applications. In profiling. The interest is in the details of the surface height or roughness of a particular article. Surface profilers are used to inspect surfaces for defects such as cracking, pitting, or the presence of foreign materials such as sludge or corrosion. Gages are used for absolute measurements such as diameter and thickness.

2.7.1 Characteristics of laser-optical triangulation systems

Laser-optical triangulation systems are characterised by three features: high speed, high accuracy, and non-contact. It is these three characteristics of laser-optical triangulation that serve to differentiate it from other non-destructive testing (NDT) techniques such as ultra-sonic and eddy current techniques and to determine those applications to which it is most ideally suited. In many instances laser-optical triangulation, when used in conjunction with these other technologies, can provide

the inspection engineer with a more powerful data set than either technique alone [18].

2.7.2 Construction of laser-optical triangulation systems

Recent advances in micro-optics and micro-electronics have enabled the construction of very tiny optical triangulation engines or probes that are capable of inspecting cavities with dimensions as small as 5 mm. A laser-optical triangulation system ideally consists of an optical triangulation head, a motion control and positioning system, and a data acquisition and analysis system. These three sub-components provide the capabilities of high speed, non-contact, and high accuracy [18].

In an active trigonometry system, the light source is provided by measuring system itself, and its light focus on the surface of object being measured and forms an illumination spot meanwhile. The spatial position of illumination spot changes with that of the object surface. The light-receiving unit records the spatial position of illumination spot by light-spot position detector such as PSD or CCD through imaging lens. The signal processing unit of measuring system can calculate the changes of displacement of the object being measured acts as a probe during measurement, and the changing of spatial position of illumination spot represents that of the surface being measured [21].

2.7.3 Types of laser-optical triangulation systems

Based on laser light incident mode laser-optical triangulation systems can be divided into two types [21]: obliquely incident mode active trigonometry [2, 13, 21-26], and vertically incident mode active trigonometry [12, 19-21, 27-35]. That means the laser light can be projected either obliquely or vertically to illuminate the surface of the object to be surveyed. But the observation apertures are always placed with an angle to the object plane. Since the latter type of technique is employed in the present work, so all the discussions about the laser-optical triangulation system are limited to this type.

2.7.4 Mechanism of laser-optical triangulation systems

The optical set-up and the relationship of object and image in vertically incident mode active trigonometry are shown in Figure 2-3.

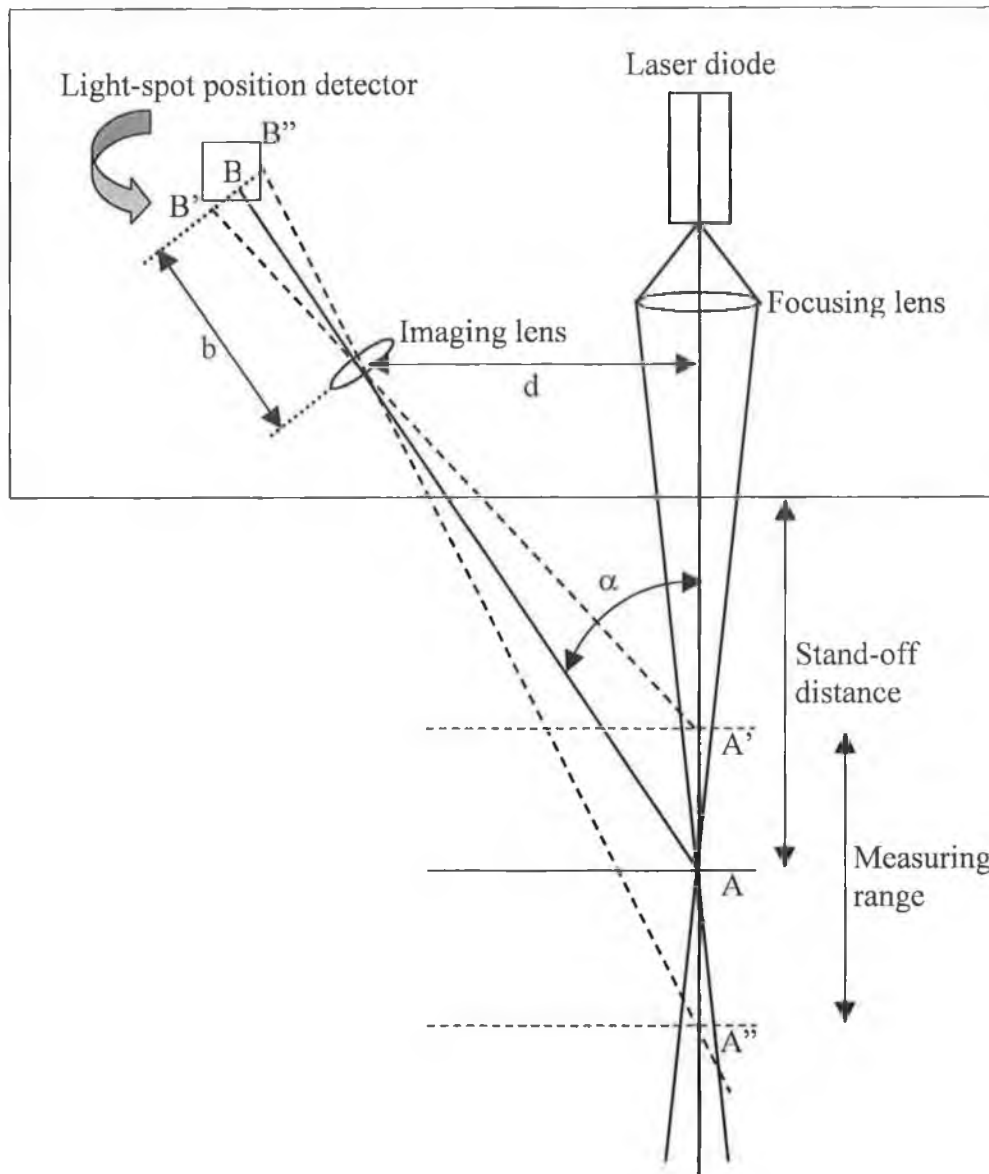


Figure 2-3: Schematic giving the arrangement of a laser-optical triangulation measurement system

In a laser-optical triangulation measurement the light beam of a laser diode is focused on the surface of the object to be measured by means of a focusing objective. The light is then subject to diffusion by reflection, i.e., the light is reflected in all directions in a hemisphere. The intensity varies in different directions depending on the properties of the surface of the object. The light spot on the surface is then viewed under an angle α onto a position sensitive detector (PSD) by a second object. Changing the distance of the object toward or away from the measurement

probe results in a displacement of the light spot, resulting in a displacement of the “centre of gravity” of the light spot on the PSD. The vertical distance between a point A’ and the imaging lens is given by geometric relationships that result in [29]:

$$A' = \frac{d \cdot b \cdot \cos \alpha}{b \cdot \sin \alpha + BB'} \quad [2.7]$$

Here **d** is the horizontal distance between the imaging and focusing lens, **b** is the image distance, α is the viewing angle, and **BB'** is the spot displacement on the detector.

2.7.5 Reflection factor of object surface in laser-optical triangulation systems

Light beams reflected by a sample comprise of a diffuse reflection component and a specular reflection component. The ratio of the diffuse reflection component to the specular reflection component depends on the material surface of the sample. Mirror surfaced or shiny samples mainly reflect specular reflection components; samples with a dull surface mainly reflect diffuse reflection components.

In principle, the sensor detects the diffuse part of the reflected laser light. It is not possible to make a definite statement on the minimum reflection factor because small diffuse parts can still be detected even from mirrored surfaces. This is done by determining the intensity of the diffuse reflection from the CCD array signal in real time and then stabilising the fluctuations in intensity [36].

Again in certain situations, where multiple reflections are present within the field of view of the collection optics, some intelligent processing of the optical signal is required before the height of the surface can be deduced. A typical example of this is the use of laser-optic profiling to measure thread forms. In these instances the radiation pattern on the focal plane may consist of one or more peaks due to the presence of multiple reflections within the field of view. For these applications a linear PDA or CCD array can be used. These detectors consist of a large number (up to 4,096) of detectors arrayed in a linear form factor. In this instance, a full profile of

the radiation scattered from the surface is obtained and intelligent algorithms can be used to locate the centroid of the optical feature of interest. This, of course, reduces the rate at which data can be acquired. Systems that use CCDs, however, have a number of other advantages and are immune from problems such as stray light, which can plague the design of tightly bundled optical systems [18].

2.7.6 Analysis of main precision factors of a laser-optical triangulation system

(1) Influences of speckle image noise – There are many factors that can cause speckle image noise and the key factor is the physical characteristics of the object surface. In a laser-optical triangulation system, diffuse reflection of the speckle is produced when the laser beam is projected onto the surface of an object. However, the surface status is diverse. When the same light beam projects onto the surface of different colours, different materials, different surface forms or different optical quality then the reflectivity or the absorbtivity of the surface is different too. Especially the surface form and the reflectance of the object affect light diffusion severely and all these make the image quality decrease. A speckle image usually takes a few pixels and it is necessary to locate the speckle centre, otherwise the measuring precision will be influenced severely. In addition, the environmental noise, the stochastic noise of CCD and an image collector, and electrical noise are other factors that can cause image noise [12].

(2) Image distortion of an imaging system – Theoretically the lens of an imaging system is supposed to be an ideal thin lens. However, all the spots do not pass through the same optical centre when they are imaged onto the image plane. When the lens is larger or the object deviates from the lens axis, the image distortion is severe. Image error will be caused when the co-ordinates of the imaging system or the camera axis does not cross the image plane at right angles, and when a video signal is transformed into a digital signal the synchro error of the transformation will cause image vibration or image distortion. In addition, image distortion can be caused by the stochastic noise and the geometric error of CCD. Image distortion can decrease measuring precision severely.

(3) Influence of surface leaning – To study the distribution of the diffuse field of an object's surface, it is supposed that the surface is a Lambert reflector and that the

intensity of diffused light is a function of the diffusion angle. This is because the light power taken by the lens is asymmetric and the energy centre of the speckle image usually deviates from its geometric centre, all of these causing a measurement result differing from the calculating result, and the maximal error level of which can be centi-micrometers. This is one of the key factors of image distortion.

(4) Influences of the relationship between the object and the image and the error of the measuring system structure – The relationship between the position of the object and the co-ordinates of the image is a transformation from 3-D to 2-D. From Figure 2-4 it is seen that the diffused light of the object passes through the lens centre and comes to the image plane. The relationship between the spatial point P and its image p is [12],

$$\frac{x}{-x_w} = \frac{f_0}{z_w - f_0}, \quad \frac{y}{-y_w} = \frac{f_0}{z_w - f_0} \quad [2.8]$$

This provides an equation set as follows:

$$x = \frac{f_0 x_w}{f_0 - z_w}, \quad y = \frac{f_0 y_w}{f_0 - z_w}, \quad z = z_w \quad [2.9]$$

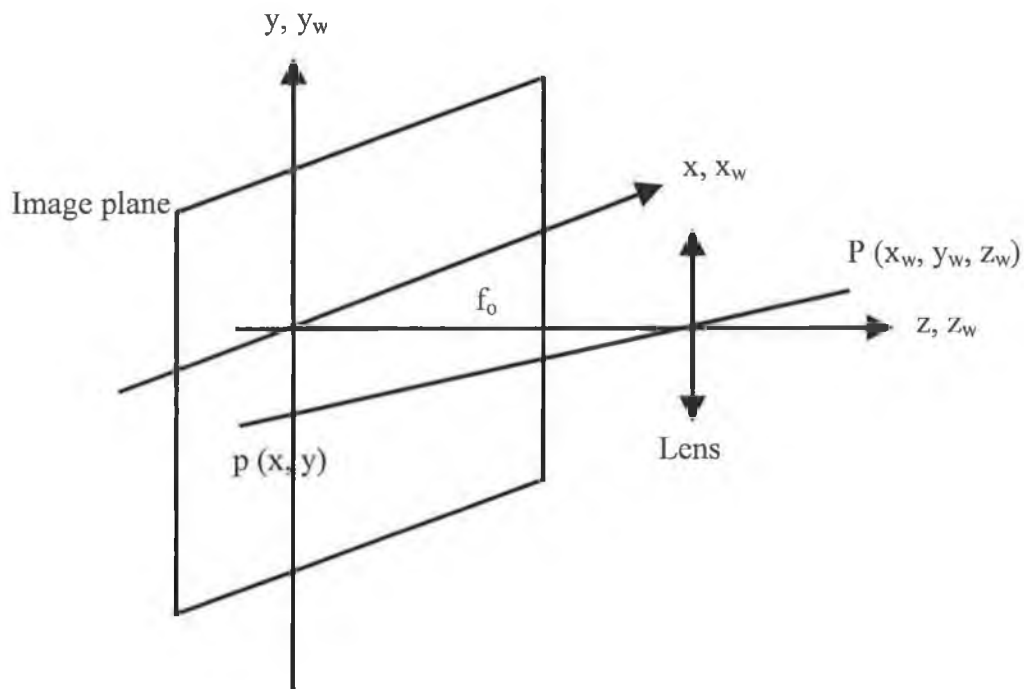


Figure 2-4: The relation between the spatial point P and its image p

In the above equations x_w , y_w and z_w are the co-ordinates of the spatial point P, x and y are the co-ordinates of p, the image of spatial point P, and f_0 is the focal length. From the equation set 2.9 it is found that the mapping relationship between the object and the image is non-linear. One cannot designate the object's co-ordinates only by considering the image co-ordinates, because each pixel on the image plane expresses a projecting line. When the camera axis and the light plane are not in parallel then the object and the image corresponds one by one. Therefore, the object's co-ordinates can be learned from the image co-ordinates by mean of the corresponding relationship of 2-D to 3-D. The key problem of gaining an object's 3-D co-ordinates is how to calibrate the non-linear relationship between the object and its image. In a laser-optical triangulation system, the light plane should project onto the object vertically and the CCD plane should cross at right angles to the lens axis. But the real structure of the measurement system cannot eliminate the error what decreases the measurement precision. Figure 2-5 shows the case of structure error.

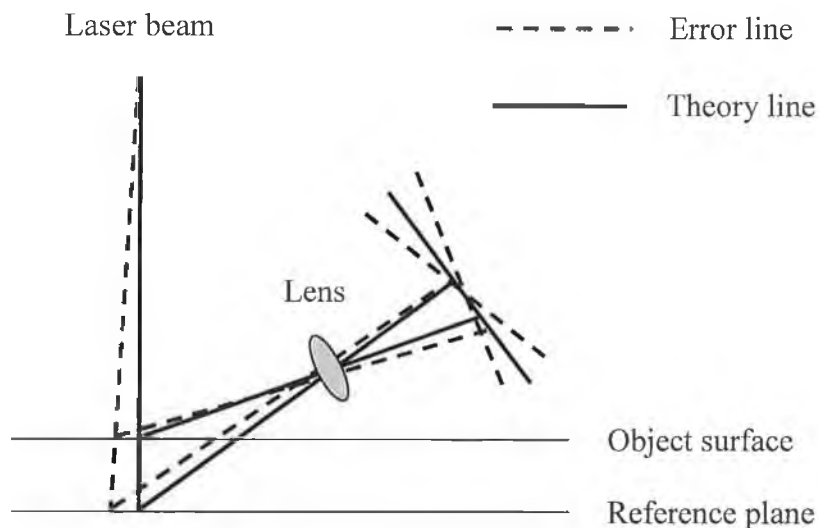


Figure 2-5: Measuring error caused by system structure

2.7.7 Methods of increasing measurement precision in a laser-optical triangulation system

In order to increase the measurement precision in a laser-optical triangulation system, three tasks should be done. They are (1) the elimination of image noise, (2) the accurate locating of the speckle image centre, and (3) the accurate calibration of

the measurement system [12]. Here the methods for decreasing image noise are discussed briefly.

Methods for decreasing image noise – At present, there are two kinds of filter for decreasing image noise: a linear filter and a non-linear filter. The linear filter is efficient for Gauss distortion but is helpless for pulse noise and most of the image noise in laser-optical triangulation system is pulse noise.

A median filter is a typical non-linear filter, which can decrease the influence of distortion and keep the detail of the image. The equation of a normal median filter is [12],

$$g(x, y) = \text{median} \{ f(x - k, y - l), (k, l) \in W \} \quad [2.10]$$

where $f(x, y)$ is the image function, W is the size of filter window, and median is to gain the middle value.

However, a median filter has some shortcomings. First, the noise can be controlled efficiently when its pulse width is less than $W/2$. But when the pulse width is greater than $W/2$ then the noise is out of control. Secondly, the median filter is ineffective for Gaussian noise. Obviously, edge image detail may be lost when using a median filter, and the case becomes worse when the filter window is enlarged [12].

2.7.8 Limitations of laser-optical triangulation systems

Although the principle of optical triangulation is relatively easy to understand, there are many hidden factors that make it difficult to design a robust and accurate system. The usual considerations for electronic noises must be taken into account when designing an optical detector system [18]. These principal noise factors include shot noise from the detected photons, Johnson noise from the resistive elements within the detector and circuit, amplifier noise, and quantisation limitations due to the use of an analogue-to-digital (A/D) converter. The first three noise terms can be reduced to applicable levels through good electronic system design. The quantisation uncertainty is a fundamental limitation due to the digitisation process, and in many

systems it is the practical limit to the amount of resolution that can be obtained in a system.

Again, variations in surface reflectivity can introduce fundamental limitations to accuracy. Since the lateral-effect photo-diode is detecting the centroid of radiation, a mottled surface with variable reflectivity within the laser spot size can result in intensity distributions for which the centroid has shifted due to variations in reflectivity. This effect can limit the sensitivity to a quantity on the order of 0.1 to 0.5 of the laser spot size, which is typically on the order of 0.025 mm.

For the case of machined surfaces, the scattered radiation may be diffractive into several orders or modes. This effect results in a non-uniform illumination of the collection aperture. Unless the collection optics are well designed, the resulting stigmatism and coma may result in a variation of the centroid of the radiation field in the focal plane, which in turn limits accuracy.

2.7.9 Advantages of laser-optical triangulation systems

The laser-optical triangulation measurement systems have a good reputation as being robust, reliable, reasonably fast and acceptably accurate. This technology can easily provide high data rates on a kilohertz to megahertz basis. In many situations this speed of measurement is an important consideration for economic reasons and the measurement itself is usually only one step in an overall engineering problem. Adequate resolution is also achieved with “sub-pixel” techniques where the resolution actually achieved is greater than that of the fundamental image element itself [30].

The advantage of this measuring method is that the measuring system is not sensitive to the detailed shape of object surface, thus a constant measuring precision will be kept during continuous measurement [21].

The another advantage of laser-optical triangulation by using a sheet beam and a plane array of CCD cameras is that 2-D scanning can be achieved by moving the object relative to the sensor only in one direction. This simplifies the measuring system and endless convenient operation [19].

2.7.10 Disadvantages of laser-optical triangulation systems

One problem common to all triangulation based inspection systems is the existence of shaded (hidden) areas that go uninspected on the surface of the object to be analysed [7]. The measurement does not take place coaxial with the light source, leading to problems of occlusion and in the physical size of the measuring instrument. If the distance between the sensor and the light probe is reduced to minimise these problems then, the non-linearity inherent in the simple triangulation geometry becomes a serious limitation. The light source used has to maintain a high signal to noise ratio at the detector compared to the ambient light reflection in the area of interest and this can lead to problems of eye safety.

This geometrical configuration has a disadvantage that as the surface profile changes, the spatial location of the sample height moves slightly. This can be corrected by using data processing software; however, it adds a degree of complexity to the system [18].

Another disadvantage of this measurement system is the occurrence of stray light with the same wavelength as the light being measured. Stray light can come from internal reflections or from secondary reflections from the measured object. A displacement in the light spot's "centre of gravity" on the PSD, as pointed out in section 2.7.4, occurs and a measurement inaccuracy results. Recent development shows using advanced optronics many of the stray light problems can be eliminated [29].

This method is not suitable to the measurement of quasi-smooth surfaces, the reflective surfaces [21]. Furthermore the lens system may present problems in dirty environments with ensuring clear optical surfaces.

2.7.11 Measurement errors in laser-optical triangulation systems

In a laser-optical triangulation system, the errors in measurement may be split into two groups: distance measuring errors and the errors in determining the spatial coordinates of the measured points [30]. In both categories there are systematic and random errors. The systematic errors can be estimated and, in many cases, a correction can be made. The random errors are best treated statistically. Figure 2-6

presents a hierarchical structure of measurement errors in laser-optical triangulation system.

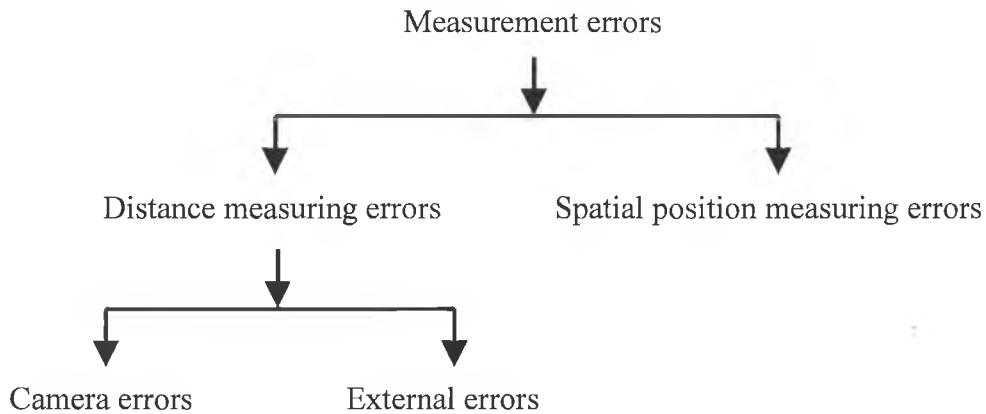


Figure 2-6: Measurement errors in LOTS

Spatial position measuring errors:

Measuring the distance from a laser-optical triangulation system to a structure is effected by means of mechanically holding the measuring system while a measurement is made. If, in addition, a number of measurements are required to a multiplicity of positions on the structure surface and these measurements are required to a number of areas on the given structure then additional errors will be accumulated to the individual measurements points. Thus the errors in determining the spatial co-ordinates of the measured points are occurred.

Distance measuring errors:

There are many sources of errors in laser-optical triangulation systems which reduce the maximum resolution available for a given configuration. A laser-optical triangulation system is made up of mechanical and optical components. Some of which are amenable to design considerations, such as, choice of laser, sensor, lens and others which are beyond the capabilities of the designer to adjust. For example, reflectivity of the surface to be measured and nature of the medium through which light is transmitted and received, e.g. air.

(1) Camera errors – The measuring system uses a lens and sensor as a distance measurer. This camera will produce errors of measurement due to temperature change, image processing and mathematical modelling limitation.

Location of image with respect to CCD linear array – The precision with which the Gaussian peak of the laser spot can be identified with respect to the sensor determines one of the fundamental limitations of the resolution of the system as a whole.

Sensor position changes with temperature – The sensor is mounted on a printed circuit board which is held in the camera/lens housing. It is assumed that the camera unit cannot move in relation to the laser, but that it is possible for the CCD sensor itself to expand with temperature.

Change in camera image distance with temperature – The lens camera system will expand or contract with temperature changes. This will affect the focus on axis, but off axis it will alter the position of the image with respect to the sensor chip and hence alter the accuracy of distance measurement.

(2) External errors – The remaining analysis of distance measurement errors concentrates on the factors which are outside of the camera measuring system, such as, base line expansion, laser pointing stability, beam stability and surface characteristics.

Base line expansion – The laser-optical triangulation system is constructed from a laser, sensor and lens mechanically held in a fixed configuration. The system is operated via calibration at a specific time and subsequent interpolation. There is an implicit assumption that the system is still in the same configuration as it was at the time of calibration which may not be the case, due to temperature changes, system straining, etc. The main resulting cause of error is the variation of base line length due to the thermal expansion of the material over its operating temperature range. It is assumed that the design is such that the camera and the laser are not able to change in orientation with respect to each other.

Laser pointing stability – A laser provides a source of well collimated light which is able to illuminate a small portion of the object. The successful use of this light spot depends critically upon the pointing stability of the source. Lasers have very low pointing angle variation. The pointing stability of all lasers is maintained by a proprietary control technology which actively stabilises the laser pointing to within $\pm 20 \mu \text{ Rad} / \text{C}$. The stabilisation is active under all operating conditions. This technology avoids power fluctuations due to changes in mirror pointing and allows for precise, long term pointing of the laser output under changing ambient and operating conditions. The laser alignment remains constant over the long term without tweaking [37].

Beam stability – The laser beam and the reflected light all pass through air before entering the camera. During this period it is possible for the light to encounter temperature, pressure or humidity gradients which can affect the direct path of the light to the camera, so giving a false reading.

Surface characteristics – The image location with respect to the CCD array can cause errors if the surface to be measured has sharp discontinuities either in form or contrast, is aligned at unfavourable angles, or is outside the optimum range of reflectivity required by the sensing system [30].

2.7.12 Requirements in laser-optical triangulation systems

For the laser-optical triangulation scheme to operate successfully the light source must be able to accurately illuminate the point on the structure to be measured. This requires, of the laser, the following [30]:

Low beam divergence – This is required because with a small spot size there is maximum signal to noise ratio.

High directional pointing stability – The system is calibrated once and then based on this, an interpolation takes place. Errors will result from a lack of reproducibility.

Power output stability – This requirement allows measurement over a greater range of surface reflectivity and allows prediction of the exposure level based on the past exposure level, this would not be possible if the power output changed between exposures.

Environmental stability – The system will be used in a range of temperature, humidity and pressure situations and also for long periods of time.

Low cost – Each component in an optical system will contribute to the overall cost and the laser is likely to be a significant cost in the development of the system.

2.7.13 Recent advancements of laser-optical triangulation systems

In recent days techniques have been developed to overcome the limitations of laser-optical triangulation systems using a differential optical head that approximately compensates for spatial variations of reflectivity [18]. Since the laser-optical triangulation head operates over a range of depth of focus design, lens design must be carefully constructed to minimise the effects of image form on the focal plane over the measurement range.

In many instances, the use of high-speed electronics can overcome many of the limitations imposed by the physics of the situation. One example is that they can convert non-linear response functions of an optical triangulation head into a linear and accurate set of engineering unit.

Despite the various design constraints, mentioned here, optical triangulation heads are routinely built with resolutions down to the 0.05 μm range and absolute accuracies on the order of 5 μm . Due to the laser's ability to be focused to an extremely small spot size, the spatial resolution of these samples can be taken on a grid as small as 0.025 mm by 0.025 mm. These sampling rates are typically orders of magnitude higher than those of other NDT techniques and enable the acquisition, presentation, and analysis of large, information-rich data sets. Speed of measurement is limited by the time it takes to collect enough light and to clock the data from the

array and process it. This implies a maximum data rate of 10kHz for a 2048 pixel CCD chip typical of what is available commercially.

2.7.14 Applications of laser-optical triangulation systems

Until now, the use of laser-optical triangulation system has been restricted to the field of mechanical engineering and optics. In industry, however, laser-optical triangulation sensors are extensively and routinely used for fast, non-contact distance measurement.

Laser-optical triangulation inspection systems provide the user with the ability to obtain high-speed and high-accurate non-contact measurements of surface profiles or dimensional gaging. Data are presented to the user in the form of two-dimensional height profiles that resemble the image from a borescope but provide quantitative relief information about the presence of details such as cracking, pitting, corrosion, and erosion. These systems are limited to detecting surface features and are not capable of detecting flaws below the surfaces and so do not directly compete with non-destructive technologies that are designed to examine flaws below the surface such as ultrasonic and eddy current detection.

Laser-optical triangulation heads have been built to penetrate spaces as small as 5 mm in diameter. Systems are routinely produced with the ability to acquire 20,000 height readings per second or higher with accuracy in the 5 μm range. The laser-optical triangulation systems have finite resolution and so they are suitable for bounded situations where it is known that all objects of interest will fall within the range of the measuring equipment.

More applications are found daily for the use of laser-optical triangulation systems. The quality control market for precious, non-contact measurement of internal surfaces in production is rapidly growing. Applications for automotive and aerospace products ranging from rubber hoses to ceramic gyroscope bearings for missiles have been successfully developed.

The two most important, appropriate, and useful fields of applications where the laser-optical triangulation system are frequently used are surface inspection and distance measurement. These two topics are also the key points of interest of the present research. So they are studied here extensively with more details.

2.8 Surface inspection

In manufacturing processes of industrial products, the importance to grasp surface properties of products is increasing as the requirements for improvement of function and performance of products are becoming keener. Especially in advanced automated production system, detection systems of surface defects are often introduced aiming not only to eliminate defective products by performing appearance inspection but also to reduce costs like raw material costs or labour charges by prevention of anticipated failure detection with feedback of inspection results to preceding processes [38]. As a result, surface geometry is the basic information required for process control and product quality monitoring in a variety of industrial applications [27].

In modern manufacturing, quality control requirements are stringent and subjective, although valuable, human visual inspection of the production process is giving way to faster, more reliable, more objective and less expensive electro-optical techniques [22]. To diverse in-line, in-process sensors, fulfilment of conditions like non-damaging, high response speed, circumstantial resistance is strongly required. For those sensors, the system using nature of light is the most useful for such conditions, also it is excellent for safety, stability, easiness of handling which are important in practical applications [38].

Among the quality control tasks, surface inspection is a major one. The advance in manufacturing automation has created the need to develop in-process measurement techniques, on-line quality control, and on-line machining compensation. Amongst these the real time measurement of roughness on surfaces under dynamic conditions is important in many industrial processes. The monitoring of finished work piece roughness in a machining process can increase the machining rate up to the required

surface finish such that the productivity can be enhanced. In-process roughness measurements can be taken as a process control parameter and/or a feedback for the optimisation of a machining process [39].

2.8.1 Conventional method for surface inspection

Surface roughness is commonly measured mechanically with a stylus device. For a long time, invasive stylus-based systems were widely accepted [22]. The conventional method for measuring surface roughness is to pass a stylus probe across the surface and measure its movement such that the surface profile can be traced.

Most of the traditional methods use contact sensors which may bring errors from measuring force into the final results, and the friction between the sensor and the objects to be measured are so serious after a period of time that frequent changing the sensor become inevitable, and this will bring not only much inconvenience and low efficiency but also bad economic benefits. Besides, if the object is of large size, the size of the contact-sensor may be rather large as well, this may cause unnecessary cost in manufacturing the contact sensor [40].

Though the technique has been developed to a very sophisticated level, however, the finite radius of the tip of the probe limits the accuracy of the measurements. For peaks and crevices with dimensions smaller than the tip of the probe, the traced profiles are smaller than the actual sizes. Furthermore, the technique is not particularly suitable to soft surfaces and it is susceptible to environmental disturbance due to its contact nature. Moreover, the roughness measurement is along a line on the surface and a large number of such lines must be traced if topographical information of the entire surface is required. It is a slow process. Hence it is not suitable for the use of in-process measurements [39].

2.8.2 Optical method for surface inspection

Compared to stylus method, an optical method is often preferred because it is non-contacting and the process is non-destructive to any surface [39]. A considerable amount of research has been conducted to measure the surface roughness of engineering surfaces by using optical methods [41]. The principles of the optical

methods mainly rely on the focusing, interference, light scattering, speckle, and reflective beam positional variation concepts [39].

Over the past decade optical methods to characterise surface finish have been used increasingly in industrial applications. The use of optical methods to evaluate the surface roughness has many advantages over the use of mechanical measurement methods. In addition to a high speed of response, greater accuracy and reliability are important features of the optical system. The absence of mechanical contact with the measured surface and non-destructiveness make the optical method most in demand by industry. Indeed, there is some evidence that optical methods are encroaching on the typical domain of the stylus. There are, obviously, non-contacting methods available such as capacitance, pneumatic, and ultrasonic methods, but these are not in general use and do not offer the same versatility [41].

On the other hand, an optical method relying on the reflected beam peak power intensity variation may not be reliable for fine surfaces, since this method uses diffusive reflection, which plays an important role only for considerably rough surfaces. Consequently, the use of a Gaussian curve parameter of a Gaussian function approximating the reflected beam intensity may be fruitful in measuring the surface roughness of engineered surfaces by an optical method [41].

Topographic and micro-topographic inspection of rough surfaces is a field of potential application for triangulation method [22]. This is an attractive method to measure surface geometry because of its simplicity; performances such as reliability, speed, accuracy and cost can generally be tailored to fit specific task requirement and environmental constraint [27].

2.9 Distance measurement

Triangulation has been used for a long time as a basis for distance measurement sensors. Particularly in long-distance range sensing and mid-range 3-d sensing the method has extensively proved its usefulness [22].

The distance measuring technology based on active trigonometry has been widely used recently as the rapid development of laser diode technique and light spot position-detecting device such as CCD and PSD. These kinds of technique and devices have been successfully used in robots and industrial production. In these cases, the surfaces of the objects to be measured are all diffuse reflecting surfaces. Laser beam illuminates the object surface vertically, and the object surface reflects the laser light diffusely in all directions. An optical receiver unit to which is fixed obliquely is used to collect certain part of the diffuse reflecting light and then light-spot position detectors and signal processing unit transfer the optical information into distance information. This traditional distance measuring is called active trigonometry with vertically incident mode [21].

2.9.1 Uncertainty limit in distance sensing

Distance measurements by laser-optical triangulation system suffer from a fundamental uncertainty that speckle introduces. Speckle arises because of the coherent illumination in combination with rough surfaces. Theory and experiments show that the uncertainty is mainly from the observation aperture, the speckle contrast, and the angle of triangulation. For short-range microscopic applications the distance uncertainty is in the range of a couple of micrometers to more than ten micrometers. The uncertainty does not depend on the size of the projected light spot as long as this spot is larger than the observed subjective speckle. For sufficiently rough surfaces the uncertainty can be reduced more than twice by low temporal coherence illumination. The introduction of low spatial coherence offers a significant improvement too. Design criteria for a sensor with minimum distance uncertainty should be small temporal coherence, small spatial coherence, and a large observation aperture [20].

2.9.2 Displacement sensors

Displacement sensors and meters measure the distance covered by an object which has moved from one place to another. It can also be used for such measurements as object height and width. There are two types of instruments for displacement measurement: the contact type (dial gauge, differential transformer, etc.) and the non-contact type (utilising magnetic fields, laser beams, sonic waves, etc.).

Operating principle of non-contact type laser displacement sensors:

The semiconductor displacement sensors and meters, comprising a light emitting element and a light receiving element such as PSD (Position Sensitive Detector) or CCD (Charged Couple Device), detect samples by using the optical triangulation technique. Figure 2-6 displays the schematic diagram of the measurement arrangement of a typical laser displacement sensor.

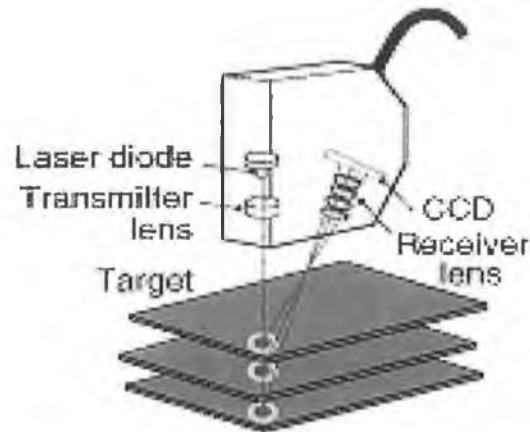


Figure 2-7: Schematic of the measurement arrangement of a typical laser displacement sensor [42]

A semiconductor laser beam is focused on the sample surface by the lens. The sample reflects the beam, which is then focused on the PSD or CCD, forming a beam spot. The beam spot moves on the PSD or CCD as the sample moves. The displacement of the work-piece can then be determined by detecting the movement of the beam spot.

During the scanning process the sensor always compares the image received from the sample surface with the one on its imaginary reference plane and then it returns the relative displacement distance of the sample surface from the imaginary reference plane.

Comparison between PSD and CCD as light receiving object:

Conventional laser displacement sensors employ a PSD as the light-receiving element but the laser displacement sensors used in this work use a CCD as the light-receiving element. The light reflected by a sample passes through the receiver lens

that focuses the light on the PSD or CCD. PSD type sensors use the light quantity distribution of the entire beam spot on the PSD to determine the beam spot centre and identify this as the sample position. However, the distribution of light quantity is affected by the surface condition of the sample, causing variations in measured values. The CCD detects the pixel where the peak value of the light quantity distribution of the beam spot identifies this as the sample position. Therefore, the CCD enables stable, highly accurate displacement measurement, regardless of the light quantity distribution of the beam spot. The light quantity distribution on a PSD and a CCD sensor is shown in Figure 2-7.

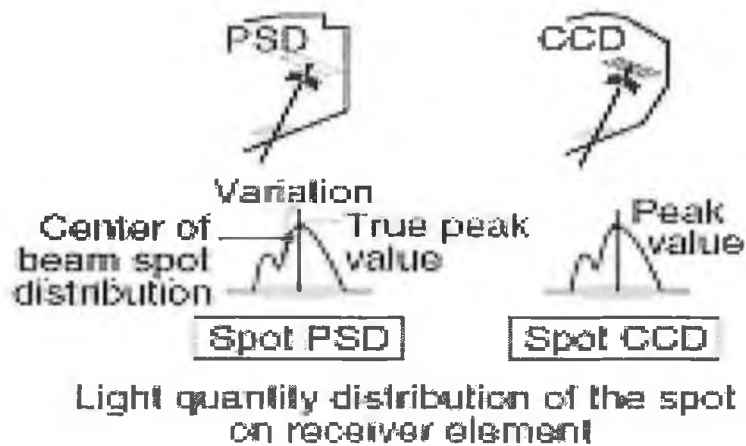


Figure 2-8: Light quantity distribution on PSD and CCD [42]

Chapter 3

System Set-up and Result for Surface Profile Measurement

This chapter presents the laser scanning system that was used for surface profile measurement. It includes system set-up, description, and experiment procedures. Results and discussion on these results are also covered up in this chapter.

3.1 A system for study

Before moving to the main project work, a preliminary work was done with a similar system. A laser scanning system was studied with a view to understanding scanning mechanism with laser technology. The system was built for surface defect detection. It could detect any change or variation in vertical displacement of the object surface surveyed and thus it was able to recognise surface defect with micrometer resolution. The system was initially designed and developed by S. Beary [44] in 1996. It was repaired, re-assembled, and modified in present work.

During the experiments a few samples were scanned. In every case the scanning data was analysed for sample profile measurement. Conclusions were made through discussing each individual result. Finally merits and demerits of the system were characterised and further development of the system was proposed.

3.2 System set-up

The schematic diagram of system set-up is shown in Figure 3-1. The X-Y plotter (Roland DXY 1300) was used to move the sample underneath the laser sensor (Micro-Epsilon optoNCDT 2000). The sample to be scanned was held in a sample holder attached to the pen-carriage of the plotter. The plotter was connected to the PC and could communicate with AutoCAD software. It moved the sample according to the drawing in AutoCAD as if it plotted a drawing in a paper. Two sample travel

to the drawing in AutoCAD as if it plotted a drawing in a paper. Two sample travel speeds were possible on the plotter: 5 mm/s (normal mode) and 20 mm/s (fast mode). The operation of the laser sensor was controlled through a dedicated software package (ILD2000 Demo Version 3.1), provided by the laser sensor manufacturer. The data interface card (Micro-Epsilon IFPS 2001) was used to interface the laser sensor with the PC. Figure 3-2 displays a photograph of the system used.

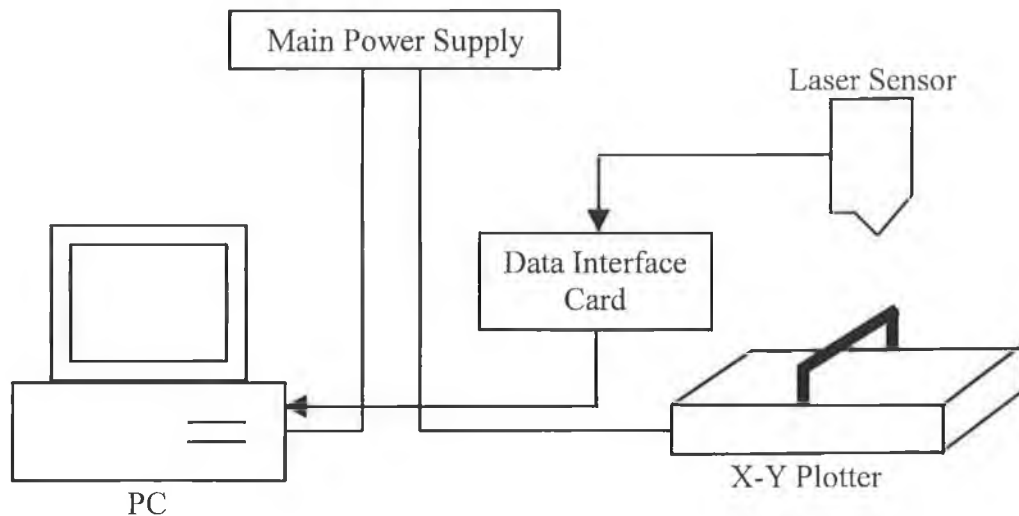


Figure 3-1: Schematic diagram of system set-up

The sensitivity of this laser scanning system was one volt per millimetre. It was capable of recording displacement data at 10 kHz. A typical accuracy of $\pm 2 \mu\text{m}$ in height measurement may be expected from this measurement system (see Table B-1 in Appendix B). The maximum number of data values that could be stored using the software provided was 8,000 and the maximum scan rate using the digital interface for the PC used (Intel 486 Processor with Windows 3.1) was 1 kHz. Before taking any measurement the system was needed to be turned on for 20 minutes to warm up to steady state and it was capable of operating in the temperature ranging from 0 °C to 40 °C. More specific details on hardware and software of this system can be found in Appendix B.

3.2.1 Laser displacement sensor, Micro-Epsilon optoNCDT 2000

The laser sensor light source is a red semiconductor laser with the wavelength of 670 nm. It is operated with a stand off distance of 58mm and has a measurement range of



Figure 3-2: Photograph of system set-up for surface profile measurement [44]

± 2.5 mm. The measured value is output simultaneously in analogue (± 5 V) and digital (RS 485/687.5 k Baud) format. It works on the principle of laser-optical triangulation method [36]. Charged-coupled device (CCD) is utilised as the light detector array of the sensor. The intensity of the diffuse reflection is determined in real time from the CCD signal. This allows the sensor to stabilise fluctuations in intensity during measurement over a very wide reflection factor range (from almost total absorption to almost total reflection). A high degree of immunity from interference is achieved by early digitalisation of the signal. The signal processing by the signal processor offers the possibility of adapting the sensor to material surfaces through the digital interface. This achieves a high linearity even on weakly reflective materials (e.g. black rubber).

3.3 Commissioning experiments

3.3.1 Safety measures

The maximum optical output power of Micro-Epsilon optoNCDT 2000 sensor was 1 mW. Before proceeding to carry out any experiment the following safety measures must be ensured.

- The sensor is classified as laser class 2. Operation of the laser should be indicated by an audible or visual warning signal as a precaution. See Appendix A for more information on the laser safety standard classification.
- Despite the low laser power, one should avoid looking directly into the laser beam.

3.3.2 Experiment considerations

The following experiment considerations should be taken into account.

- The sample to be measured should always be placed perpendicular with the optical axis of the sensor.
- The distance between the sensor head and the sample must be within the calibrated range.

- Air vents in the main housing must be free.
- While taking measurement any kind of mechanical vibration of either the sample or the sensor must be avoided.
- The experiment should be carried out in a dry and clean room that is free from dust, a strong source of illumination, and strong air currents.

3.3.3 Experiment procedures

The sample to be measured was placed on the sample holder attached to the pen-carriage of the plotter. The PC and the plotter were powered on. The laser sensor operating software, ILD2000 Demo Version 3.1 was then executed. The program had options to take measurements in two ways – single shot measurement and continuous measurement. Below is the step-by-step procedure of how this program was used and a sample was scanned. Figure 3-3 displays the measurement window of Micro-Epsilon ILD2000 Demo Version 3.1.

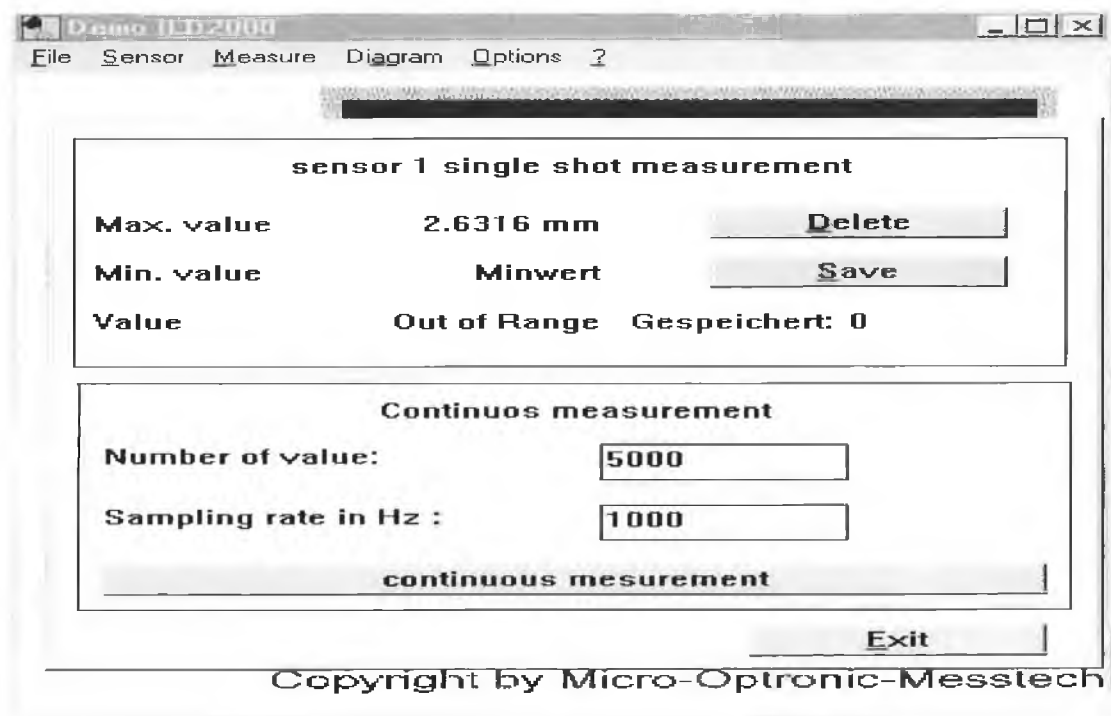


Figure 3-3: Measurement window of Micro-Epsilon ILD2000 Demo Version 3.1

Within the laser sensor operating software the menu options were selected as Sensor → Sensortype → 5mm, and Sensor → Power → on. The LED indicators of the sensor were then checked to ensure that the sensor was powered from PC via the

interface card. After at least 20 minutes the menu option was chosen as Measure → Sensor1. The program then opened up with a dialogue box for 'Sensor 1 single shot measurement' and for 'Continuous measurement' (see Figure 3-3). At this stage the system displayed the reading of a single point measurement. Data was found in millimetre scale that indicated the distance of a specific point on the sample surface from the reference plane of the sensor. The Save button was then selected from the open dialogue box. This saved the scan data into the system memory. This later step was repeated to obtain single point measurements. Upon exiting, the program prompted for a file name and the drive location to save the scan data.

In order to take continuous measurements the menu option was chosen as Measure → Sensor1. At this point any integer could be entered for '*Number of Value*' and for '*Sampling rate in Hz*' to specify the number of scan data points to be collected and the desired sampling rate respectively. Next the 'Continuous measurement' button of the open dialogue box, see Figure 3-3, was selected to start the measurements. The X-Y plotter was also set in motion at the desired speed at this point in order to move the sample beneath the sensor. After completing the measurement task, the system beeped automatically and went back to the previous screen. Again upon exiting, the program prompted for a file name and the drive location to save the scan data. All the data captured by the above program was opened up in Microsoft Excel, and plotted into graphs to view and analyse the sample surface profiles.

3.3.4 System parameters

In order to analyse the system output, a set of system parameters was considered. These are discussed below.

- **S** = the sampling cycle of laser sensor (Hz)

It was the scanning frequency of the laser sensor used. The value of this parameter was determined by the user input.

- **N** = the total number of scan data points

It was the total number of data to be acquired during a set of scan and was also determined by the user input.

- S_p = sample travel speed (mm/s)

During the experiments it was equivalent to the speed of the pen-carriage of the plotter which was 5 mm/s at the normal mode and 20 mm/s at the fast mode. (The figure was not exact rather approximate.)

- t = the total time elapsed for a set of scan (s)

This was the total time elapsed for a set of scan. $25 \text{ s} > t > 16 \text{ s}$ and $6 \text{ s} > t > 3 \text{ s}$ were recommended for the sample 80 mm in length at the normal mode and the fast mode respectively.

- S_r = scan resolution (mm)

This was the horizontal distance between two consecutive scan points on the sample surface.

The relationship among these system parameters is presented in Table 3-1(a) and Table 3-1(b). The tables indicate some possible combinations of these parameters. It can be seen from these tables that for a given sample travel speed the higher the sampling rate, the lower the scan resolution is. From the last entry in the last row of Table 3-1(b) it can also be seen that, for the set-up used in this work, it was possible to take a scan every 20 μm on the sample surface.

Table 3-1(a): Relationship among system parameters when $S_p = 5 \text{ mm/s}$

Sampling cycle S (Hz)	Total number of scan data points, N	Total time of scan $t = N / S$ (s)	Scan resolution $S_r = S_p / S$ (mm)
2	50	25	2.50
5	100	20	1.00
10	200	20	0.50
20	400	20	0.25
50	1000	20	0.10
100	2000	20	0.05

Table 3-1(b): Relationship among system parameters when $S_p = 20$ mm/s

Sampling cycle S (Hz)	Total number of scan data points, N	Total time of scan $t = N / S$ (s)	Scan resolution $S_r = S_p / S$ (mm)
100	500	5	0.200
200	1000	5	0.100
400	2000	5	0.050
500	2500	5	0.040
600	3000	5	0.033
800	4000	5	0.025
900	4500	5	0.022
1000	5000	5	0.020

3.4 Results and discussion

The measurement system was able to measure the maximum vertical displacement of 5 mm of a sample. The displacement measurements were recorded to a maximum resolution of 0.25 μm . Samples of different shapes and materials were tested. A few of them are presented here along with the description of the experiments carried out and the results obtained from these scans. The objectives of the experiments were to investigate the scanning performances of the system in different situations and to determine how accurate the system can represent sample profiles, such as, diameter or depth of a hole on a sample surface.

In the following experiments two thin brass plates of 1 mm thickness was used. There were a series of through holes on one plate and blind holes of approximately 0.45 mm in depth on the other one. Scans were performed on both series of holes and also on a flat section of the sample plate. During the experiments the sample was placed on a piece of white paper to ensure good contrast for the scanner head. Scans were done only in horizontal direction and the height measurements were acquired through the scans. In each sample picture the dashed arrow indicates the direction of scan performed. The system parameter, S_p (sample travel speed), was 5 mm/s and 20 mm/s. Lots of choices were made on S (sampling cycle of laser sensor) and N (the

total number of scan data points) to achieve lower S_r (scan resolution) as shown in Table 3-1(a) and Table 3-1(b).

3.4.1 Scan of through holes area of brass plate

In this experiment the through holes of the brass plate were scanned. Figure 3-4 is a picture of this sample plate. It shows the seven through holes of different sizes on the plate. See Figure F-1 in Appendix F for the drawing of the sample in AutoCAD with detailed dimensions. The aim of this experiment was to observe how perfectly the system could detect a hole on the sample surface and how closely it could measure the diameter or the depth of each hole. During the experiment the height measurements were acquired through the scan. The system parameters were selected as follows:

$$N = 200, S = 10 \text{ Hz}, t = 20 \text{ s}, S_r = S_p / S = 0.5 \text{ mm}$$

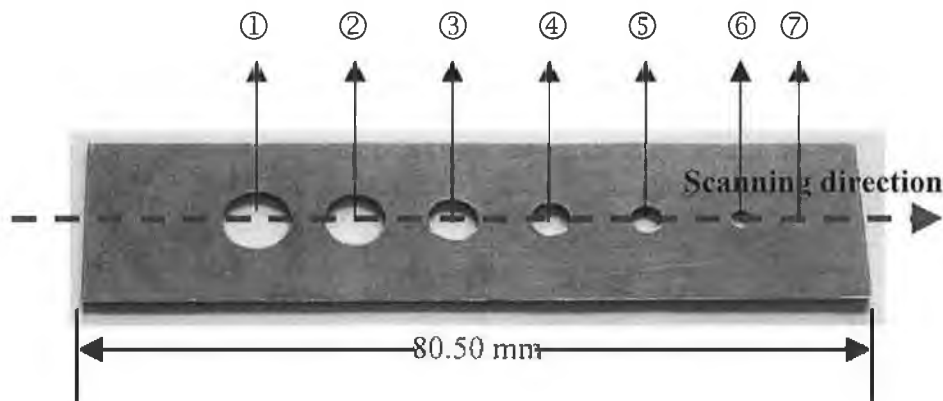


Figure 3-4: Picture of brass plate with 7 through holes (scan-1)

As the full length of the sample was 80.50 mm and the scan resolution (S_r) was 0.5 mm, so a total of 160 data points should represent the actual scan of the sample. This is seen in Figure 3-5 (note data points in the region of data point from 12 to 180). The sample was initially in an out of range position (-2.6315 V reading) with respect to the sensor head and then gradually it came closer to the sensor. The sample came within the measurement range over the first 5 data points collected (see Figure 3-5). At the end of the scan the sample again left the sensor measuring range (the last 6 data points). These 11 data points individually returned the lowest measurement value of the sensor (-2.6315 V reading). The data points in the region of point 6 to

point 11 and point 182 to point 194 in Figure 3-5 represent the scan reading from the paper surface. The location of the corresponding through holes is also indicated in Figure 3-5. The following measurements can be performed from this scan.

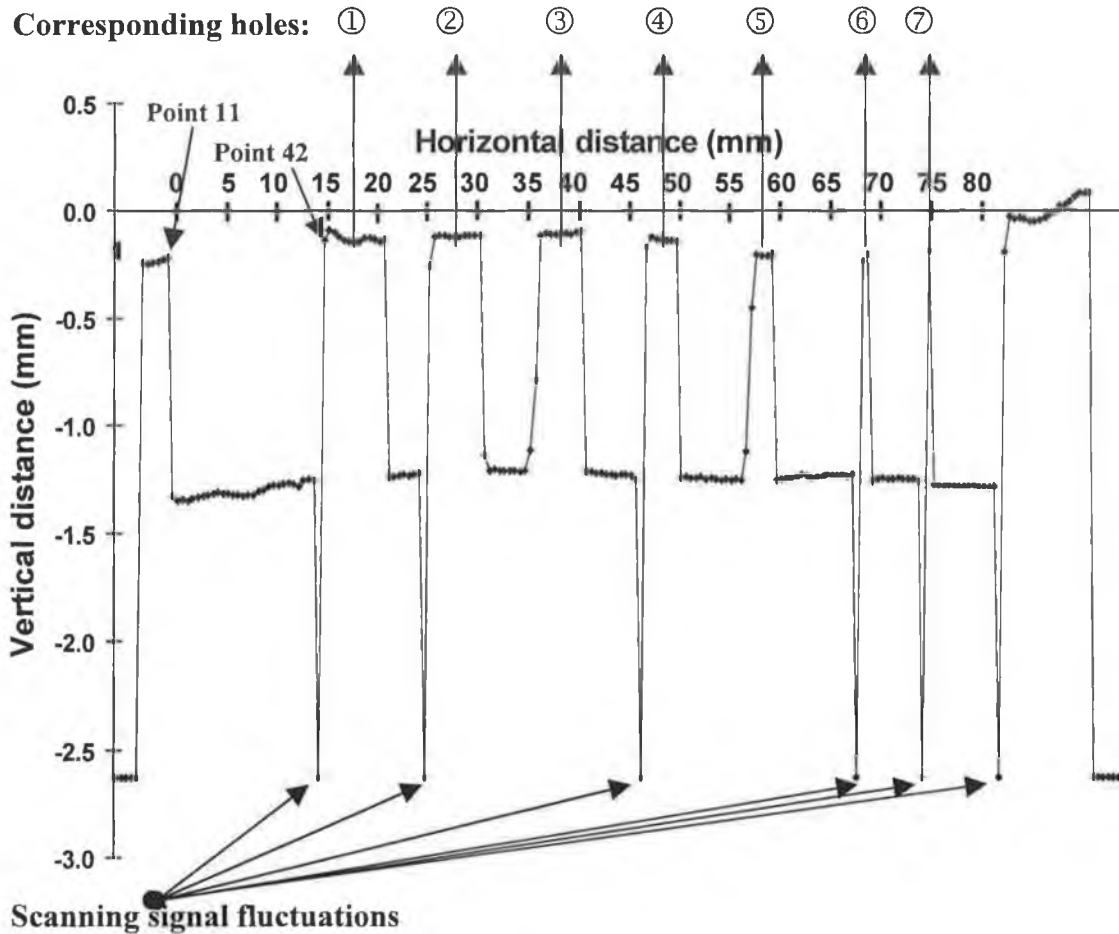


Figure 3-5: Scan of through holes area of brass plate

(1) **Diameter of through holes** – It can be calculated by multiplying the total number of scan data points of a single through hole with the value of S_r (scan resolution), provided that the scan is performed through the centre line of the hole. Based on the graph in Figure 3-5, Table 3-2 produces the calculation and comparison of the diameter of 7 through holes of the sample.

(2) **Thickness of sample plate** – It should be the height difference of any two points on the graph representing scans of the paper and the sample surface respectively. If point 11 and point 42 in Figure 3-5 are assumed to be from the paper surface and all other points between these two (except the point 41) are assumed to be from the

brass surface, then the thickness of the sample plate can be determined from the graph as approximately 1 mm.

Table 3-2: Comparison in dimension on the scanned brass plate

Through holes number	①	②	③	④	⑤	⑥	⑦
Total scan data points	13	12	10	7	6	2	1
Measured diameter (mm) (with scanning system)	6.50	6.00	5.00	3.50	3.00	1.00	0.50
Actual diameter (mm) (with Vernier callipers)	6.89	6.04	4.94	3.97	2.95	1.00	0.50

The few data points of the graph as indicated represent the scanning signal fluctuations on edge of the sample due to diffuse reflection of the laser beam from the sharp edge area. The concept is explained in Figure 3-6. The reflected laser beam of the laser sensor hits the sharp edge of the sample before it reaches the receiving lens of the sensor. Thus the scan produces an error in measurement. There was also some inclination in the sample relative to the scanning head evident in this graph.

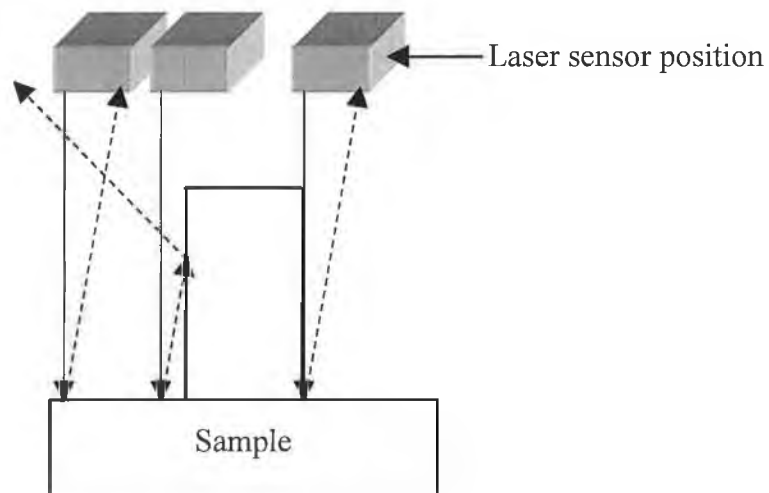


Figure 3-6: Scanning signal fluctuation on sharp edge area

3.4.2 Scan of flat area of brass plate

In this experiment the flat area of the brass plate was scanned. Figure 3-7 is a picture of this scan. The aim of this experiment was to observe the surface roughness of the sample in a range of sub-micrometer. The height measurements in horizontal

direction were taken through the scan. Degree of variation of the height signals would be reckoned as degree of roughness of the sample. The system parameters were selected as follows:

$$N = 50, S = 2 \text{ Hz}, t = 25 \text{ s}, S_r = S_p / S = 2.5 \text{ mm}$$

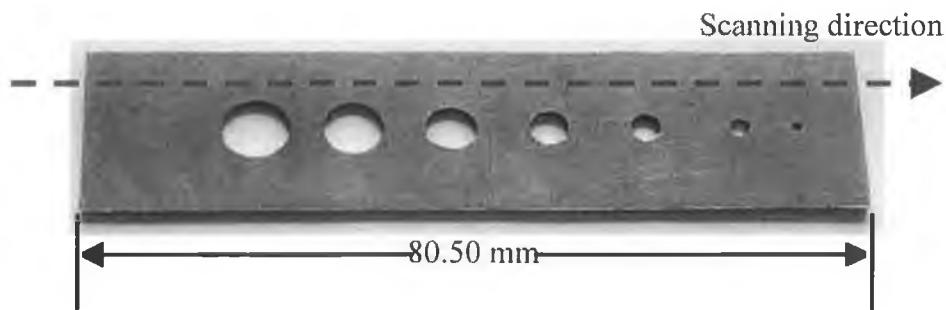


Figure 3-7: Picture of brass plate (scan-2)

As the full length of the sample was 80.50 mm and the scan resolution (S_r) was 2.5 mm, so a total of 32 data points should represent the actual scan of the sample. This is seen in Figure 3-8 (note data points in the region of data point from 11 to 41).

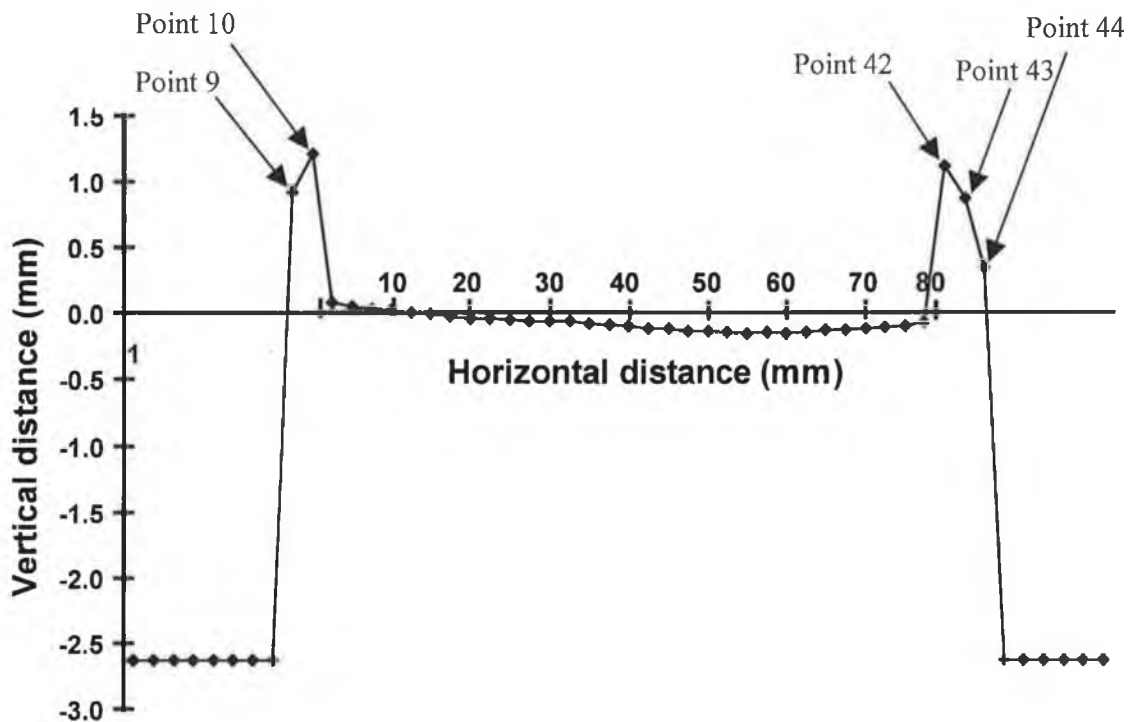


Figure 3-8: Scan of flat area of brass plate, showing the vertical displacement of the plate (mm) versus the scanned points

Similar to the previous experiment, the sample was initially in an out of range position (-2.6315 V reading) with respect to the sensor head. The sample came within measurement range over the first 8 data points collected (see Figure 3-8). At the end of the scan the sample again left the sensor measuring range (the last 6 data points). The data points 9, 10, 42, 43, and 44 in the graph represent the scan reading just off the edge of the sample. If point 10 and 42 are assumed to be from the paper surface and the points between these from the brass surface, the thickness of the sample plate can be determined from the graph as approximately 1 mm.

3.4.3 Scan of blind holes area of brass plate

In this experiment the blind holes of the brass plate were scanned. Figure 3-9 is a picture of this sample plate. It shows the five blind holes of different sizes on the plate. See Figure F-2 in Appendix F for the drawing of the sample in AutoCAD with detailed dimensions. The aim of this experiment was to observe how perfectly the system can detect a hole on the sample, and how closely it can measure the diameter or the depth of each hole. During the experiment the height measurements were acquired through the scan. The system parameters were selected as follows:

$$N = 50, S = 2 \text{ Hz}, t = 25 \text{ s}, S_r = S_p / S = 2.5 \text{ mm}$$

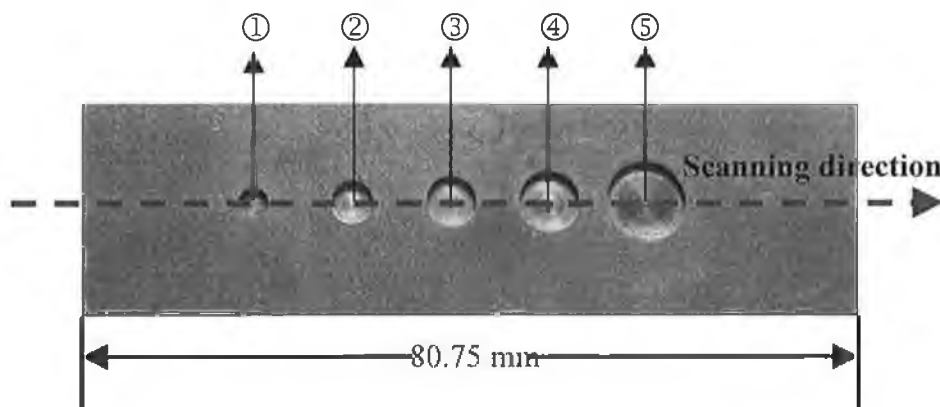


Figure 3-9: Picture of brass plate with 5 blind holes (scan-3)

As the full length of the sample was 80.75 mm and the scan resolution (S_r) was 2.5 mm, so a total of 32 data points should represent the actual scan of the sample. This is seen in Figure 3-10 (note data points in the region of data point from 10 to 40).

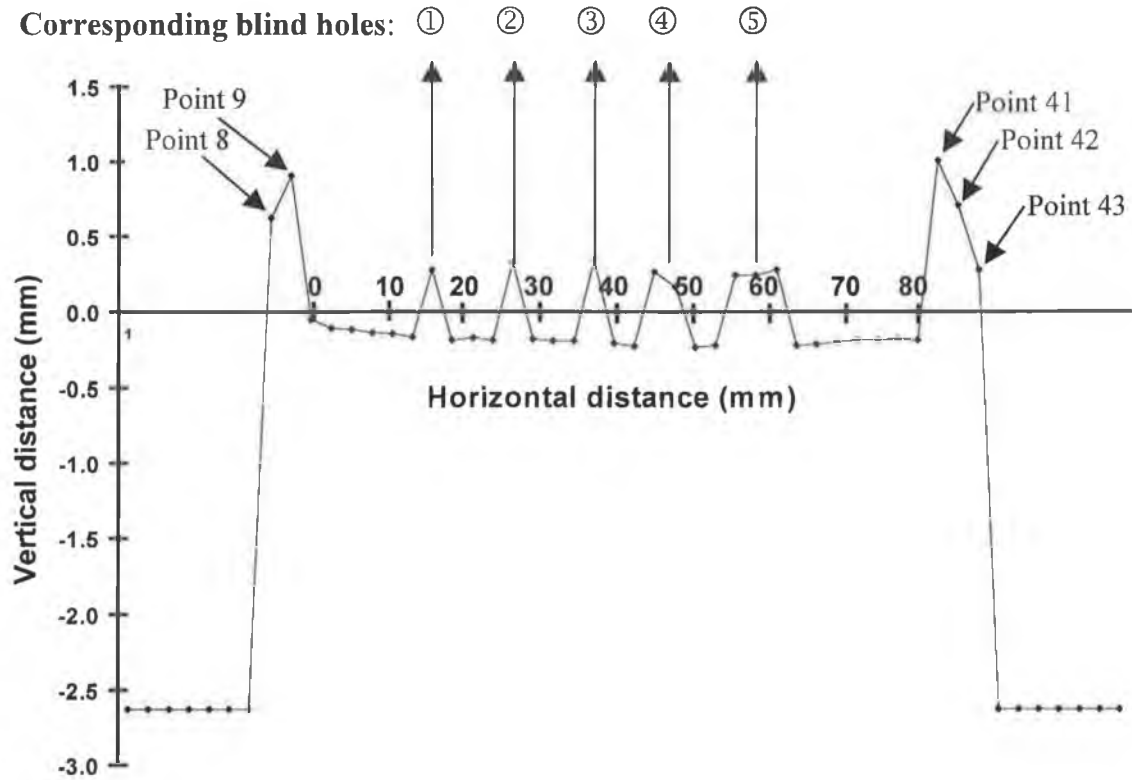


Figure 3-10: Scan of blind holes area of brass plate

Similar to the previous experiments, the sample was initially in an out of range position with respect to the sensor head and then gradually it came closer to the sensor. The sample came within measurement range over the first 7 data points collected (see Figure 3-10). At the end of the scan the sample again left the sensor measuring range (the last 7 data points). These 14 data points individually return the lowest measurement value of the sensor (-2.6315 V reading). The data points 8, 9, 41, 42, and 43 in the graph represent the scan reading just off the edge of the sample. The location of the corresponding blind holes is also indicated in Figure 3-10. The following measurements can be performed from this scan.

(1) Diameter of blind holes – It can be calculated by multiplying the total number of scan data points of a single blind hole with the value of S_r (scan resolution), provided that the scan is performed through the centre line of the hole. For example, the graph in Figure 3-10 shows a total of 3 points (point 31, 32, and 33) indicating scan data of corresponding blind hole ⑤. So the diameter of the blind hole ⑤ is 7.5 mm.

(2) Depth of blind holes – It should be the height difference of any two points on the graph representing scans of the sample surface and the bottom of a particular blind hole respectively. For example, if point 30 and 34 in Figure 3-10 are assumed to be from the brass surface and the points 31, 32, and 33 from the bottom of the blind hole ⑤, then the depth of the blind hole ⑤ can be determined from the graph as approximately 0.45 mm.

(3) Thickness of sample plate – It should be the height difference of any two points on the graph representing scans of the paper and the sample surface respectively. If points 9 and 41 in Figure 3-10 are assumed to be from the paper surface and the points 13,14, and 15 are assumed to be from the brass surface, then the thickness of the sample plate can be determined from the graph as approximately 1 mm.

3.5 Characterisation of the system

In order to characterise the surface profile measurement system the merits and demerits of the system are analysed here. The displacement measurement error producing factors of the laser system is also figured out for this purpose.

3.5.1 Merits of the system

The merits of the system mostly depends on the characteristics of the laser scanner (sensor head) itself. These are discussed below:

(1) Scanning frequency

The laser scanner offers a very high speed scanning facility. Its sampling frequency is 1 kHz, that is, it can take 1000 measurement data in a second.

(2) Scanning resolution

The scanning resolution* of the laser scanner is 0.25 μm , that is, it can detect a displacement variation along the Y-axis of the sample surface as small as 0.25 μm . This is illustrated in Figure 3-11. The laser scanner returns the same measurement

data for those points on the sample surface that are below the line indicating $0.25 \mu\text{m}$. [* 0.005 % FSO (Full Scale Output)]

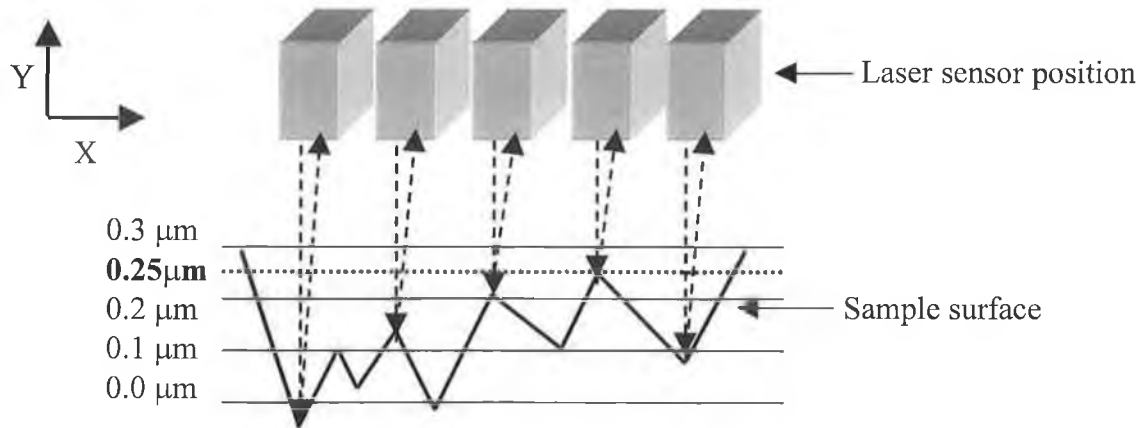


Figure 3-11: Scanning resolution

(3) Non-linearity

The non-linearity* of the laser scanner is $\pm 1.5 \mu\text{m}$ what indicates the high accuracy in surface profile measurement. [* 0.03 % FSO (Full Scale Output)]

(4) Non-contact nature of measurement

The laser scanner takes measurement in a non-contact way. So, it is possible to inspect the surface defect of a sample without being touched and keeping it in a reasonable distance from the sensor head.

(5) Stand-off (reference) distance

In this measurement system the samples must be placed with a distance about 58 mm ($\pm 2.5 \text{ mm}$) from the sensor head plane. Thus it facilitates to take the measurement of those samples that produce considerably heat and vapour in the production line.

(6) Laser beam spot diameter

At the start of the measuring range the smallest laser beam spot size is $50 \mu\text{m}$ and it becomes $130 \mu\text{m}$ at the end of the measuring range (see Figure 3-12). The laser scanner displays the measurement data after calculating the average data of all points available on the sample surface that is equal to the area of its laser beam spot. As a result the smallest the area of laser beam spot is, the smallest area of sample surface

will be scanned and it leads the measurement as accurate as possible. Thus even a tiny defect on the sample surface can easily be detected with this measurement system.

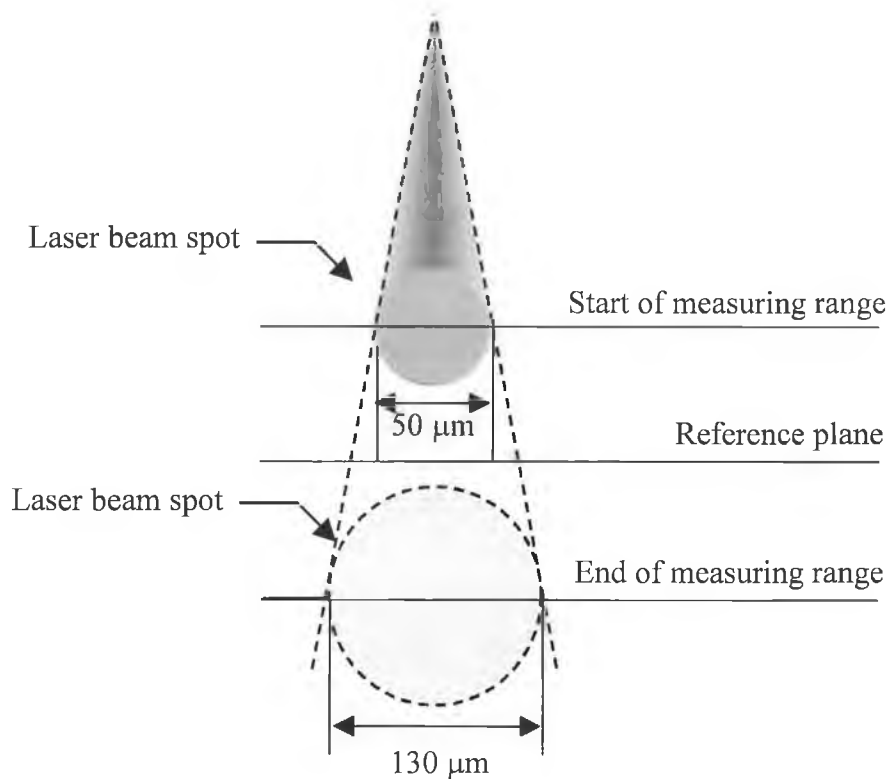


Figure 3-12: Dimension of laser beam spot

3.5.2 Demerits of the system

Although the system delivers very high speed laser scanning, high resolution, and better non-linearity, but it also has some demerits that can not be neglected where high precision measurement is the main goal.

(1) Measuring range of the laser scanner

The laser scanner can only measure the vertical displacement of sample up to ± 2.5 mm from its reference plane what may not be sufficient for some particular applications. This is explained in Figure 3-13. The laser scanner can detect any point on the sample surface that is within ± 2.5 mm from the reference plane and can measure the distance of this point from the reference plane. Any point on the sample surface that is above the line AA' or below the line BB' will be considered as out of

the measuring range of the laser scanner and in such a situation the point cannot be identified.

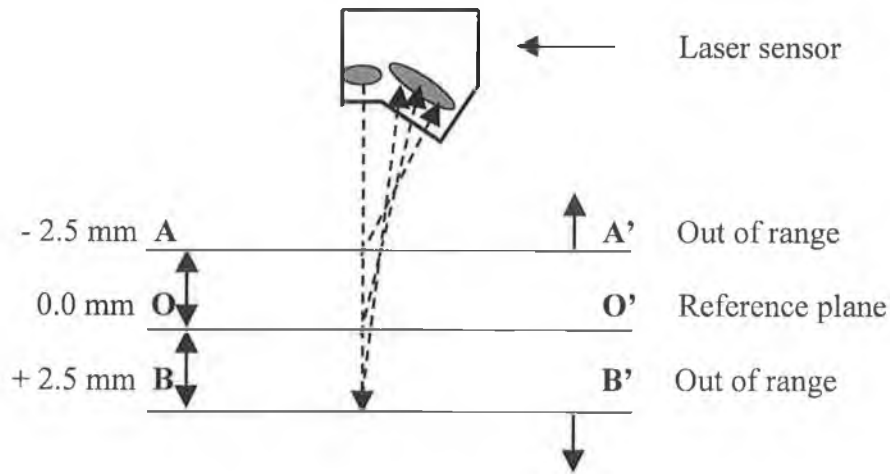


Figure 3-13: Measuring range of the laser scanner

(2) Kinetic vibration and noise

When the sample to be scanned is travelled by the plotter then it produces considerable amount of kinetic vibration and noise what is very normal to a plotter. But the measurement data captured fluctuates within a specific range what is not desirable for such a precise application.

(3) Sample inclination

Due to the poor design and fixture of holding the sample to be scanned, the plotter also produces some sort of inclination while it carries the sample. As a result slopes are found when the data from the experiments are transferred to a spreadsheet program and graphs are drawn using those data.

3.5.3 Displacement measurement error producing factors

The following factors are related with the laser sensor that can affect the displacement measurement and thus can produce significant errors. These are taken from the manufacturer's reference documents [36].

(1) Differences in colour

Differences in colour of samples affect the measuring result of the laser sensor only slightly due to the intensity adjustment. However, these differences in colour are

often combined with different penetration depths of the laser light. Different penetration depths also cause apparent changes in the size of the measuring point. Therefore, changes in colour in combination with changes in penetration depth can result into measuring errors. This phenomenon also affects the linearity behaviour of the sensor if it has been adapted to white diffusely reflecting reference material. If, on the other hand, the sensor is optimised for black material, a much better linearity behaviour is achieved.

(2) Temperature fluctuation

The internal housing temperature of the laser sensor is measured by an integral temperature sensor. So the measured displacement values are temperature-compensated. A warm-up time of at least 20 minutes is necessary before taking data in order to achieve a uniform temperature distribution in the sensor. If the measurements are to be made in the micrometer accuracy range, the effect of the temperature fluctuations on the sensor holder must be considered. Fast temperature changes are damped by the sensor's heat capacity.

(3) Mechanical vibration

If the laser sensor has to achieve resolutions in the micrometer to sub-micrometer range, particular attention must be paid to a stable or vibration-damped sensor and sample installation.

(4) Surface roughness

Surface roughness of 5 micrometer and above creates an apparent change in distance if the surface is scanned (also called surface noise). These can be suppressed by averaging.

(5) Ambient light influences

Due to the narrow band optical filter used, measurement can be made reliably even when a diffusely reflecting sample is exposed to direct sunlight (maximum 30,000 lux).

(6) Angle influences

Angles of tilt of the sample around both the X-axis and the Y-axis of less than 5° only cause errors with surfaces giving strong direct reflection. Table 3-3 gives an idea regarding error of angle influence. An angle of tilt of 15° causes an apparent change in distance of approximately 0.1% of the measuring range and an angle of tilt of 30° causes an apparent change in distance of approximately 0.5% of the measuring range. These influences must be noted particularly when scanning structured surfaces. In principle the angle behaviour is also subject to the reflectivity of the sample surface.

Table 3-3: Error of angle influences [36]

Angle (°)	X - axis	Y - axis
5	0.04%	0.03%
15	0.12%	0.1%
30	0.5%	0.5%

3.6 Further development of the system

Though the existing system is good enough to measure the surface profile of a sample, but there is more scope to develop this existing system to a further extent. Following is a discussion on further development of this system in the range of experimental development, hardware development, and software development.

3.6.1 Experimental development

In order to achieve this goal, it is needed to repeat the experiments by increasing S (sampling cycle of laser sensor) and N (the total number of scan data points). Thus the value of S_r (scan resolution) will decrease and it will be possible to reach even to sub-micron range. Another way to improve the system is to find out a better solution to increase the value of S_p (sample travel speed). So the value of t (total time elapsed for a set of scan) will decrease and the system will be faster.

3.6.2 Hardware development

The X-Y plotter is basically designed to plot a drawing on a paper. But it is used as a tool for sample holding and movement in current system. So, there exists some sort

of kinetic vibration and noise in the system while the sample is being carried and moved by the pen-carriage of the plotter. In order to eliminate this error and improve the system performance, one solution would be to make an accurate fixture on the pen-carriage of the plotter so that it can carry the sample and move it in every direction smoothly without having any vibration, noise or inclination.

Another solution to the problem would be to use a linear guide instead of an X-Y plotter to move the sample to scan. A stepper motor can be used in conjunction with the linear guide to automate the process. Thus vibration and noise can be eliminated and no inclination will be produced. Furthermore a high speed in sample movement can also be achieved.

3.6.3 Software development

There comes a software program with the existing system in order to operate the laser scanner, take the measurement, and view the results. But it is also possible to develop a stand-alone software what can work with the system independently and more sophisticatedly. The new user-friendly software can provide more features than the existing one and can work in a better way, such as, controlling sample movement, scanning properties, analysing measurement data, etc.

Chapter 4

Experiment Set-up for Thickness Measurement

This chapter describes the laser scanning system for thickness measurement that was designed, developed and analysed in present work. It contains system organisation, description, principle of measurement, experiment set-up, procedures and calibration of the system.

4.1 Laser scanning system components

A laser displacement sensor set, see Figure C-1 through Figure C-3 in Appendix C, comprised of two sensor heads (Keyence LK-031), two controllers (Keyence LK-2001), an analogue sensor output display unit (Keyence RD-50RW), and two power supply units (Keyence KV-U6W). The sensor heads emitted the laser beam, took the measurement, and then sent the signals back to the controllers, which in turn sent the signals to the analogue sensor output display unit. The controllers also supplied power to the sensor heads, automatically adjusted different measurement parameter ranges (such as, brightness, sensitivity, stability etc.), and displayed the status in or out of range for these parameters with individual LED lights.

The LK series laser displacement sensor of Keyence Corporation features a newly developed CCD and 32-bit processor for precise measurement of height, width, and position. Some of the key features are discussed below [42].

Highly accurate measurement – Utilising CCD as the light-receiving element and an ultra-high speed RISC processor for signal processing, the LK series provides highly accurate measurement regardless of sample surface properties. It delivers a resolution of 1 μm and linearity of $\pm 0.1\%$ of FS (Full Scale).

Stable measurement of various sample surfaces – The LK series includes an LFTC (Laser Flash Time Control) circuit that can automatically control the laser

emission time based on the sample surface condition. This function enables stable measurement of glossy metal samples and multicoloured or patterned samples. Samples of low reflectivity, such as black rubber, can also be measured without any additional adjustment.

Visible laser beam spot of 30 µm diameter – Keyence's unique optical system minimises lens aberration to give the LK-031 a minimum spot diameter of 30 µm. This enables the surface contour of a sample to be accurately measured.

Auto Gain function – With a glossy sample, the receiving light quantity is large but with a low-reflective sample the receiving light quantity is small. The AUTO GAIN function automatically adjusts the amplification factor of the light-receiving signal according to the receiving light quantity. This function enables stable measurement regardless of the light-receiving characteristics of the sample.

Response speed selection function – This function switches the measurement averaging time between 0.5 ms and 4 ms. When the LK series measures a sample with a wide range of reflectivity or with a large colour difference then this function enables the LK series to ignore sporadic changes in measurement data to ensure stable measurement.

Analogue output hold function in alarm condition – When the alarm output is activated due to a large vibration of the sample for an instant during measurement, the LK series holds the analogue output (measured value) immediately before the alarm output is activated. When the alarm output is reset, the LK series continues the output measurement from the previous voltage level.

4.2 Measuring principle of the laser sensor, Keyence LK-031

The laser sensor, Keyence LK-031, is placed perpendicular to the sample plane. The distance between the laser sensor and the sample is first set at a stand off distance of 30 mm. This is called *reference distance* or *stand-off distance* of the laser sensor. This distance offers the maximum measurement range for the sensor.

The measuring range of this laser sensor is ± 5 mm. This means it can measure a total of 10 mm (maximum) vertical displacement of the sample. Thus the laser sensor is capable of detecting the sample if it is placed between 25 mm and 35 mm from the sensor plane. Anything beyond this limit is its *out of range*. Figure 4-1 demonstrates this measuring principle. The figure shows the displacement corresponding to voltage reading for sensor A.

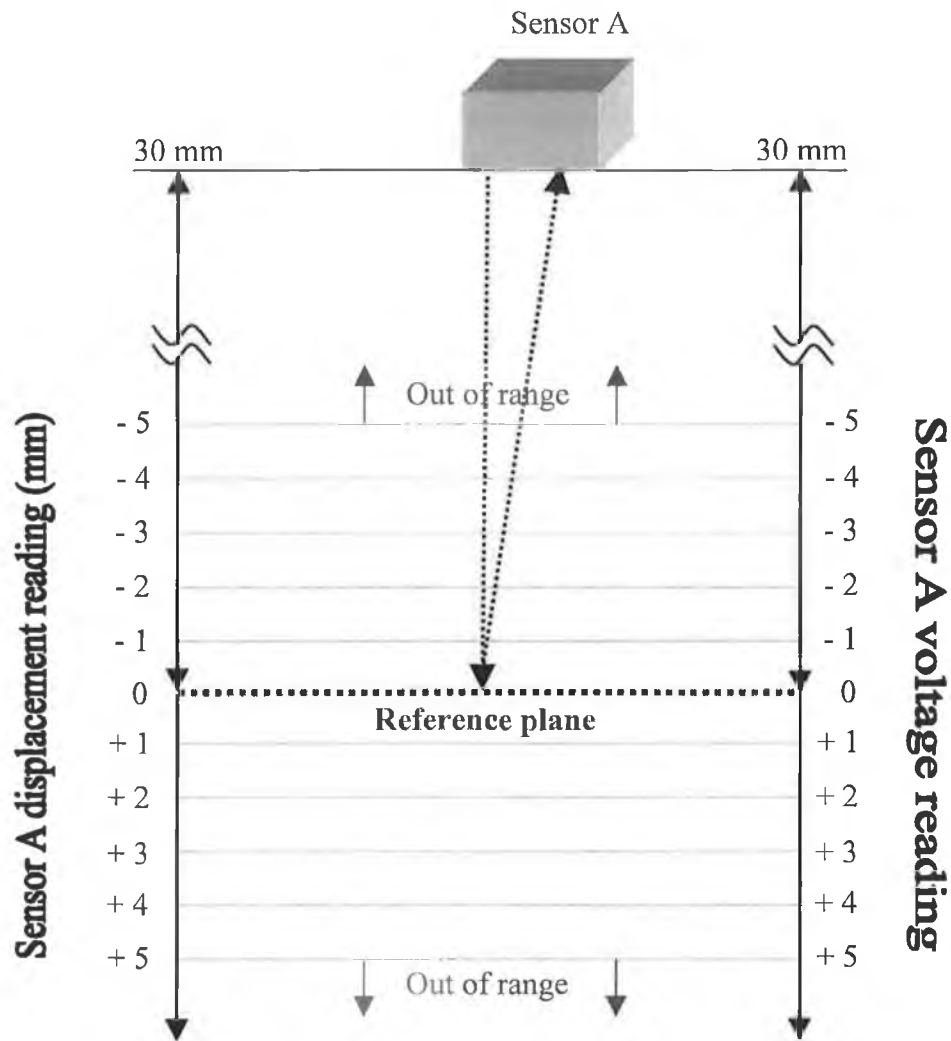


Figure 4-1: Measuring principle of the laser sensor

4.3 Laser scanning system calibration

When the thickness measurement principle was initially set-up, the sample could only be held stationary between the sensor heads as shown in Figure 4-2. This initial

set-up enabled the sensor heads to be calibrated and the capabilities of the system to be analysed.

As part of the calibration objective for the scanning system, the accuracy of the system was also to be determined. The individual components were examined first. Then both of the laser sensors were tested and calibrated separately. During this experiment, the sample was fixed at its position but the sensor head was moved up and down with the micrometer stage. The following points outline the step-by-step procedure that was carried out in order to calibrate and test a single laser sensor.

(1) All the components of the system were set up as it is shown in Figure 4-2 and the sample was placed over the holding pins.

(2) The power to the controllers and the analogue sensor output display unit was switched on.

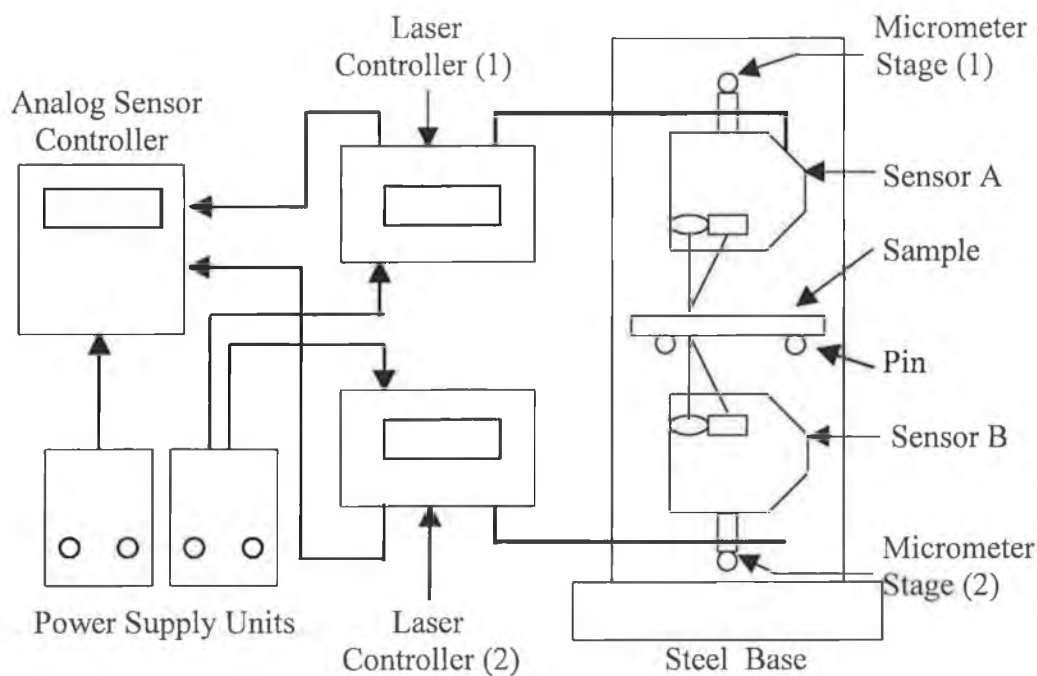


Figure 4-2: Initial system set-up without sample translation

(3) The key-operated laser switches of the controllers were positioned to ON. The LASER ON indicators on the sensor heads lighted up. This meant power had gone

through the sensor heads. The sensor heads were then continuously emitting the laser beam and taking the measurements.

(4) At this stage the apparatus was left for 30 minutes to allow the sensor units achieve a uniform temperature distribution. (For more general information on the environmental conditions under which the laser system should be used, see Appendix C.)

(5) The sample and the sensor head were positioned such that the output voltage of the sensor head was zero volt on the RD-50RW display unit.

(6) The reading was noted from the micrometer stage. The voltage output of the sensor head is directly related to the displacement ($1 \text{ V} = 1 \text{ mm}$) for this system.

(7) Using the micrometer stage, the distance between the sensor head and the sample was then incremented by 0.5 mm at a time and the output voltage noted.

(8) Step (6) was repeated until half the displacement range of the sensor head had been traversed (5 mm). At this point the measurement went out of range for the sensor head. This was indicated on a sensor head LED and on the display output as "FFFF".

Having traversed a known displacement and obtained the corresponding sensor head displacement output, an indication of the error in the system was obtained. Data found from the above experiment was tabulated and the calibration graph was drawn. Calibration results and discussion will be presented in the next chapter.

4.4 Principle of thickness measurement

In order to achieve accurate thickness measurement, it is necessary to examine co-axial position of the laser beam spots emitting from sensor A and sensor B and identical position of the reference planes of those two sensors. The following steps can be taken to check whether the laser beam spots are co-axial to each other.

- Position sensor A and sensor B opposite to each other and adjust the distance between them to the desired one (approximately 60 mm)
- Hold a piece of clean, thin, white paper crosswise between the two sensors at their reference plane
- Power on sensor A. Look at the position of the laser beam spot and then power on sensor B
- Observe whether the position of two laser beam spots are co-axial

For accurate measurement the beam spots should be co-axial to each other. So after following the above procedure, if the two laser beam spots are found not co-axial, the lateral displacement for either sensor needs to be adjusted until the beams are in line with one another.

During the measurement process it is also necessary to keep the reference distance of both sensors at 30 mm. This means the distance between sensor A and sensor B should be 60 mm. For some particular applications if it is not possible to maintain this distance, then the exact distance between the two sensors must be determined.

Failure to providing these two conditions will produce errors in thickness measurement. This will be explained more in details in the next chapter while characterising system errors.

The principle of thickness measurement is illustrated in Figure 4-3. When the system is run to take the measurement, sensor A returns the distance from its reference plane to the top of the sample surface and sensor B returns the distance from its reference plane to the bottom of the sample surface. These two distances are defined as A and B respectively throughout the rest of this chapter. The thickness of the sample, T_h , is determined by the following equation (assuming the reference planes for sensor A and sensor B are in the same position):

$$T_h = | A + B | \quad [4.1]$$

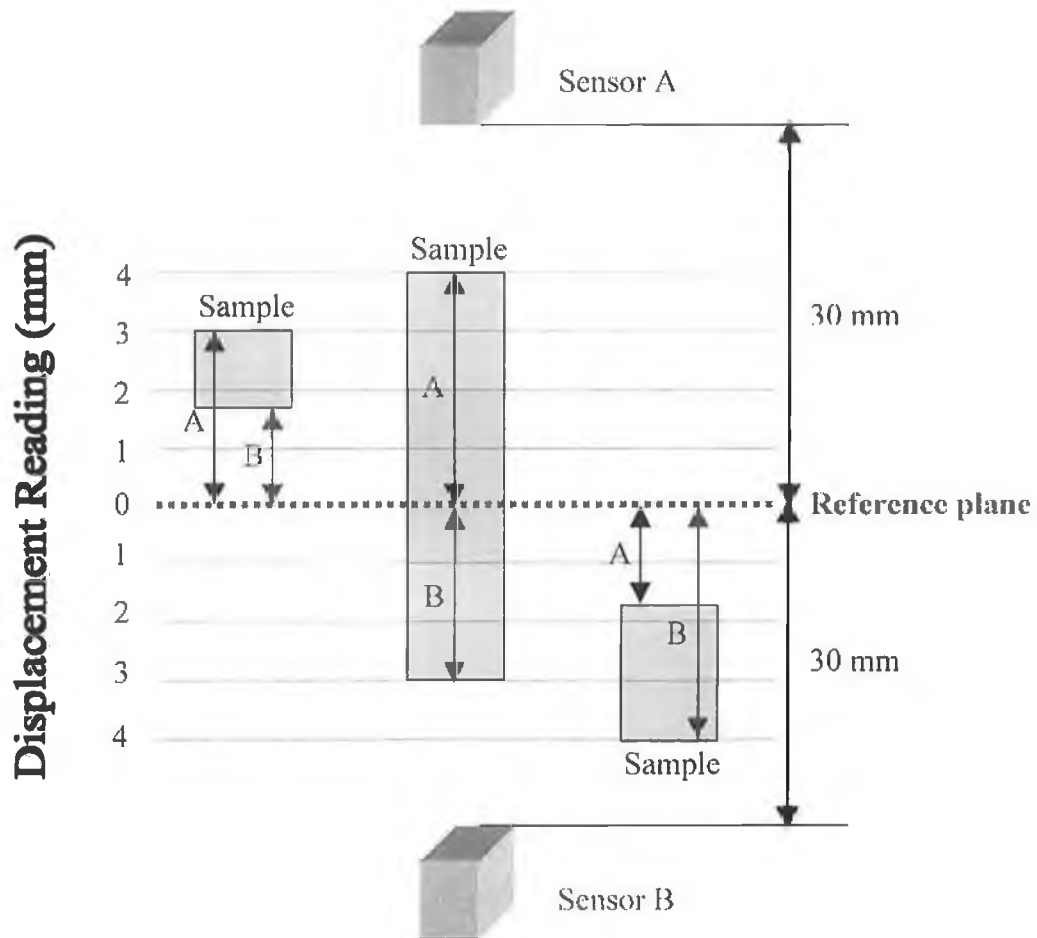


Figure 4-3: Principle of thickness measurement

Figure 4-3 shows the three different possible positions of the sample to be scanned and the relevant distances of A and B. Figure 4-4 along with Table 4-1 presents various examples of thickness measurement. All together nine samples of different thickness are considered in Figure 4-4. A1 through A9 and B1 through B9 are the values for the distance of sensor A and sensor B respectively from the reference plane. Again, it is assumed that the reference planes for sensor A and sensor B are in the same position.

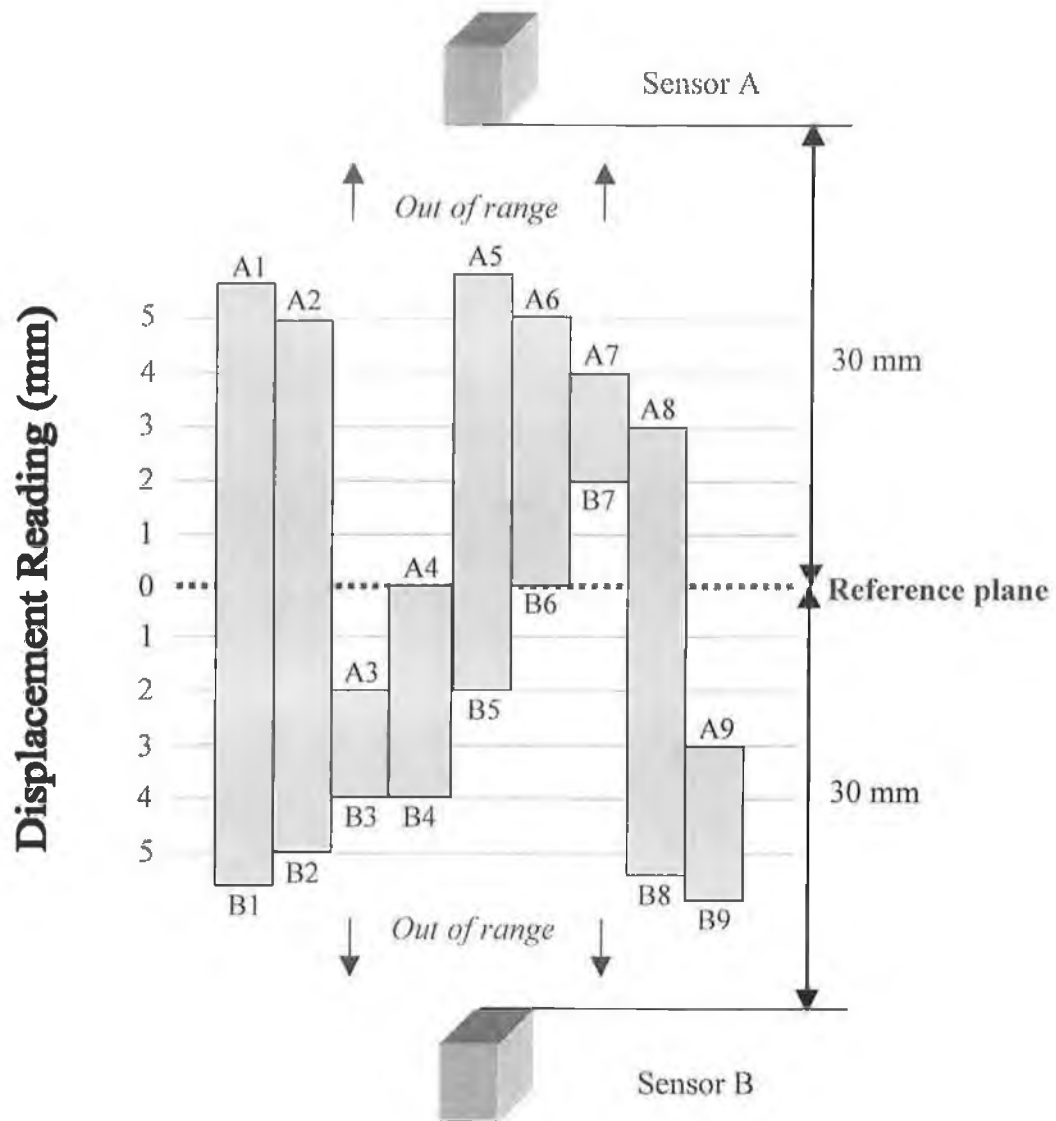


Figure 4-4: Examples of thickness measurement

Table 4-1: Calculation of thickness measurement

Sample No	Reading of Sensor A	Reading of Sensor B	Value of A	Value of B	Thickness A+B
1	A1	B1	∞	∞	∞
2	A2	B2	-5	-5	10
3	A3	B3	+2	-4	2
4	A4	B4	0	-4	4
5	A5	B5	∞	-2	∞
6	A6	B6	-5	0	5
7	A7	B7	-4	+2	2
8	A8	B8	-3	∞	∞
9	A9	B9	+3	∞	∞

Note: ' ∞ ' is marked where measurement is not possible because the sample is out of the measuring range.

4.5 Thickness measurement of moving samples

Before going to manufacture the final rig for the thickness measurement of moving samples, several options were considered. The set-up shown in Figure 4-7 was finally chosen. This includes a lead screw table, which was used to hold the sample to be measured for moving between the two sensors. The apertures are photographed in Figure 4-8. See Appendix E for the engineering drawings of the assembly components.

4.5.1 Procedures for thickness measurement of moving samples

All of the system components, as shown in Figure 4-8, were powered on and the keys for both laser controllers were turned on. Applying the procedures stated in the earlier section the co-axial condition of the laser beam spots was examined. The location of reference planes for both sensors was determined too by measuring the distance between the top surface of lead screw table and the individual sensor.

Hyper Terminal program was executed for establishing communication between the sensors and the PC. The desired input mode and display format in the analogue output display unit were set. The LabVIEW program was also run and the pre-built VI for thickness measurement system was opened.

The sample to be measured was clamped on the surface of the lead screw table. Using the MINI-LAB 603B, the desired frequency for sample movement speed was selected. The switches on the motor control unit was turned on to run the stepper motor and the lead screw table as well.

At this stage the sample was being scanned by the both sensors as it was travelling between them. Scanning data was being displayed simultaneously on Keyence RD-50RW panel, on the Hyper Terminal user interface and also on the control panel of the VI built in LabVIEW. Scanning signal, in a range of analogue voltage or current, was also obtainable on Keyence LK-2001 ports 14 and 15 respectively.

Both of the software programs had the options to capture scanning data and save them into a file. This file could be opened later in any spreadsheet program for

further analysis and demonstration of the thickness measurement of the sample scanned.

4.6 Kinetic system

Kinetic sub-system was used to facilitate the movement of sample for scanning. This mainly comprised of a lead screw table, a stepper motor, MediStep euro 01/3005, a motor control unit and a power station, BWD Instruments MINI-LAB 603B, for supplying power and generating frequency.

4.6.1 Lead screw table

The lead screw table, see Figure 4-9, was used to hold the sample. A small window (100mm X 30mm) was cut in the slide of the table to let laser beam from the bottom sensor head hit the sample. An aluminium sample wedge can be seen, in the figure, on the top of this window. Samples were clamped tightly in order to reduce mechanical vibration. The bottom of four supporting posts of the lead screw assembly was also covered with rubber pads to avoid system vibration.

4.6.2 Stepper motor

A stepper motor, MediStep (model reference: euro 01/3005), was used in the system to drive the lead screw table. It had the following features:

- Power supply from 15 to 50 V maximum
- Run by micro steps
- Step frequencies to 50 kHz
- Dissolution of step full -, half -, quarter -, eighth step-by-step operation
- Automatic current sinking with deadlock
- LED displays for supply and phases
- Protection and disconnection with temperature rise, over current in the engine
- Inputs clock, direction, Boost, RESET and ding activate

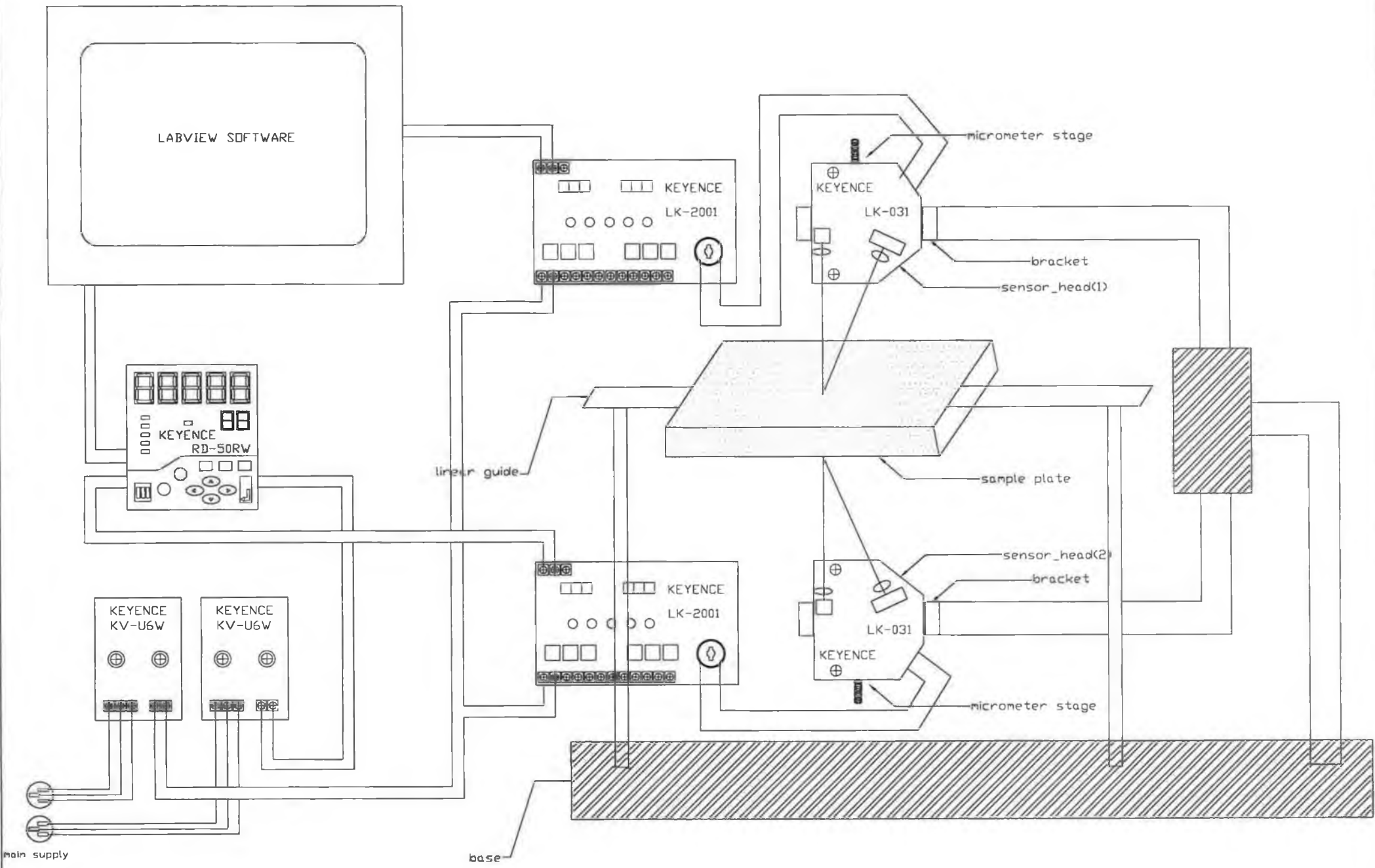


Figure 4-5: Schematic of system set-up for thickness measurement of moving samples

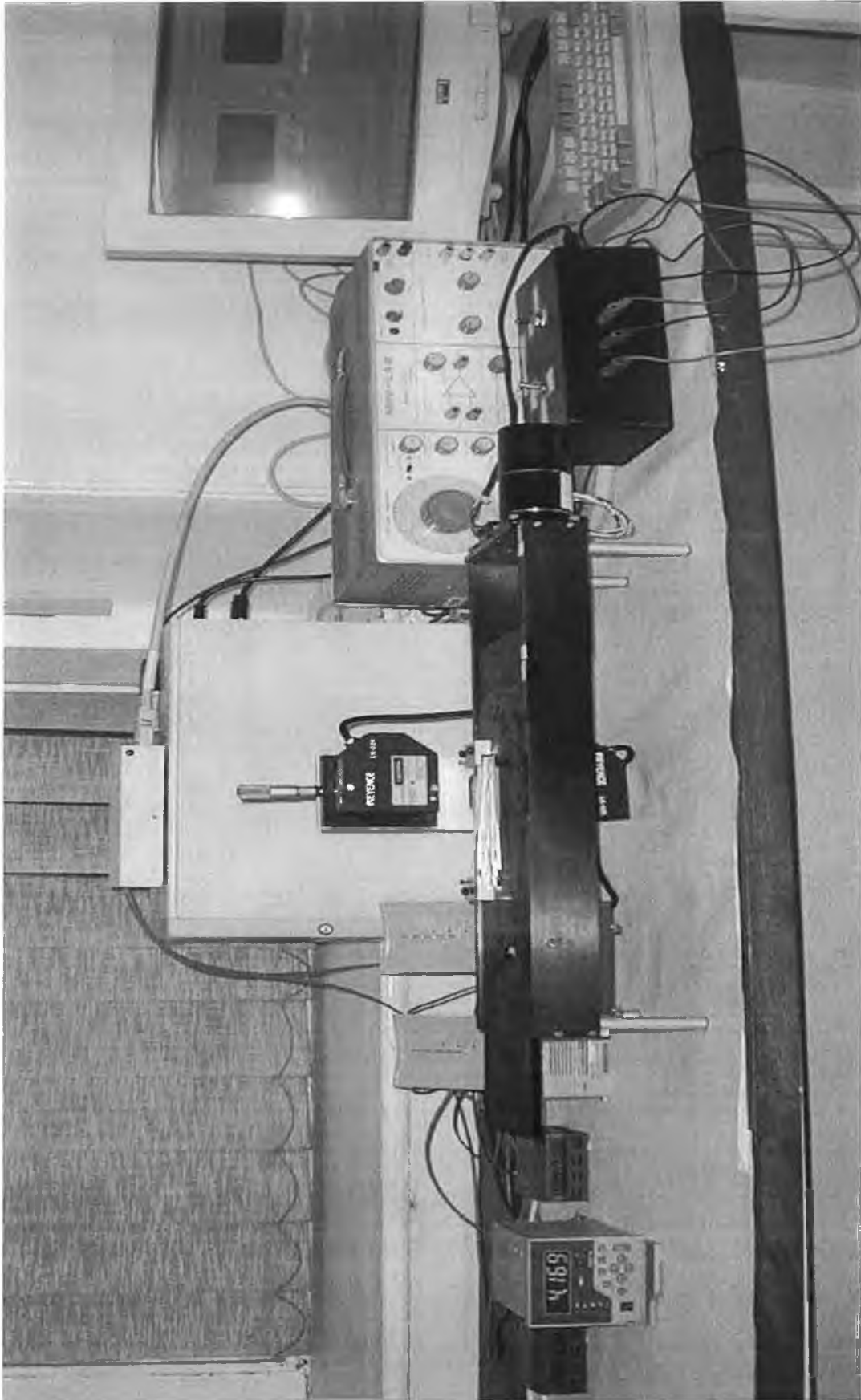


Figure 4-6: Photograph of system set-up for thickness measurement of moving samples

4.6.3 Motor control unit

The motor control unit included a motor driver card, an on/off switch and a direction switch. The motor driver card performed the overall control of the stepper motor. The on/off switch let the motor run/stop and the direction switch changed the direction of the motor movement.

4.6.4 Motor power and frequency supply

A power supply station, MINI-LAB Model 603B manufactured by BWD Electronics Pty. Ltd, was used to supply the necessary DC voltage and to generate adequate frequency for the motor driver card in order to drive the stepper motor. A picture of this is shown in Figure C-4 of Appendix C.



Figure 4-9: Lead screw assembly and clamped sample

4.7 Data acquisition and analysis (DAQ) system

4.7.1 Break-out box

The break-out box, National Instruments SCB-68, was a 68-pin shielded connector block, see Figure C-6 in Appendix C. The shielded board with 68 screw terminals was used for easy connection to National Instrument 68-pin products. In the thickness measurement system the analogue signals coming from the sensor controllers were fed to this break-out box in order to pass the signals to the computer through the data acquisition card for further use in the LabVIEW environment.

4.7.2 Data acquisition card

The data acquisition card, National Instruments AT-MIO-16E, was used to receive analogue signals from the sensor controller (LK2001) through the break-out box and then to convert these signals into digital form so that LabVIEW software could be easily used to access the data, see Figure C-5 in Appendix C. The LabVIEW software was then be used to convert this into the displacement reading and graph it.

4.7.3 Communication software

The first communication software that was used was Hyper Terminal. This was developed by Hilgraeve Inc. for Microsoft and was used to establish a communication with the sensor, Keyence RD-50RW, through RS-232C communication parameters via the serial port. Once the RS-232C communication parameters of Keyence RD-50RW were set the same as that of the Hyper Terminal program, communication was established. The user interface of this program provided some menu driven options to display, capture and save the scanning data coming from the controllers, Keyence LK-2001. It could also transfer any keyboard-driven command to the Keyence RD-50RW, such as changing input mode or output display pattern, etc. Figure 4-10 is a snap shot of this software. It shows that a dialogue box was popped up while the communication was being run between the scanning system and the computer.

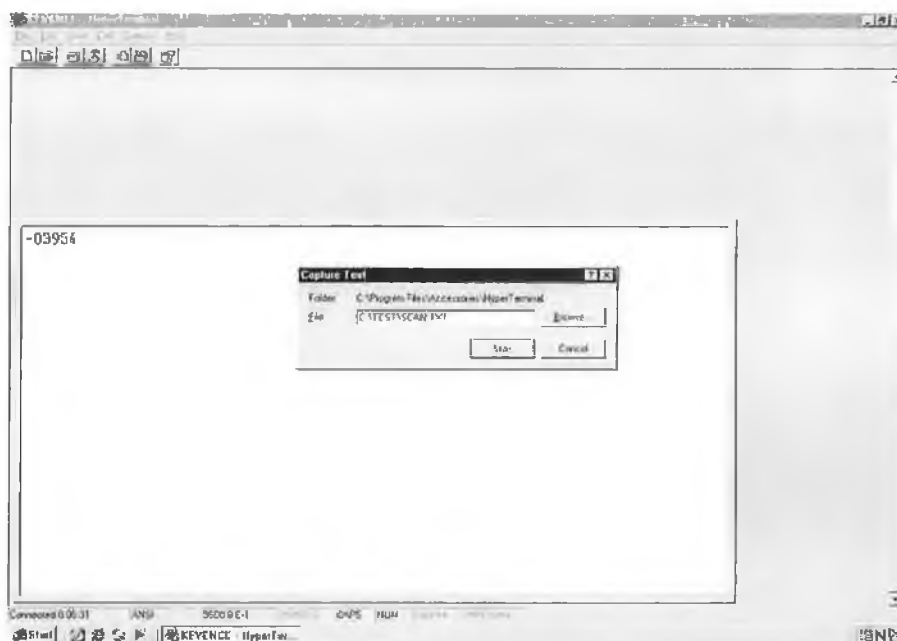


Figure 4-10: Interaction in Hyper Terminal program

4.7.4 Data analysing software

The data analysing software, LabVIEW 6i, developed by National Instrument Inc. [44], is a powerful graphical programming language that has been widely adopted throughout industry, academia and government labs as the standard for data acquisition, instrument control software, and analysis software. LabVIEW (short for *Laboratory Virtual Instrument Engineering Workbench*) is ideal for science and engineering applications. LabVIEW programs are called Virtual Instruments, or VI's for short. LabVIEW is different from text-based programming languages (such as Pascal or C) in that LabVIEW uses a graphical programming language, known as G programming language, to create programs relying on graphic symbols to describe programming actions. It uses a terminology familiar to scientists and engineers, and the graphical icons used to construct the G programs are easily identified by visual inspection [45].

In the thickness measurement system, LabVIEW was used to log and display data. A virtual Instrument or VI was created for the thickness measurement application. When this VI was run, then it was able to capture the scanning signals coming from the sensors through data acquisition card, manipulate them and lastly display them both numerically and graphically. It had some other features too, such as, controlling data flow speed (delay in transferring data), saving data to storage devices, etc. Figure 4-11 and Figure 4-12 are the snap shots of the front panel (user interface) and the diagram (program codes) of the VI that was created in LabVIEW for the thickness measurement application respectively. Below is the description of the elements used in the diagram to build the VI.

The upper and lower corners of the most left part of the diagram are the data acquisition part of the VI. The two corners are identical where the upper one is for Sensor A and the lower one is for Sensor B. An one-channel system pre-built sub-VI is used in each corner to capture the scanning signals from the sensor. The amplitude of the incoming signals is given a range of 10.00 V (as high limit), and -10.00 V (as low limit).

The left middle part is used for thickness measurement. The two scanning signals are added together first and then the added value is again subtracted from 10.00 (the

distance between the reference planes of the two sensors as set-up) to get the thickness of the sample to be measured.

The right middle part is created to accommodate data display functions. The scanning signals of each sensor are passed separately from the left to this part and subtracted from 30.00 (the reference distance of the sensor) to show the numerical display of the distance between that sensor and the surface of the sample. These can be seen on top and bottom of this part. Again the scanning signals of two sensors are bundled together to be displayed in one graph dynamically as they are acquired by the data acquisition system. The measured thickness is also displayed in another graph.

The elements in the upper right corner are for controlling the data flow between the data acquisition system and the user interface in the form of time delay. A variable is used to perform this task, namely DFS (Data Flow Speed). It takes the user input in the range of 0, 0.1, 0.2,...,0.9. This value is then multiplied by 1000 to get the desired time in millisecond (ms) and this amount of time is the delay to pass between two incoming signals. As a result the data in the two graphs mentioned earlier can be seen moving slower or faster according to the value of DFS. The purpose to use this control is to help the user tracking the signals more conveniently and efficiently.

The elements in the lower right corner are used for data storage utilities. These facilitate the output values (measured thickness, scanning signals from Sensor A, and Sensor B) to save into a storage system. A system pre-built sub-VI is used here to create a file. The output values are accumulated together in an array first and then they are written in a spreadsheet file. The location of the file will be entered by the user. There is an option to append data in an existing file or save those into a new file.

The whole program is placed in a loop where the loop will be repeated until the desired condition is fulfilled, hence when the STOP button in the front panel is pressed.

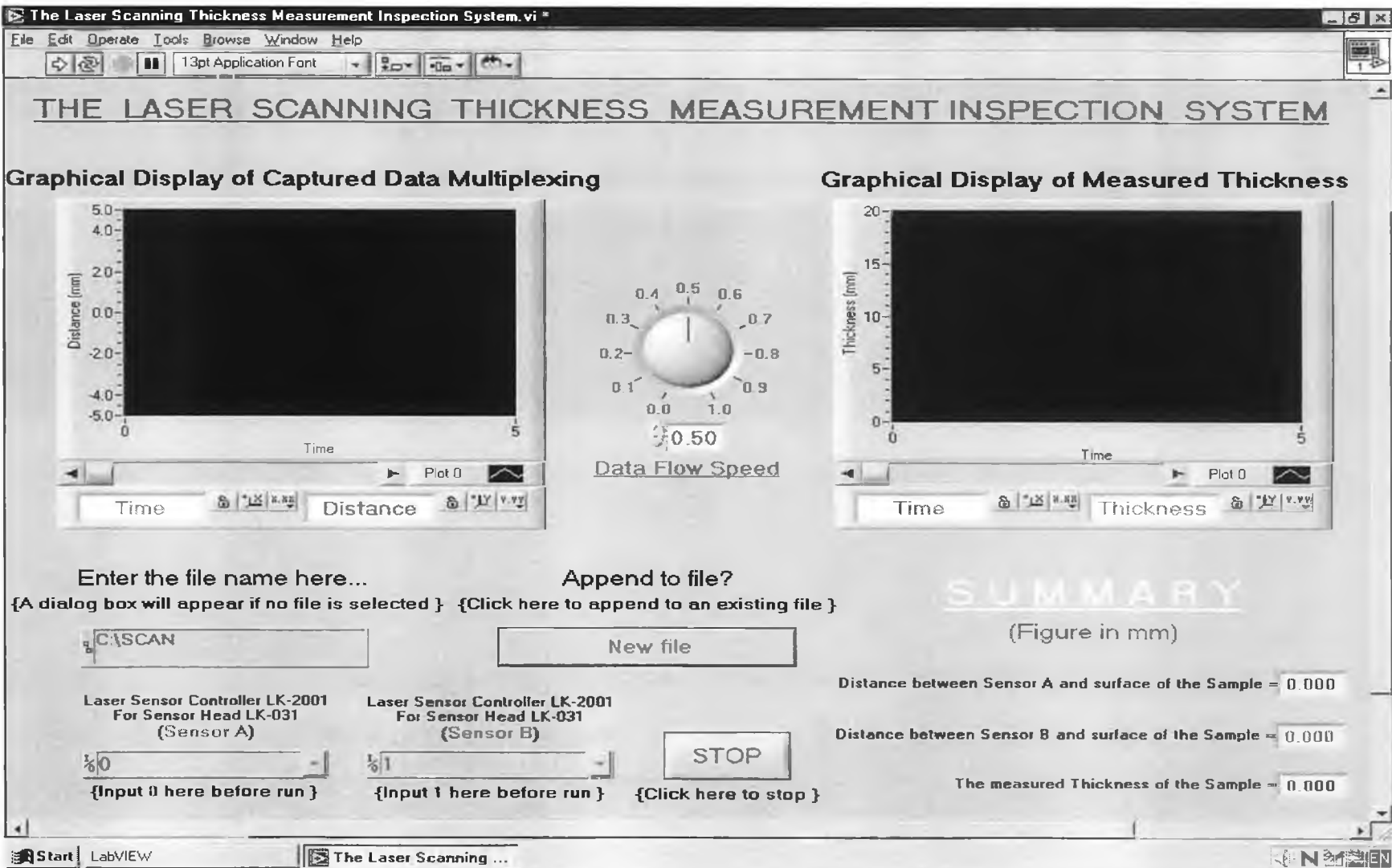


Figure 4-9: Control panel (user interface) of the VI created in LabVIEW

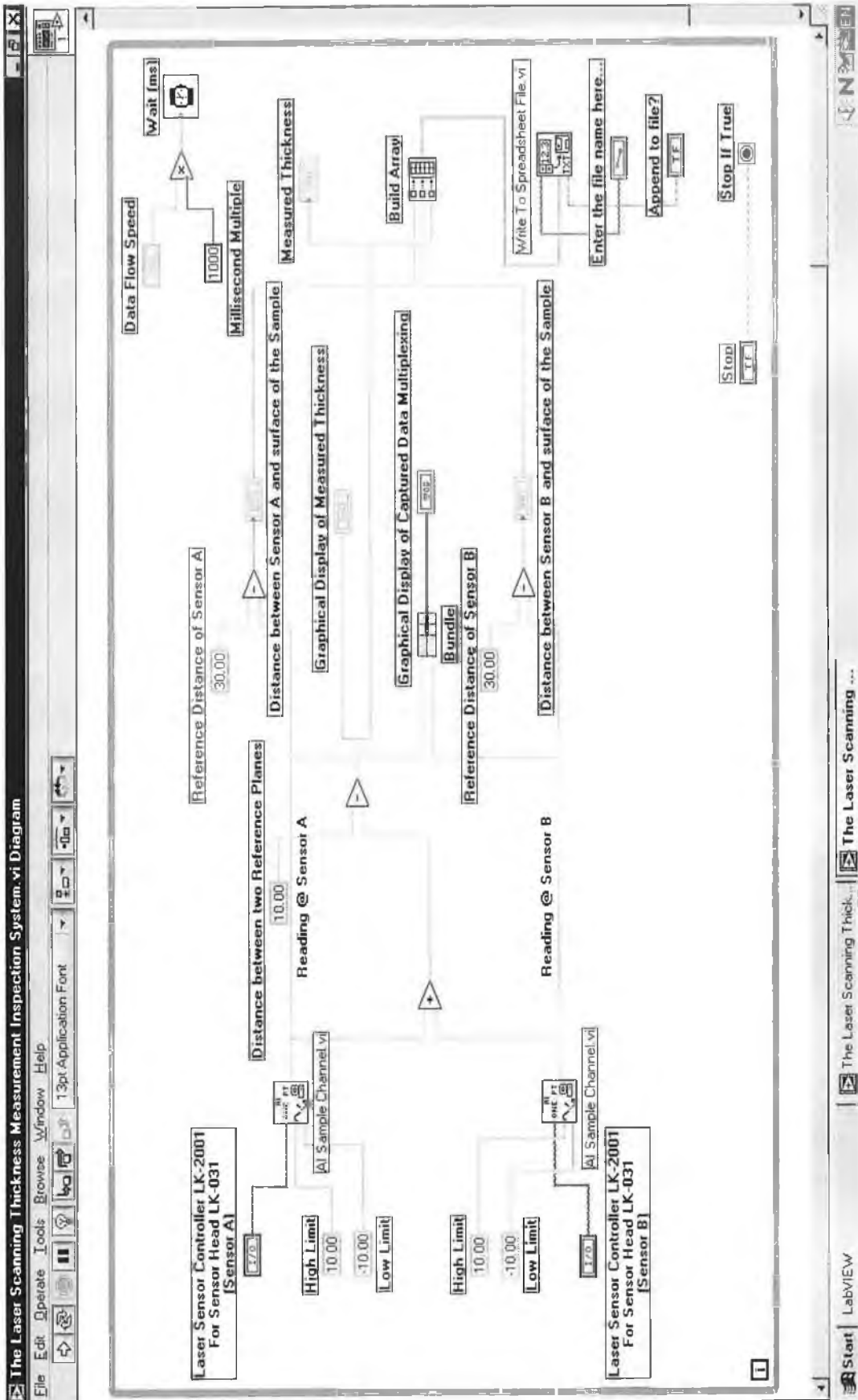


Figure 4-10: Block diagram (program code) of the VI created in LabVIEW

Chapter 5

Thickness Measurement System Results

This chapter contains all the results of the experiments carried out using the thickness measurement system. It also discusses the results with the scope of errors. Finally system accuracy and error analysis are calculated in the chapter too.

5.1 System parameters

System parameters are those variables found in the system upon which the system performance is reliable. A list of all system parameters of the thickness measurement system is given with their definitions as follows:

S_p	=	sample travel speed (mm/s)
f_m	=	the frequency of motor (Hz)
P	=	the path travelled by sample (mm)
t	=	the total time elapsed for a set of scan (s)
N	=	the total number of scan data points, i.e. the total number of data to be acquired during a set of scan
L_S	=	length of the sample (mm)
S_r	=	scan resolution, i.e. the horizontal distance between two consecutive scan points on the sample surface (mm)
DFS	=	data flow speed
DAR	=	data acquisition rate (Hz)

The length of the sample (**L_S**) can be calculated from the following equation,

$$L_S = S_r \times N \quad [5.1]$$

The scan resolution (**S_r**) can be determined by the following equation (the values for **S_p** and **DAR** can be found in Table 5-2, Table 5-3, and Table 5-4),

$$S_r = S_p / \text{DAR}$$

[5.2]

These two equations are used later in this chapter to analyse the resolution of the scanning system in performing horizontal measurements.

5.2 Calibration results and discussion

In Table 5-1, the experimental voltage value displayed on the analogue output display unit, Keyence RD-50RW, is referred to as the measured voltage. A linear relationship over the measuring range of the system exists of 1V to 1 mm, as per the manufacturer's specification. The theoretical voltage can also be calculated and is shown in Table 5-1 along with measured results against displacement increments.

Table 5-1: Calibration data

Displacement Increment (mm)	Measured Voltage (V)	Theoretical Voltage (V)
0	-0.011	-0.011
0.5	0.471	0.489
0.5	0.956	0.989
0.5	1.441	1.489
0.5	1.923	1.989
0.5	2.404	2.489
0.5	2.892	2.989
0.5	3.382	3.489
0.5	3.871	3.989
0.5	4.352	4.489
0.5	4.836	4.989
0.45	5.275	5.439
0.005	5.279	5.444
0.005	FFFF	

From Table 5-1 it can be seen that over each millimetre distance there is a difference (error) of 0.033 mm between the measured and the theoretical voltages. Thus a total

error of 0.153 mm results over a distance measurement of 5 mm (a measurement error of 3.06%). The calibration graph, see Figure 5-1, is obtained by plotting the last two columns of data of Table 5-1 against the overall displacement.

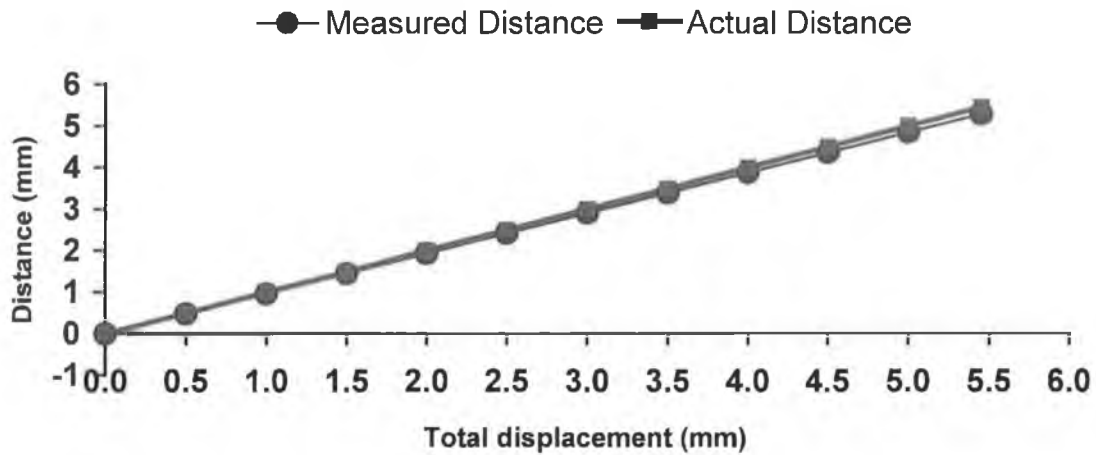


Figure 5-1: Calibration graph

5.3 System performances

5.3.1 Laser scanning system

The following experiment was carried out to determine the stability of laser scanning signal over time. During this experiment the sample was held stationary and the height signal was acquired from the same point on the sample surface.

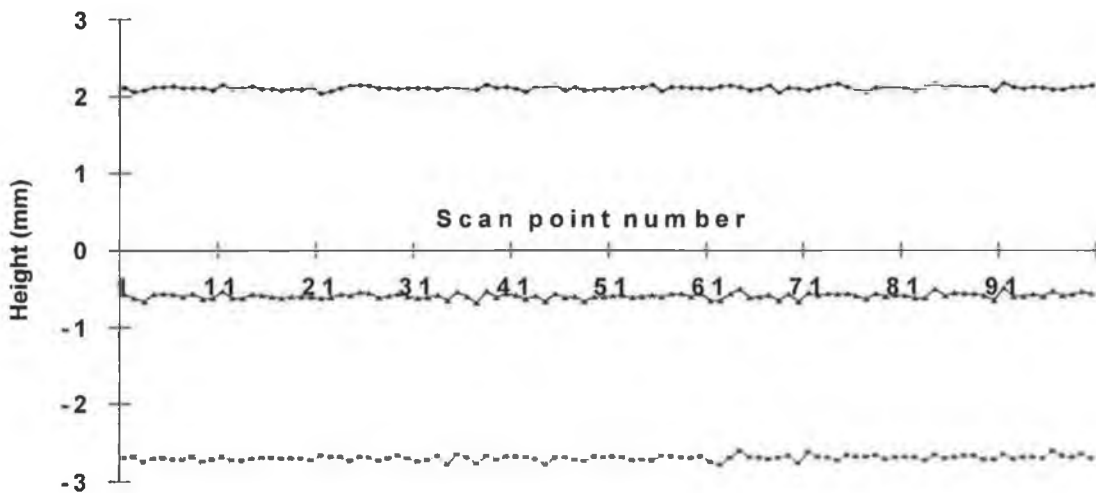


Figure 5-2: Signal recorded while holding the sample and the scanner head stationary

The signal was recorded over a period of 60.61 second. The signal acquired was stable over this time period. Figure 5-2 shows the first 100 data points, which are very representative of the 2548 data collected during this period.

5.3.2 Kinetic system

The following experiment was carried out to measure the linearity of the sample travel speed (S_p) over various motor frequencies (f_m) supplied from the MINI-LAB 603B (power station and frequency generator).

Table 5-2: Performance of kinetic system

Motor frequency f_m (Hz)	Path travelled P (mm)	Average time elapsed t (s)	Sample travel speed $S_p = P / t$ (mm/s)
400	150	23.530	6.37
420	150	22.315	6.72
440	150	21.435	7.00
460	150	20.555	7.30
480	150	19.730	7.60
500	150	18.820	7.97
520	150	18.190	8.25
540	150	17.310	8.67
560	150	16.710	8.98
580	150	16.200	9.26
600	150	15.745	9.53
620	150	15.270	9.82
640	150	14.880	10.08
660	150	14.400	10.42
680	150	14.030	10.69
700	150	13.630	11.01
720	150	13.340	11.24
740	150	12.905	11.62
760	150	12.430	12.07
780	150	12.275	12.22
800	150	11.985	12.52
820	150	11.820	12.69
840	150	11.460	13.09
860	150	11.195	13.40
880	150	10.980	13.66
900	150	10.860	13.81
920	150	10.485	14.31
940	150	10.360	14.48
960	150	10.190	14.72
980	150	9.770	15.35
1000	150	9.645	15.55

At each frequency selected the time to traverse 150 mm was recorded. After repeating this procedure 3 times at each frequency, the average time to traverse the 150 mm at each frequency was noted, see Table 5-2. Figure 5-3 was then generated from Table 5-2.

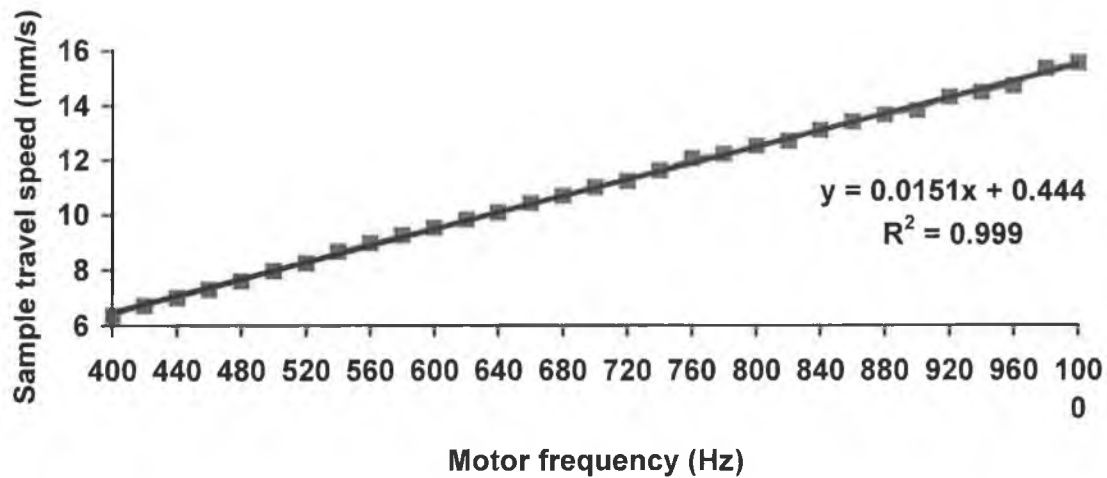


Figure 5-3: Relationship between sample travel speed and motor frequency

5.3.3 Data acquisition and analysis (DAQ) system

Data acquisition rate – The sensor head, Keyence LK-031 is capable of signal updating at 512 μ s, see Table C-1 in Appendix C. It is equivalent to a sampling rate of 1953 Hz. The data acquisition systems used were not capable of acquiring or displaying this large amount of data. Data acquisition rate was examined with the Hyper Terminal program, the LabVIEW VI without data flow speed (DFS) control and the LabVIEW VI with data flow speed (DFS) control. Table 5-3, Table 5-4, and Table 5-5 present the data acquisition rate of different program used. The data acquisition rate obtained using the Hyper Terminal program is shown in Table 5-3.

Table 5-3: Data acquisition rate in Hyper Terminal environment

Time elapsed t (s)	Number of data recorded N	Data acquisition rate DAR (per second)
30.59	2657	86.86
30.35	2638	86.92
30.41	2645	86.98
60.72	5281	86.97

In the LabVIEW environment, two VI's were created to operate the system. In the first VI there were additional program components to support various features, such as, data visualisation and data flow speed (DFS). DFS consisted of a program time delay and was used to facilitate the task of graphical representation of sensor signals and thickness measurement. As a result of having these additional program components, the first VI ran slowly and the data acquisition rate was lower (see Table 5-4) than for the second program. The second VI was relatively simple and resulted in a data acquisition rate, which was comparatively high (see Table 5-5). Figure 5-4 displays an inverse power relationship between data acquisition rate and data flow speed used in the first LabVIEW program.

Table 5-4: Data acquisition rate in LabVIEW environment (with DFS control)

Data flow speed DFS	Time elapsed t (s)	Number of data recorded N	Data acquisition rate DAR (per second)
0.00	30.37	1293	42.57
0.05	30.48	500	16.40
0.10	30.16	266	8.82
0.15	30.56	183	5.99
0.20	30.76	142	4.62
0.25	30.39	114	3.75
0.30	30.07	94	3.13
0.35	30.05	86	2.86
0.40	30.17	76	2.52
0.45	30.34	68	2.24
0.50	30.13	61	2.02
0.55	30.34	56	1.85
0.60	30.70	52	1.69
0.65	30.64	48	1.57
0.70	30.20	44	1.46
0.75	30.08	41	1.36
0.80	30.46	39	1.28
0.85	30.68	37	1.21
0.90	30.70	35	1.14
0.95	30.46	33	1.08
1.00	30.06	31	1.03

Table 5-5: Data acquisition rate in LabVIEW environment (without DFS control)

Time elapsed t (s)	Number of data recorded N	Data acquisition rate DAR (per second)
30.32	3173	104.65
29.86	3133	104.92
30.16	3170	105.11
30.33	3163	104.29

Some small error may exist in the data acquisition rates in the above tables as the elapsed time was recorded by using a stopwatch where some amount of human error was certainly involved. However, even an error of ± 3 s would still result in similar results to those noted above.

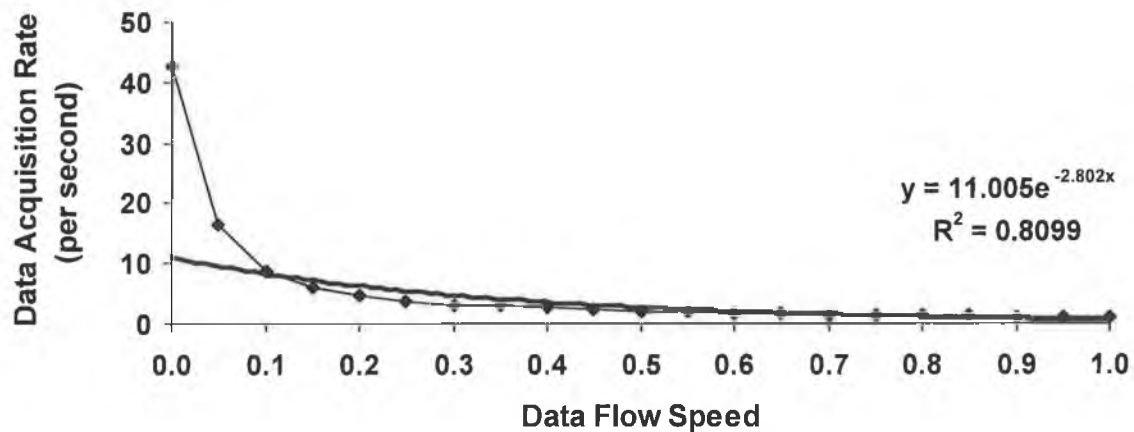


Figure 5-4: Relationship between data acquisition rate and data flow speed used in the first LabVIEW program.

5.4 Results from scans

The thickness measurement system developed here was able to measure many different types of sample materials up to 20 mm thick. The thickness measurements were recorded to a maximum resolution of $1\mu\text{m}$. Samples of different thickness, shape and material were tested. A few of them are presented here along with the description of the experiments carried out and the results obtained from these scans. The objectives of the experiments were to investigate the scanning performances of the system in different situations and measure the system accuracy. Although the main goal was thickness measurement but it was also an interest of the present work to determine how accurate the system can represent sample profiles, for example, length of sample, etc.

Scan was done only in horizontal direction and the height measurements were acquired through the scan. In each sample picture the dashed arrow in the figures

indicates the direction of scan performed. During the experiments, the system parameters were defined as follows:

S_p (sample travel speed) was set at 11 mm/s, and **DFS** (data flow speed in LabVIEW) was set at 0.00. **DAR** (data acquisition rate) was 87 Hz in Hyper Terminal program, and 104 Hz in LabVIEW program. S_r (scan resolution) was found 0.13 mm in Hyper Terminal program, and 0.14 mm in LabVIEW program.

For those graphs obtained from LabVIEW program, the scanning signals coming from sensor A and sensor B are represented by thin and thick data series respectively. The thicker data series represent the thickness of the sample measured. In the graphs, the heights of the data series of sensor A and sensor B are displayed with negative signs because of the nature of data acquisition by the sensors described in section 4.2. For most cases, the lower surface of the sample was flat, so the reading of sensor B does not change significantly. As a result the thickness of the sample mainly depends on the reading of sensor A. So the data series of sensor A and that of thickness are found parallel to each other.

5.4.1 Scan of aluminium taper block

An aluminium taper shaped block was used in this experiment. Figure 5-5 is a picture of this sample. See Figure F-3 in Appendix F for the drawing of the sample in AutoCAD with detailed dimensions. The aim of this experiment was to see the taper shape (slope in the sample surface) in the scanning result to compare the physical dimension of the sample with the scanned one. During the experiment the height measurements were acquired through the scan.

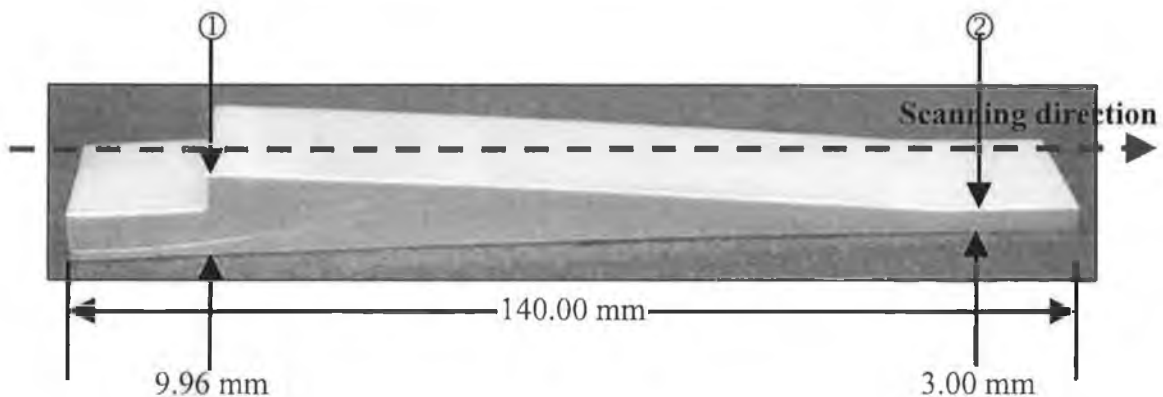


Figure 5-5: Aluminium taper block (sample-1)

Figure 5-6 displays the scanning result of sample-1 obtained in LabVIEW environment. As the length of the window on the lead screw slide was only 100 mm, see Figure E-6 in Appendix E, so the actual scan started at point ① and ended at point ②, see Figure 5-5. The first few points of data, see Figure 5-7, represent the scanning signal fluctuations on edge of the sample due to diffuse reflection of the laser beam from the sharp edge area. The signal got quite uniform for the rest of the scan. The altitude of the highest peak was 9.7 and then it gradually dropped to 3.39. It corresponded to the physical thickness of sample-1 from 9.96 mm to 3.00 mm.

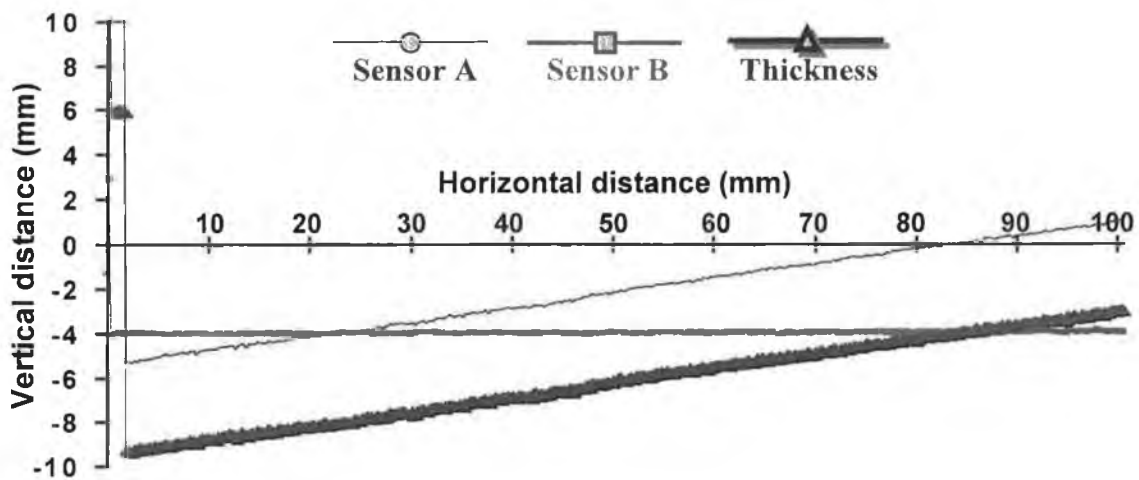


Figure 5-6: Scanning result of sample-1 in LabVIEW environment

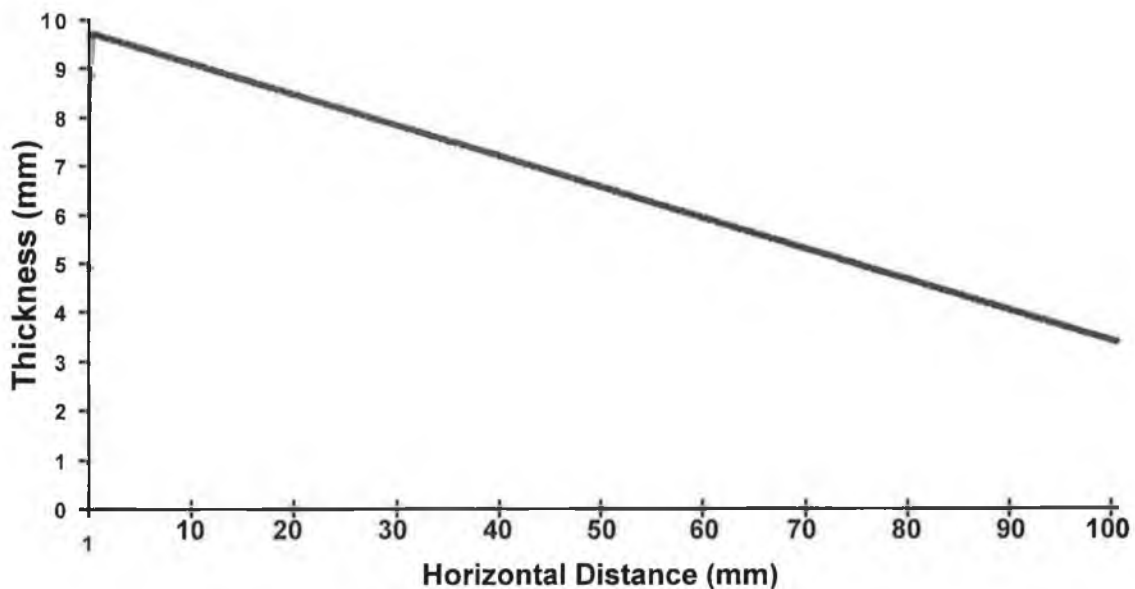


Figure 5-7: Scanning result of sample-1 in Hyper Terminal environment

5.4.2 Scan of aluminium block with various thickness

An aluminium block with various thickness was used in this experiment. Figure 5-8 is a picture of this sample. There were 7 regions of different length and thickness in the sample. The length and thickness corresponding to each region of the sample are given in Table 5-6. See Figure F-4 in Appendix F for the drawing of the sample in AutoCAD with detailed dimensions. The aim of this experiment was to observe how precisely the system could represent the sample. Further aim was to measure the length and thickness of each region and to compare the physical dimensions with the scanned one. During the experiment the height measurements were acquired through the scan.

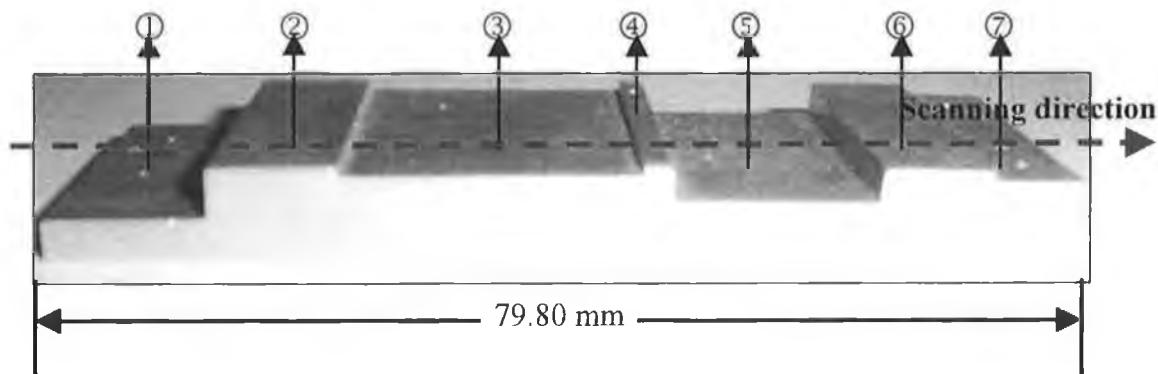


Figure 5-8: Aluminium block with various thickness (sample-2)

Table 5-6: Dimension of sample-2

Region	①	②	③	④	⑤	⑥	⑦
Length (mm)	12.90	9.90	22.90	2.30	15.70	8.70	7.40
Thickness (mm)	3.61	8.22	7.20	8.17	4.91	8.09	7.03

Figure 5-9 and Figure 5-10 display the scanning results of sample-2 obtained in LabVIEW and Hyper Terminal environment respectively. In Figure 5-10 the first few points of data represent the scanning signal fluctuations on edge of the sample due to diffuse reflection of the laser beam on the sharp edge area. This happened again every time the laser beam passed a sharp edge area on sample surface (note data points in the region of data point: 183, 378, 379, 569, 570, 626 and 627). This error was caused by shadow and dispersion effect indicated in Figure 3-6 of Chapter 3. However, a total number of 630 scanning data points was collected from this scan (i.e. $N = 630$). By using the equations 5.1 and 5.2 it can be calculated that the length

of sample (L_s) was 79.66 mm. It was very close to the actual length of the sample what was 79.80 mm. The scan resolution (S_r) was found to be 0.13 mm i.e. the scanning data was collected in every 130 μm on the sample surface.

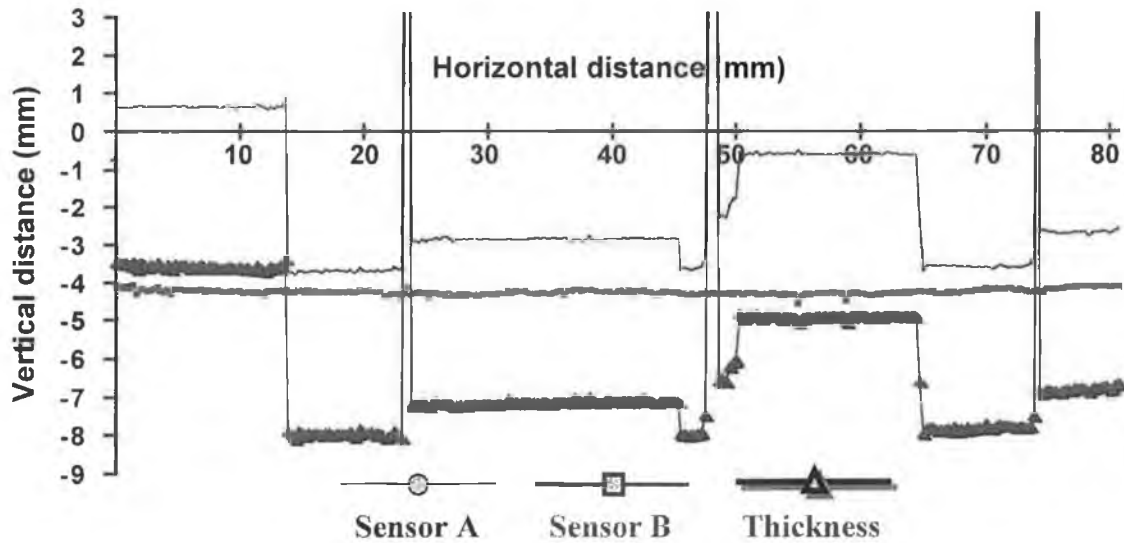


Figure 5-9: Scanning result of sample-2 in LabVIEW environment

The distribution and height calculated on the graph correspond well with the physical length and thickness of the different regions of sample-2. Table 5-7 with results from the above graph and the actual measurements indicates this correlation. For example, the second column of this table states that the points from 5 to 104 of the graph represent region ① of sample-2, and the length and thickness of this region are 12.87 mm and 3.60 mm respectively where the actual measurements are 12.90 mm and 3.61 mm respectively.

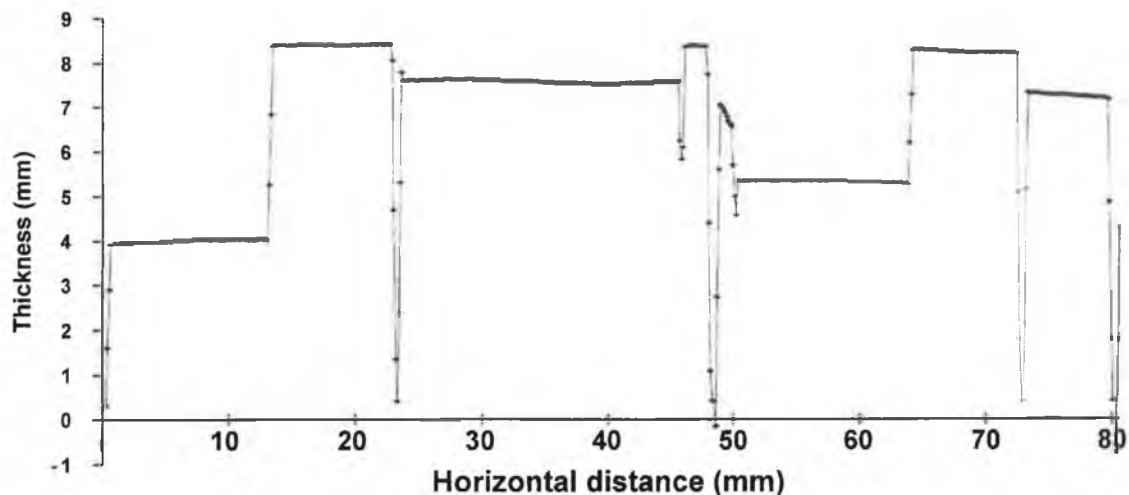


Figure 5-10: Scanning result of sample-2 in Hyper Terminal environment

Table 5-7: Comparison in dimension on sample-2

Points on graph	5-104	105-181	185-357	361-390	391-499	502-566	573-623
Region	①	②	③	④	⑤	⑥	⑦
Measured length (mm) (with scanning system)	12.87	9.88	22.36	3.77	14.04	8.32	6.50
Actual length (mm) (with Vernier callipers)	12.90	9.90	22.90	2.30	15.70	8.70	7.40
Measured thickness (mm) (with scanning system)	3.60	8.00	7.20	7.90	4.90	7.90	6.90
Actual thickness (mm) (with screw gauge)	3.61	8.22	7.20	8.17	4.91	8.09	7.03

5.4.3 Scan of kinked thin aluminium plate

A piece of kinked thin aluminium plate was used in this experiment. Figure 5-11 is a picture of this sample. See Figure F-5 in Appendix F for the drawing of the sample in AutoCAD with detailed dimensions. The main aim of this experiment was to view the scanning performance of the sensor, especially in the region of ③ and ④ on the sample plate, see Figure 5-11. During the experiment the height measurements were acquired through the scan.

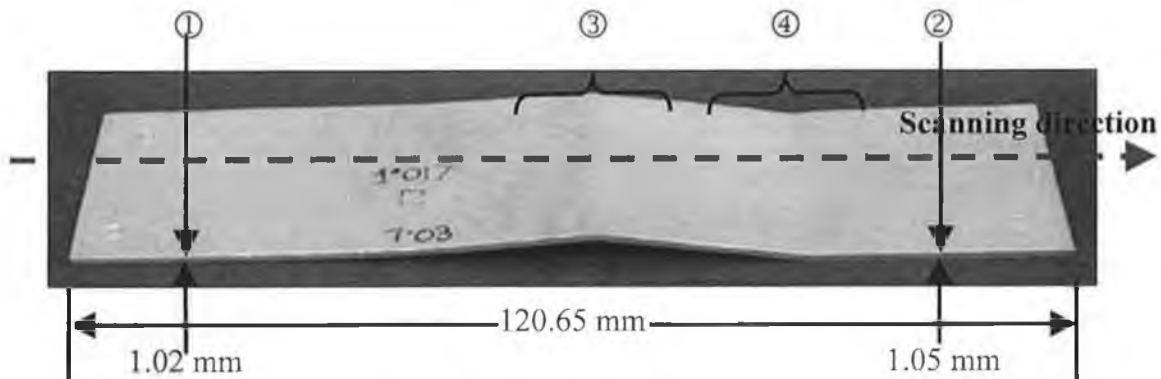


Figure 5-11: Kinked 1 mm thick aluminium plate (sample-3)

As the length of the window on the lead screw slide was only 100 mm, see Figure E-6 in Appendix E, so the actual scan started at point ① and ended at point ②, see Figure 5-11. The thickness readings from the graph, see Figure 5-12, was very similar to the actual thickness of the sample (1 mm on average) except in the pointed area of ③ and ④ in Figure 5-11. Because while taking thickness measurement the

sample was tilted by an evident amount on that two particular positions. The reason will be explained in details later in this chapter while characterising system errors.

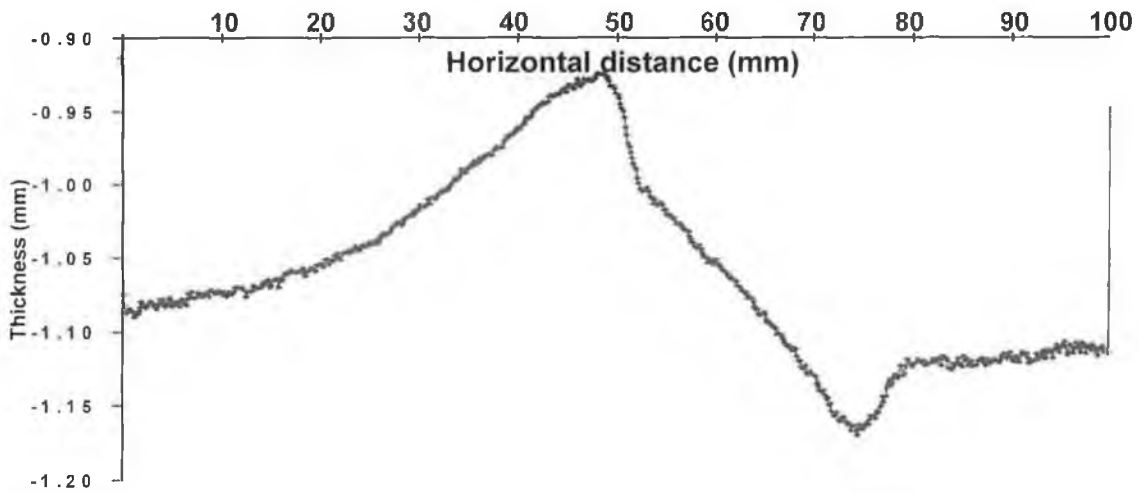


Figure 5-12: Scanning result of sample-3 in Hyper Terminal environment

5.4.4 Scan of aluminium plate with a rectangular hole inside

An aluminium plate with a rectangular hole inside was used in this experiment. Figure 5-13 is a picture of this sample. The sample can be divided into three regions for analysing purposes. Each region with its corresponding length is shown in Figure 5-13. See Figure F-6 in Appendix F for the drawing of the sample in AutoCAD with detailed dimensions. The main aim of this experiment was to find out the contrast of the scanning signals in the region of ① and ③ with the region of ②, see Figure 5-11, while the scan was being performed through the middle of the sample plate. Further aim was to measure the length and thickness of each region and to compare the physical dimensions with the scanned one. During the experiment the height measurements were acquired through the scan.

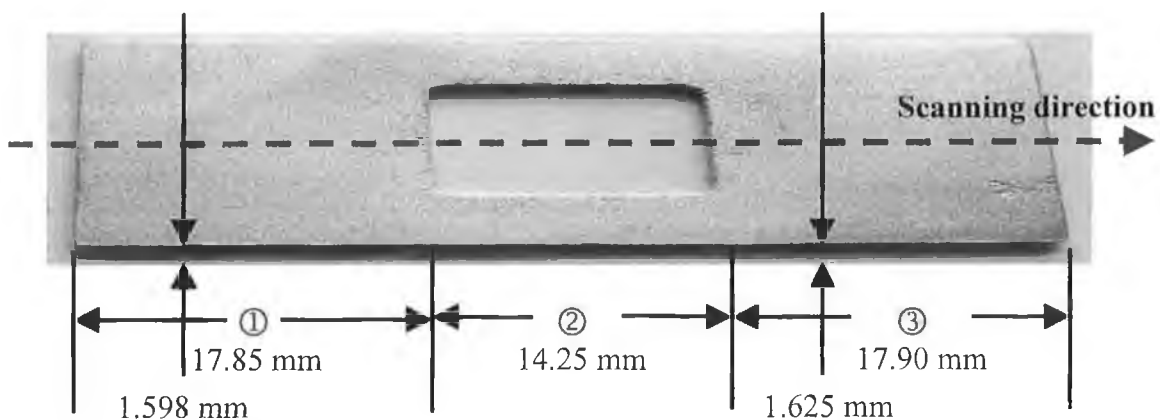


Figure 5-13: Aluminium plate with a rectangular hole inside (sample-4)

Figure 5-14 and Figure 5-15 display the scanning results of sample-4 obtained in LabVIEW and Hyper Terminal environment respectively.

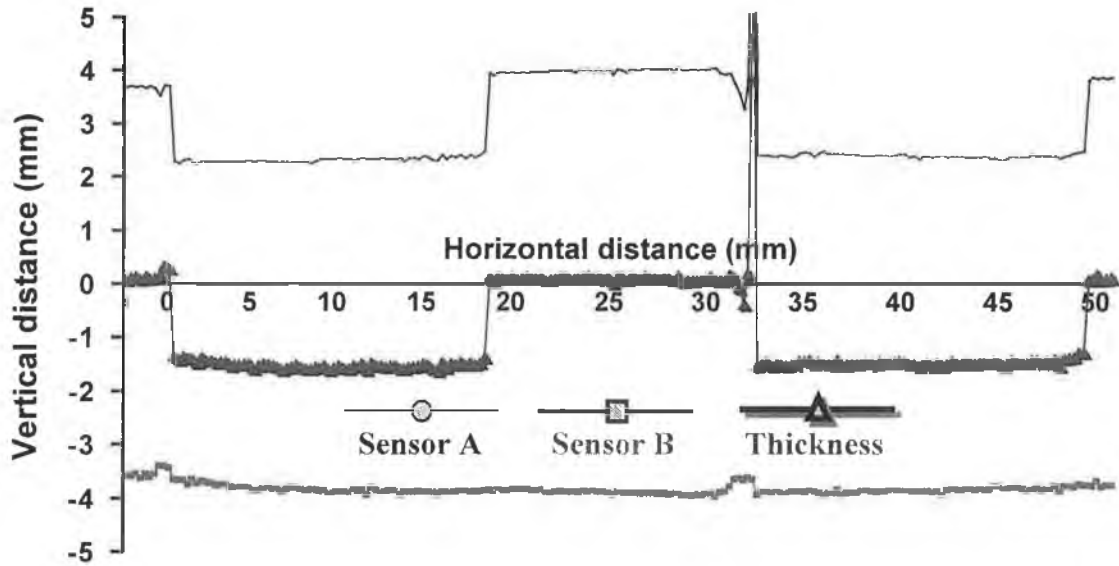


Figure 5-14: Scanning result of sample-4 in LabVIEW environment

During the experiment the sample was placed on the top of a thin white paper (0.3 mm thick) to prevent the sample falling through the window as it was small in size. The thickness of the sample and that of the piece of paper are shown separately in Figure 5-15. Scanning signal fluctuations can be seen at position 16 to 23 and 264 to 274 in this figure due to the reason explained in Figure 3-6 of Chapter 3. Another possibility of happening this was a sudden noise interference of the circuits or the mechanical vibration produced during the sample movement.

The distribution and height calculated on the graph in Figure 5-15 correspond well with the physical length and thickness of the different regions of sample-4. Table 5-8 with results from this graph and the actual measurements indicates this correlation. For example, the fifth column of this table states that the points from 275 to 412 of the graph represent region ③ of sample-4, and the length and thickness of this region are 17.81 mm and 1.60 mm respectively where the actual measurements are 17.90 mm and 1.63 mm respectively.

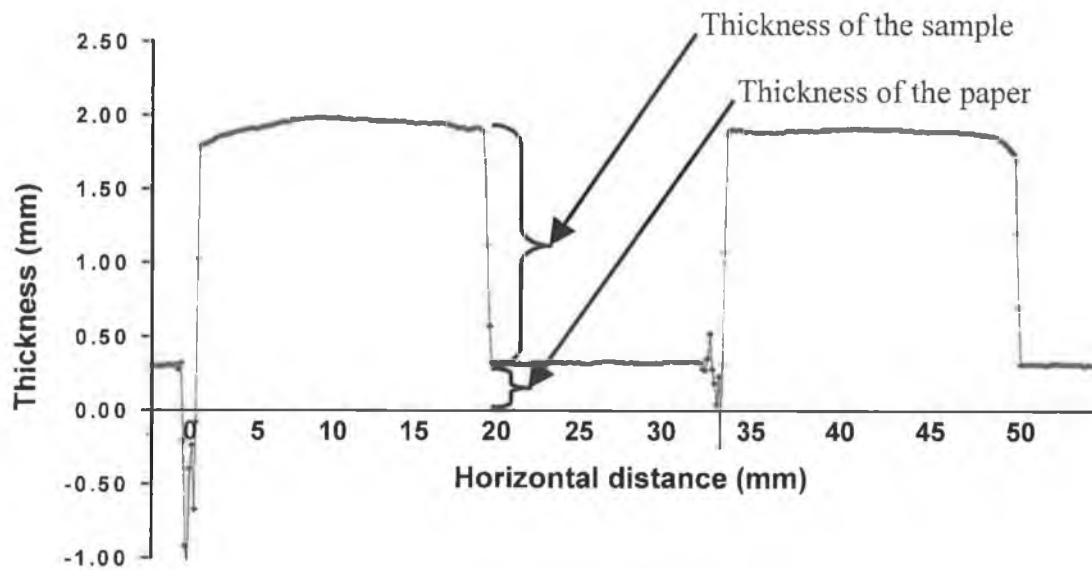


Figure 5-15: Scanning result of sample 4 in Hyper Terminal environment

Table 5-8: Comparison in dimension on sample-4

Points on graph	1-23	24-160	161-274	275-412	413-450
Region	Paper	①	②	③	Paper
Measured length (mm) (with scanning system)	2.86	17.68	14.69	17.81	4.81
Actual length (mm) (with Vernier callipers)	-	17.85	14.25	17.90	-
Measured thickness (mm) (with scanning system)	0.30	1.60	0.30	1.60	0.30
Actual thickness (mm) (with screw gauge)	-	1.60	-	1.63	-

5.4.5 Scan of double taper aluminium block

Until now all the sample plates scanned and analysed, except sample-3 in section 5.4.3, were flat on their bottom surfaces. In these situations the bottom laser sensor (sensor B) was not essential as the readings from this sensor did not affect the measurements. So an aluminium double taper shaped block was used in this experiment in order to use sensor B effectively in thickness measurement. The further aim of this experiment was to see the taper shape (slope in the sample

surface) in the scanning result to compare the physical dimension of the sample with the scanned one. Figure 5-16 is a picture of this sample. It shows the different thickness in different positions on the sample. See Figure F-7 in Appendix F for the drawing of the sample in AutoCAD with detailed dimensions.

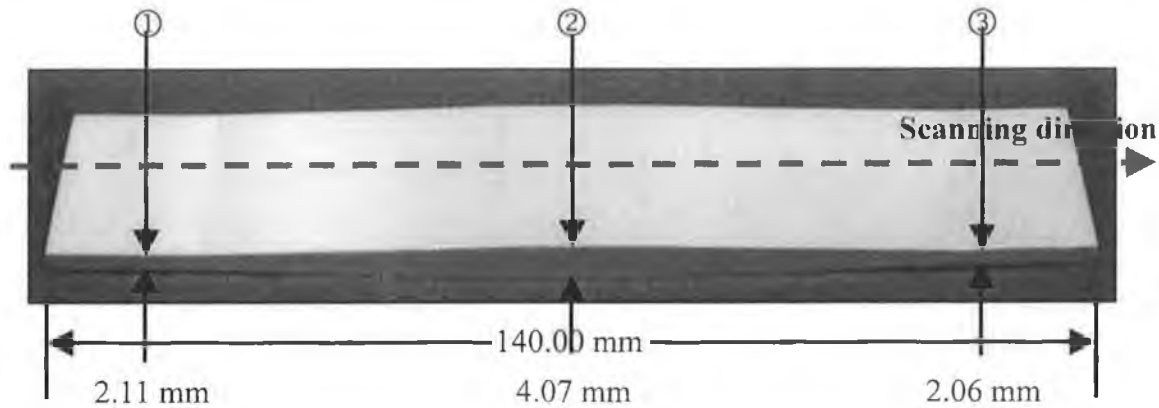


Figure 5-16: Double taper aluminium block (sample-5)

As the length of the window on the lead screw slide was only 100 mm, see Figure E-6 in Appendix E, so the actual scan started at point ① and ended at point ③, see Figure 5-16. During the experiment the height measurements were acquired through the scan. Figure 5-17 displays the scanning result of sample-5 in Hyper Terminal environment. The height distribution calculated on the graph in this figure corresponds well with the physical thickness in different positions of sample-5. Table 5-9 with results from this graph and the actual measurements indicates this correlation.

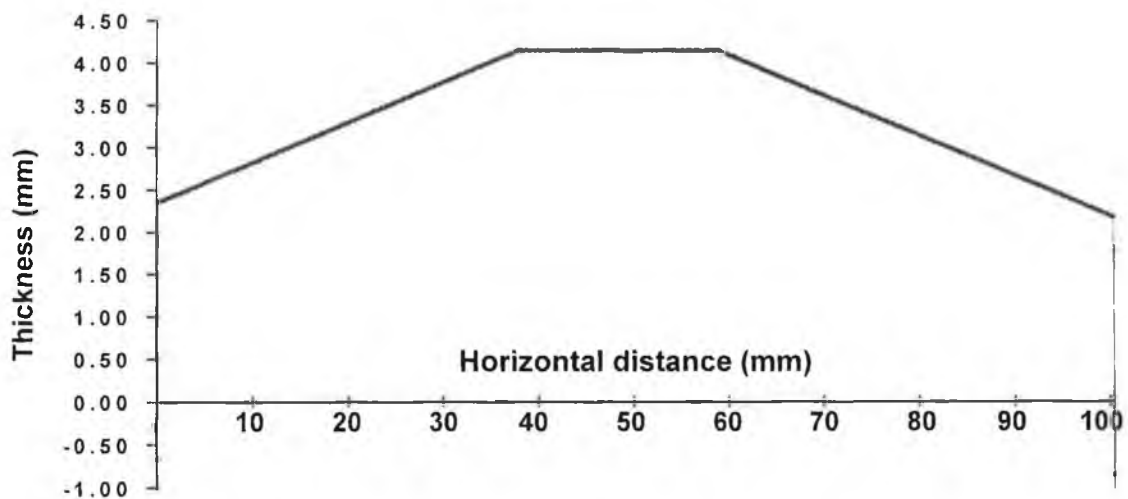


Figure 5-17: Scanning result of sample-5 in Hyper Terminal environment

Table 5-9: Comparison in dimension on sample-5

Region	①	②	③
Measured thickness (mm) (with scanning system)	2.30	4.10	2.10
Actual thickness (mm) (with screw gauge)	2.11	4.07	2.06

5.4.6 Scan of brass plate with 7 through holes

A brass plate with 7 through holes was used in this experiment. Figure 5-18 is a picture of this sample. It shows the seven through holes of different sizes on the sample plate. See Figure F-1 in Appendix F for the drawing of the sample in AutoCAD with detailed dimensions. The aim of this experiment was to observe how perfectly the system can detect a hole on the sample, and how closely it can measure the diameter or the depth of each hole. During the experiment the height measurements were acquired through the scan. Furthermore two points, namely Point A and Point B, were chosen for another experiment described later of this section.

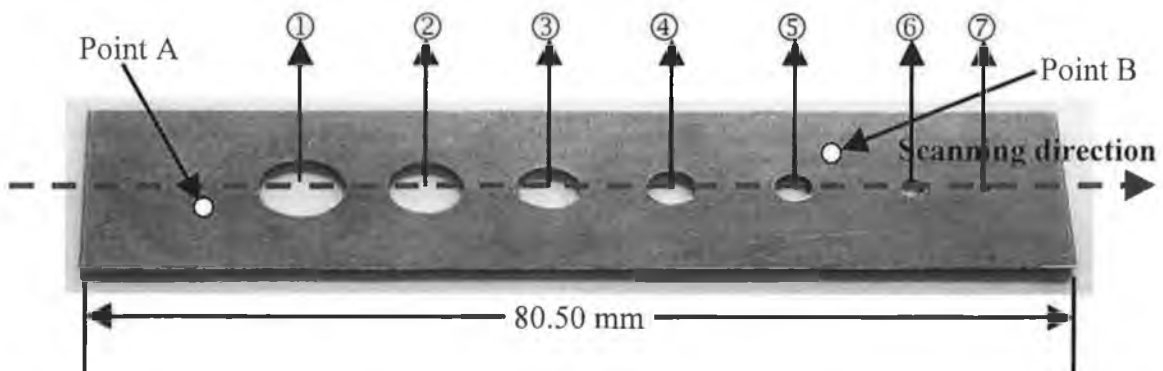


Figure 5-18: Brass plate with 7 through holes (sample-6)

Figure 5-19 and Figure 5-20 display the scanning results of sample-6 obtained in LabVIEW and Hyper Terminal environment respectively. During the experiment the sample was placed on the top of a thin white paper (0.3 mm thick) for the reason stated earlier in section 5.4.4. The thickness of the sample and that of the piece of paper are shown separately in Figure 5-19 and in Figure 5-20. The figures also indicate the positions of the corresponding holes on the sample. Scanning signal fluctuations can be seen at different positions of this figure due to the reason explained in Figure 3-6 of Chapter 3.

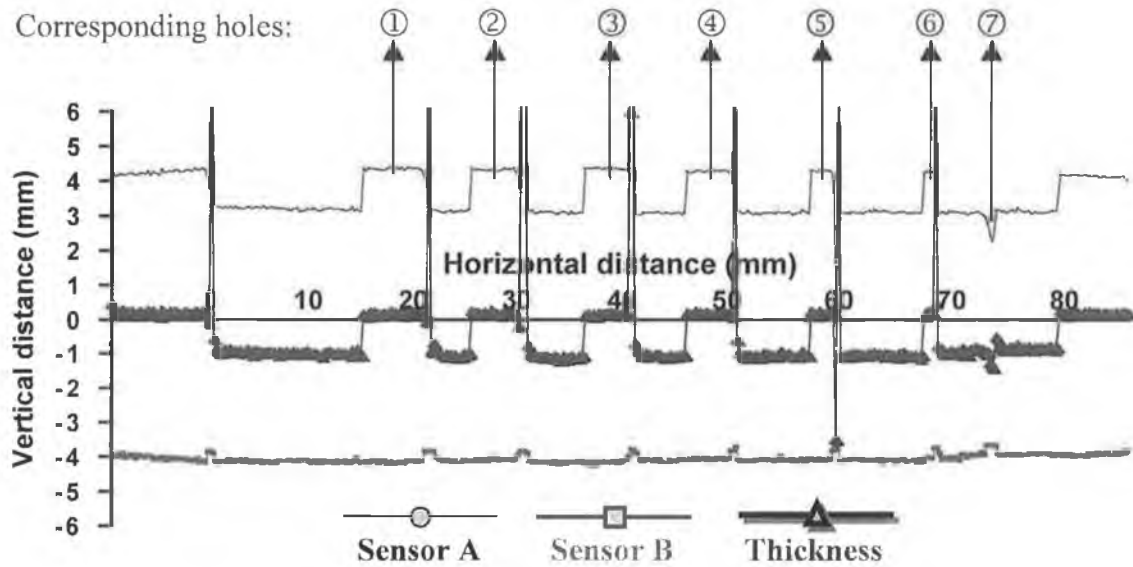


Figure 5-19: Scanning result of sample-6 in LabVIEW environment

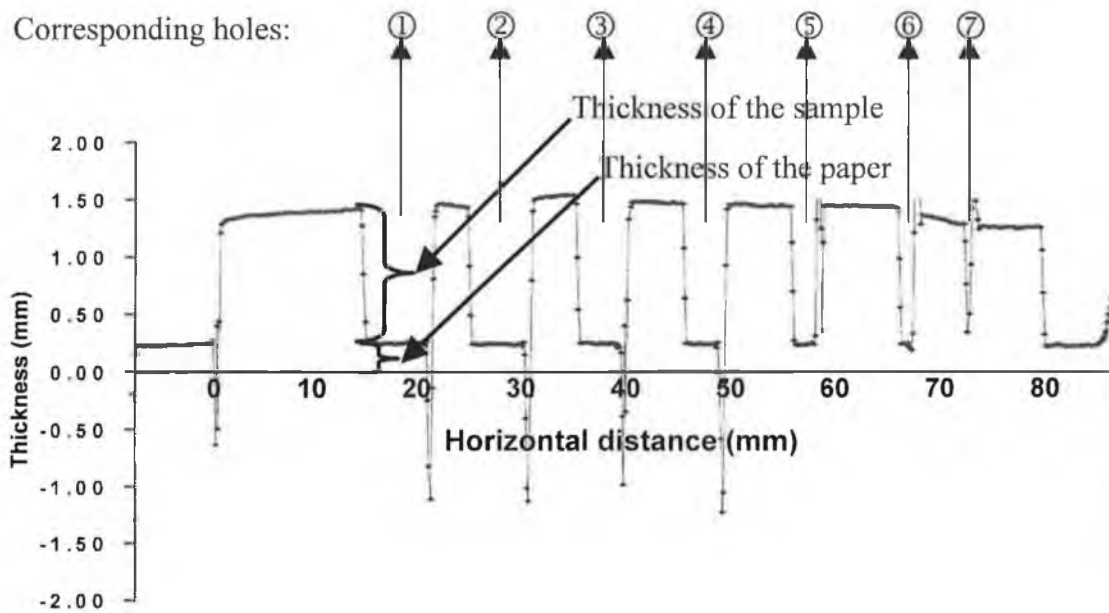


Figure 5-20: Scanning result of sample-6 in Hyper Terminal environment

A set of repetitive scanning experiments was carried out on sample-6 where the objectives were to examine the repeatability and accuracy of the system. Point A and Point B were two randomly selected points on the sample plate, see Figure 5-18. Table 5-10 is prepared on the basis of the results from this set of experiments. In this table \bar{x} , σ , and μ stand for average, standard deviation, and confidence interval

respectively. The equations that are used to calculate standard deviation and confidence interval are stated below [46],

$$\sigma = \sqrt{\frac{n \sum x^2 - (\sum x)^2}{n(n-1)}} \quad [5.3]$$

$$\mu = \bar{x} \pm t_{(\alpha/2; n-1)} \frac{\sigma}{\sqrt{n}} \quad [5.4]$$

In the above equation $t_{(\alpha/2; n-1)}$ is the value of t distribution with $n - 1$ degrees of freedom exceeded by an area of $\alpha / 2$. For 95% confidence level and 5 samples it equals to 2.571. The plus or minus part of this equation is denoted as CI in Table 5-10.

Table 5-10: Comparison in dimension on sample-6

#	Thickness of Sample plate at Point A (mm)		Thickness of Sample plate at Point B (mm)		Diameter of Hole ① (mm)		Length of Sample plate (mm)	
	Screw gauge (mm)	Scanning system (mm)	Screw gauge (mm)	Scanning system (mm)	Vernier callipers (mm)	Scanning system (mm)	Vernier callipers (mm)	Scanning system (mm)
1	0.981	1.017	0.993	1.066	6.90	6.15	80.53	80.85
2	0.990	1.046	0.984	1.071	6.87	6.60	80.47	80.55
3	0.985	1.056	0.989	1.041	6.92	6.30	80.52	80.10
4	0.997	1.031	0.993	1.056	6.82	6.45	80.51	80.70
5	0.985	1.027	0.985	1.051	6.88	6.60	80.51	80.40
\bar{x}	0.9876	1.0354	0.9888	1.057	6.878	6.42	80.508	80.52
σ	0.0061	0.0155	0.0043	0.0119	0.0377	0.1956	0.0228	0.2885
CI	0.0071	0.0179	0.0049	0.0137	0.0433	0.2249	0.0262	0.3317

The results in Table 5-10 indicate that at worst there was a 1.4 % confidence (for example, at Point A) for the measurements. The ranges given by CI for the mechanical and for the scanning system measurements largely overlap. This indicates that the scanning system was giving the same general results that were

obtained from the mechanical measurements. A slightly higher CI range is, however, noted for the scanning system measurements than for the mechanical measurements. This was due to the errors associated with the scanning system method of measurement. These will be discussed further in a later section.

5.5 System accuracy

The following experiment was carried out in order to measure the accuracy of the thickness measurement system. During this experiment a point was marked on the surface of a sample. Then the thickness of the sample on that particular point was measured with a screw gauge. The thickness of that point displayed on the screen of Keyence RD-50RW was recorded too. This procedure was repeated for a number of times with different samples and different thickness. The data recorded during this experiment is shown in Table 5-11. The last column of the table presents the accuracy of the individual measurements. The average accuracy of all the measurements was found as 98.27% what indicates the existence of errors in the system developed. The following section discusses about the system errors which were the possible reasons that had affected the system accuracy to this level.

Table 5-11: System accuracy

Thickness measured with screw gauge (mm)	Thickness measured with scanning system (mm)	Absolute error (mm)	Accuracy (%)	Error (%)
1.017	1.042	0.025	97.54	2.46
1.598	1.670	0.072	95.49	4.51
1.625	1.705	0.080	95.08	4.92
3.608	3.658	0.050	98.61	1.39
8.215	8.132	0.083	98.99	1.01
7.196	7.160	0.036	99.50	0.50
4.914	4.904	0.010	99.80	0.20
8.091	7.995	0.096	98.81	1.19
7.030	6.973	0.057	99.19	0.81
9.545	9.416	0.129	98.65	1.35
3.211	3.252	0.041	98.72	1.28
3.195	3.286	0.091	97.15	2.85
3.188	3.239	0.051	98.40	1.60
5.060	5.068	0.008	99.84	0.16

5.6 Characterisation of system errors

Although every possible measure was taken into consideration to make the thickness measurement system free from errors but existence of some sorts of errors in the system was not unexpected. For distance and thickness measurement, there are several factors, such as mechanical vibration and unstable of fixing ends of the object being measured, can make deflection in the direction of measurement. The affection of this deflection can not be entirely avoided, specially in high accurate displacement measurement, and the error caused by deflection can not be ignored for the same reason. Because light-spot position detector such as CCD can not distinguish the moving of light is due to the displacement or due to the deflection, the error will be superposed to the measuring result directly. Its influences to the measuring result are discussed below [21].

The scope of possible errors to affect the accuracy of thickness measurement can be divided into three main groups, such as, (1) set-up errors, (2) external errors, and (3) environmental error. Figure 5-21 draws the classification of errors.

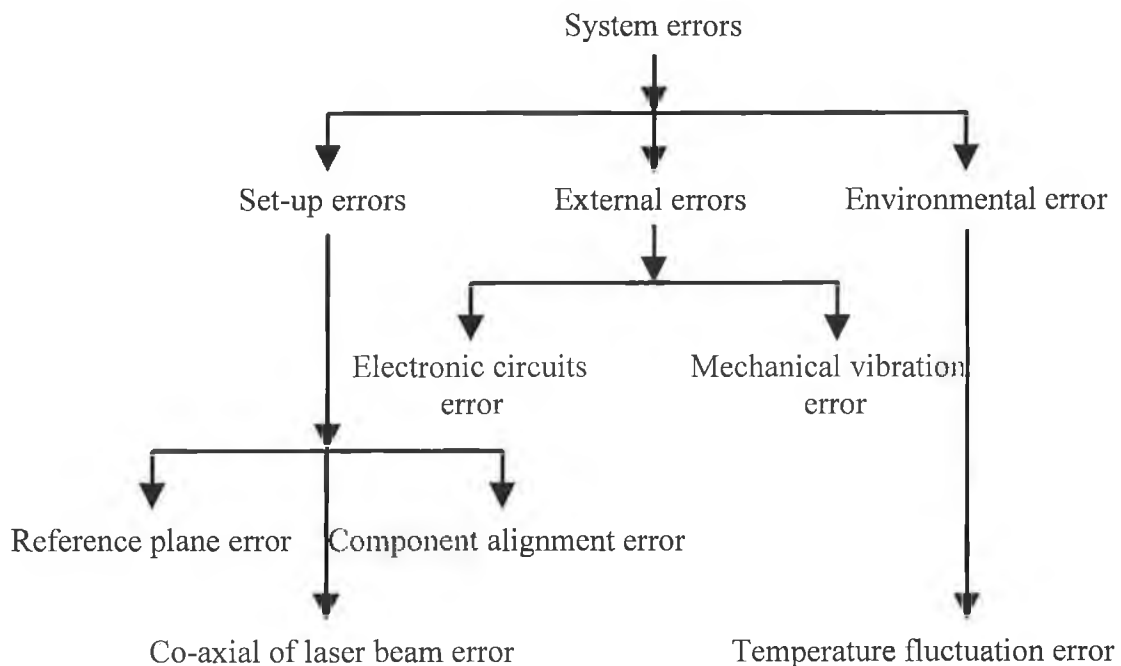


Figure 5-21: Classification of system errors

5.6.1 Set-up errors

During the thickness measurement process it is to keep the stand-off distance of both sensors at a distance of 30 mm from the sensor surface. Failure to providing so will result significant experimental error in the whole thickness measurement process. There can be three types of set-up errors, such as, error with reference plane, error with co-axial of laser beam, and error with component alignment. These errors are explained separately below.

(1) Error with reference plane: If the location of the reference planes is not previously known, then the difference between the reference planes for Sensor A and Sensor B should be examined.

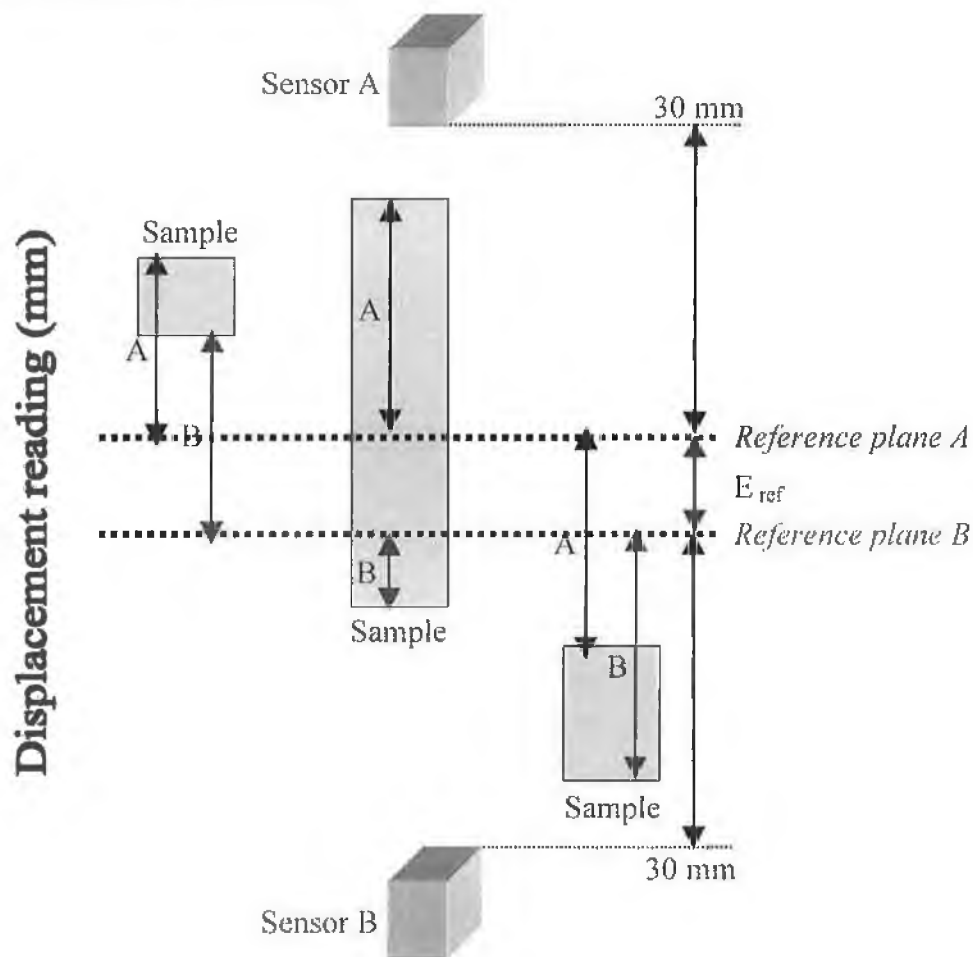


Figure 5-22: Reference planes apart from each other

The amount of difference, say E_{ref} , needs to be adjusted in equation 4.1 to calculate the thickness of the sample accurately (only when the reference planes are to be overlapped or apart from each other). Therefore,

$$T_h = |A + B| \pm E_{ref} \quad [5.5]$$

In the event shown in Figure 5-22, the thickness of the sample will be decreased by the amount of E_{ref} . So in this case,

$$T_h = |A + B| + E_{ref} \quad [5.5 (a)]$$

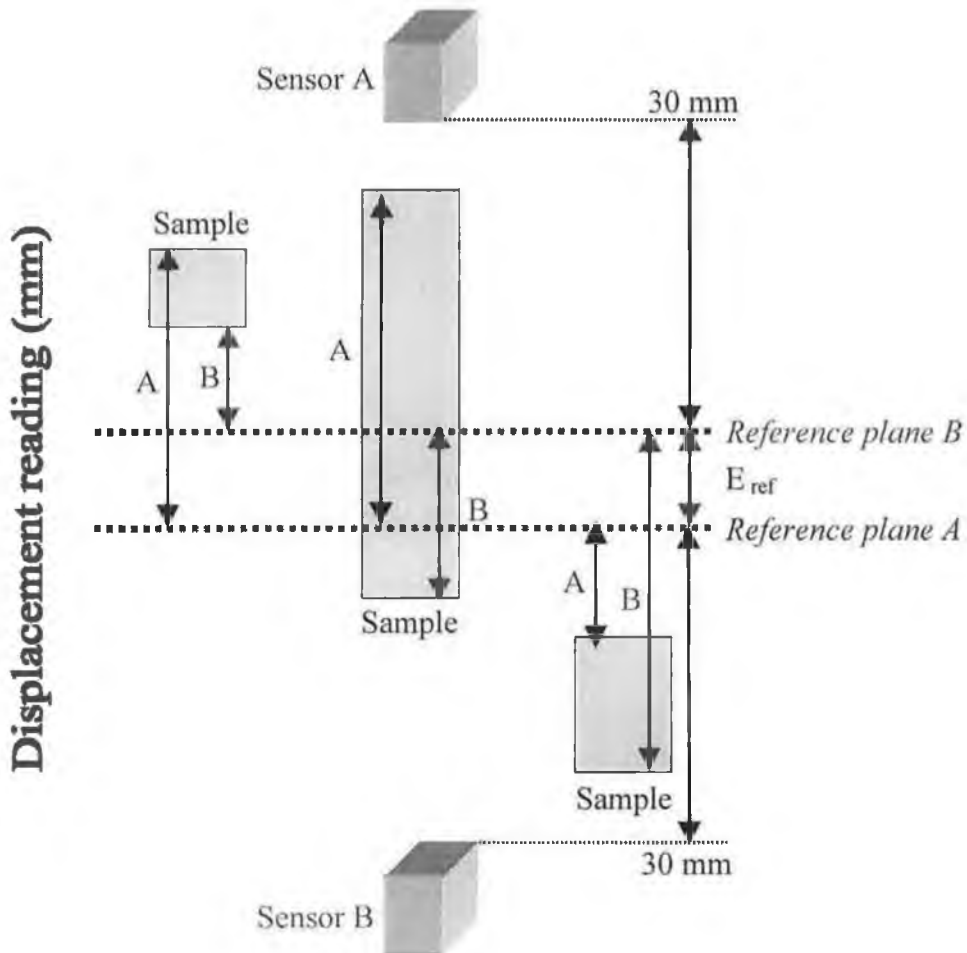


Figure 5-23: Overlapped reference planes

In the event shown in Figure 5-23, the thickness of the sample will be increased by the amount of E_{ref} . So in this case,

$$T_h = |A + B| - E_{ref} \quad [5.5 (b)]$$

(2) **Error with co-axial of laser beam:** Before proceeding for the thickness measurement, it is necessary to examine the position of the laser beam spots that are

emitting from Sensor A and Sensor B. To achieve the accuracy for the thickness measurement, the beam spots should be co-axial to each other. The set-up orientation of two sensors in Figure 5-24 (a) will give the accurate thickness of the sample whereas the other one, Figure 5-24 (b), will be error rendering. As mentioned in the previous chapter, this error was attempted to avoid by ensuring that the beam spots overlapped when viewed on a sheet of paper placed crosswise on the reference plane.

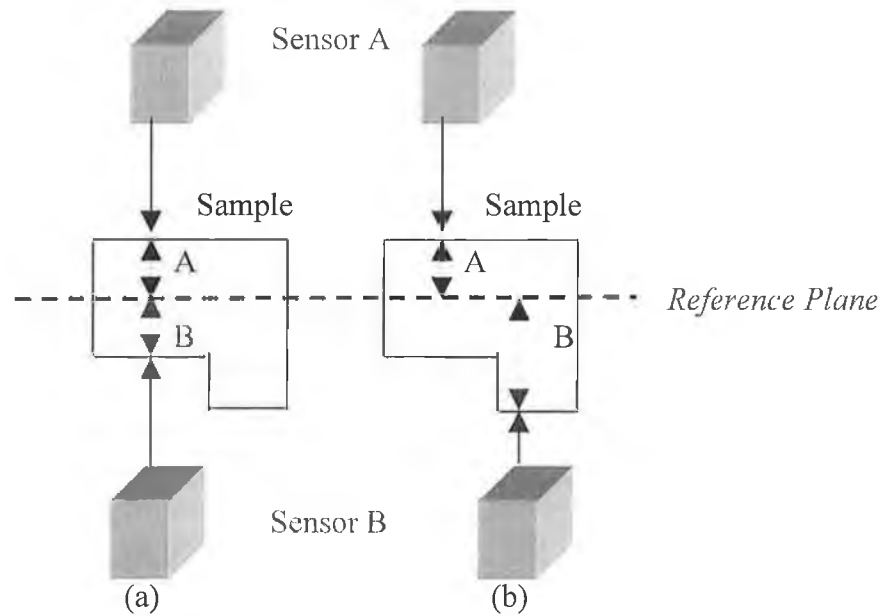


Figure 5-24: Co-axial of laser beam spots

(a) accurate measurement and (b) error rendering measurement

(3) Error with component alignment

A significant amount of error will be produced if the components associated with thickness measurement are not in the correct position. Figure 5-25 (a) indicates a scope of error where the sample itself is tilted by an amount θ while taking a thickness measurement. As a result the thickness $|AC|$ may be read incorrectly as the distance $|BC|$, see Figure 5-25 (b).

Using the trigonometry, it can be shown that $\angle ACB = \theta$, so

$$|BC| = |AC| / \cos \theta \quad [5.6]$$

Then under the tilting angle, θ , the amount of error, E_{tilt} , will be,

$$E_{\text{tilt}} = |BC| - |AC| \quad [5.7]$$

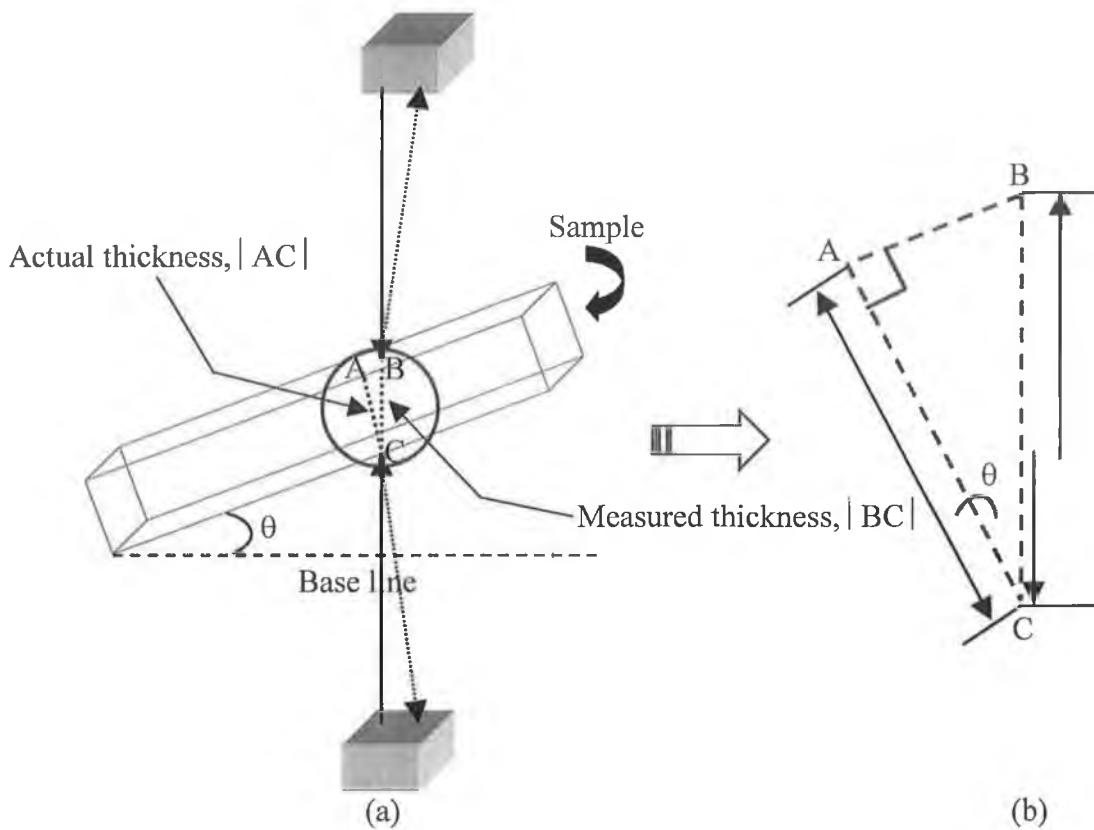


Figure 5-25: (a) Scope of error in tilting sample and (b) close-up of measured region

If the actual thickness assumed to be 10 mm then by using the equations 5.6 and 5.7, the following table (Table 5-12) can be obtained which shows the amount of error, E_{tilting} , associated with the tilting angle, θ , ranging from 1° to 5° .

Table 5-12: Error in tilting sample

Angle of tilt ($^\circ$)	Cosine	Error (mm)
1	0.99985	0.002
2	0.99939	0.006
3	0.99863	0.014
4	0.99756	0.024
5	0.99619	0.038

Now by considering the error in tilting sample, the equation for thickness measurement 5.5 will be modified as follows,

$$T_h = |A + B| \pm E_{ref} \pm E_{tilt} \quad [5.8]$$

Calibration error

At the beginning of this chapter we found that during the calibration process each of the laser sensors produced a short fall of 0.033 mm over 1 mm distance measurement, see Table 5-1 and Figure 5-1. It means that there is a certain amount of calibration error underlying in the system. Actually those three types of set-up errors discussed earlier in this section are responsible for causing this calibration error. So if the amount of calibration error is presented by E_{cal} then

$$E_{cal} = E_{ref} + E_{tilt} \quad [5.9]$$

The equation for thickness measurement 5.8 is then updated as follows,

$$T_h = |A + B| \pm E_{cal} \quad [5.10]$$

5.6.2 External errors

Errors in this category are associated with electronic circuit of hardware components and mechanical vibration of lead screw table.

(1) Error due to accuracy of electronic circuits

The linearity of Keyence LK series is $\pm 0.05V$ (max.) and the measuring accuracy of Keyence RD-50RW is $\pm 0.015V$ (max.), see Table C-1 and Table C-2 in Appendix C. There also exists $\pm 0.076 V$ accuracy on the LabVIEW data acquisition system [44]. These all figures should be considered to calculate the overall hardware error, $E_{hardware}$. So the equation for thickness measurement 5.10 needs to be corrected as follows.

$$T_h = |A + B| \pm E_{cal} \pm E_{hardware} \quad [5.11]$$

(2) Error due to mechanical vibration

Although adequate actions were taken to reduce the amount of mechanical vibration in the measurement system, there still exist some vibration while the sample is being

travelled by the lead screw table of the kinetic system. A specific experiment was carried out to measure the amount of displacement caused in the vertical position of the sample scanned due to the mechanical vibration produced from the stepper-motor / lead screw table assembly. An accelerometer, ET-ACC-02, manufactured by Ergotest [47], and an analogue to digital converter, ADC-12, supplied by Pico Technology Ltd. [48], were used in this experiment. Details of this experiment will be given in Appendix D. In theory, a body that experiences simple harmonic motion follows a displacement pattern defined by [49],

$$\chi = \chi_0 \sin(2\pi f t) = \chi_0 \sin \omega t \quad [5.12]$$

Where f is the frequency of the simple harmonic motion, $\omega = 2\pi f$ is the corresponding angular frequency, and χ_0 is the amplitude of the displacement. The velocity χ' and acceleration χ'' of the body are found by differentiating the displacement once and twice, respectively:

$$\chi' = \chi_0 (2\pi f) \cos(2\pi f t) = \chi_0 \omega \cos \omega t \quad [5.13]$$

$$\chi'' = -\chi_0 (2\pi f)^2 \sin(2\pi f t) = -\chi_0 \omega^2 \sin \omega t \quad [5.14]$$

The maximum absolute values of the displacement, velocity, and acceleration of a body undergoing harmonic motion occur when the trigonometric functions in equations 5.12 to 5.14 are numerically equal to unity. These values are known, respectively, as displacement, velocity, and acceleration amplitudes; they are defined mathematically as follows:

$$\chi_0 = \chi_0, \quad \chi' = (2\pi f) \chi_0, \quad \chi'' = (2\pi f)^2 \chi_0 \quad [5.15]$$

Following the procedures described in Appendix D, the values for f and χ'' were found from the above experiment. By utilising the equation 5.15 the following table (Table 5-13) is produced which shows the amount of vertical displacement under different sample speed selected.

Table 5-13: Maximum vertical displacement error from mechanical vibration

Sample speed (mm/s)	Frequency (Hz)	Acceleration (m/s ²)	Displacement (mm)
9.53	300	10.70	0.0030
11.01	350	8.40	0.0017
12.52	400	5.90	0.0009
13.81	450	2.45	0.0003

If the maximum vertical displacement error from mechanical vibration is denoted by E_{vib} , then the equation for thickness measurement 5.11 will be,

$$T_h = |A + B| \pm E_{cal} \pm E_{hardware} \pm E_{vib} \quad [5.16]$$

5.6.3 Environmental error

This type of error is related with the environmental phenomena, such as, temperature fluctuation.

(1) Error due to temperature fluctuation

Temperature fluctuation is one of the factors that can have an impact on displacement measurements. It is proportionally related with the co-efficient of linear expansion which is defined as follows [50]:

$$\text{Co-efficient of linear expansion, } \beta = \frac{1}{L_s} \cdot \frac{\Delta L_s}{\Delta T} \quad [5.17]$$

where L_s , ΔL_s , and ΔT refer to the original length, the change in length, and the change in temperature respectively. As most of the samples used in the experiments were made of either aluminium or brass, so we consider the values of β for aluminium and brass which are $2.4 \times 10^{-5} / ^\circ\text{C}$ and $1.8 \times 10^{-5} / ^\circ\text{C}$ respectively. If the original thickness of sample was 20 mm and a temperature fluctuation of 10°C maximum was assumed, then using the equation 5.17 the change in length, ΔL_s , would be 0.0048 mm for aluminium and 0.0036 mm for brass. The change in length can occur in both the horizontal and vertical direction of the sample. The change in length in vertical direction was mostly concerned as thickness was measured in this

position. If ΔL_T refers to the error caused by temperature fluctuation, E_{temp} , then the equation 5.16 for thickness measurement can be presented as follows,

$$T_h = |A + B| \pm E_{cal} \pm E_{hardware} \pm E_{vib} \pm E_{temp} \quad [5.18]$$

5.7 Errors analysis

A measurement system is often made up of a chain of components, each of which is subject to individual inaccuracy. The overall inaccuracy can only be computed when all the individual inaccuracies are known. A similar problem occurs in experiments that use the results (measurements) from several different instruments to compute some quantity. In order to estimate what amount of errors are allowable in the individual instrument if there must be a certain accuracy in a computed result, let us consider the problem of computing a quantity N , where N is known function of n independent variables $u_1, u_2, u_3, \dots, u_n$ [51]. That is,

$$N = f(u_1, u_2, u_3, \dots, u_n) \quad [5.19]$$

The u 's are the measured quantities (instrument or component outputs) and are in error by $\pm \Delta u_1, \pm \Delta u_2, \pm \Delta u_3, \dots, \pm \Delta u_n$, respectively. These errors will cause an error ΔN in the computed result N . The Δu 's may be considered as absolute limits on the errors or as uncertainties. If the Δu 's are considered as absolute limits on the individual errors and we wish to calculate similar absolute limits on the error in N , we could calculate

$$N \pm \Delta N = f(u_1 \pm \Delta u_1, u_2 \pm \Delta u_2, u_3 \pm \Delta u_3, \dots, u_n \pm \Delta u_n) \quad [5.20]$$

By subtracting N in equation 5.19 from 5.20, we finally obtain $\pm \Delta N$. This procedure is needlessly time-consuming and an approximate solution valid for engineering purposes may be obtained by application of the Taylor series. Expanding the function f in a Taylor series, we get

$$f(u_1 \pm \Delta u_1, u_2 \pm \Delta u_2, \dots, u_n \pm \Delta u_n)$$

$$\begin{aligned}
&= f(u_1, u_2, \dots, u_n) + \Delta u_1 \frac{\partial f}{\partial u_1} + \Delta u_2 \frac{\partial f}{\partial u_2} + \dots + \Delta u_n \frac{\partial f}{\partial u_n} \\
&\quad + \frac{1}{2} \left[(\Delta u_1)^2 \frac{\partial^2 f}{\partial u_1^2} + \dots \right] + \dots
\end{aligned} \tag{5.21}$$

Where all the partial derivatives are to be evaluated at the known values of u_1, u_2, \dots, u_n . That is, if the measurements have been made, the u 's are all known as numbers and may be substituted into the expressions for the partial derivatives to give other numbers. In actual practice, the Δu 's will all be small quantities, and thus terms such as $(\Delta u)^2$ will be negligible. Then equation 5.21 may be given approximately as

$$\begin{aligned}
&f(u_1 + \Delta u_1, u_2 + \Delta u_2, \dots, u_n + \Delta u_n) \\
&= f(u_1, u_2, \dots, u_n) + \Delta u_1 \frac{\partial f}{\partial u_1} + \Delta u_2 \frac{\partial f}{\partial u_2} + \dots + \Delta u_n \frac{\partial f}{\partial u_n}
\end{aligned} \tag{5.22}$$

So the absolute error E_a is given by

$$E_a = \Delta N = \left| \Delta u_1 \frac{\partial f}{\partial u_1} \right| + \left| \Delta u_2 \frac{\partial f}{\partial u_2} \right| + \dots + \left| \Delta u_n \frac{\partial f}{\partial u_n} \right| \tag{5.23}$$

The absolute-value signs are used because some of the partial derivatives might be negatives, and for a positive Δu such a term would reduce the total error. Since an error Δu is, in general, just as likely to be positive as negative, to estimate the maximum possible error, the absolute-value signs must be used as in equation 5.23. The form of equation 5.23 is very useful since it shows which variables (u 's) exert the strongest influences on the accuracy of the overall result. That is, if, say, $\delta f / \delta u_3$ is a large number compared with the other partial derivatives, then a small Δu_3 can have a large effect on the total E_a . If the relative or percentage error E_r is desired, clearly it is given by

$$E_r = \frac{\Delta N}{N} \times 100 = \frac{100}{N} E_a \tag{5.24}$$

So the computed result may be expressed as either $N \pm E_a$ or $N \pm E_r$ percent, and the interpretation is that we are certain this error will not be exceeded since this is how the Δu 's were defined.

In carrying out the above computations, questions of significant figures and rounding will occur. While hand calculators allow us to easily carry many digits, even here, rounding may not be entirely meaningless. The trade-off involved is between the time it takes to properly round and the time it takes (plus a greater probabilities of mis-entering a digit) to enter a long string of digits. However, irrespective of what is done in intermediate steps, the final result must always be rounded to a number of digits consistent with the accuracy of the basic data.

Calculation: With a view to perform error analysis and achieve a real figure in order to indicate absolute error or relative error of the system, the numeric values of all the errors described in the earlier section need to be known. That is the numeric values for E_{cal} , $E_{hardware}$, E_{vib} , E_{temp} of equation 5.18 should be drawn, see Table 5-14. So based on the thickness measurement system, the equation 5.23 can be written as follows:

$$E_a = \Delta N = E_{cal} + E_{hardware} + E_{vib} + E_{temp} \quad [5.25]$$

Table 5-14: Estimation of expected errors in the system

Scope of error	Defined by	Length $\pm (\mu\text{m})$	Height $\pm (\mu\text{m})$	Error due to
Set-up reference plane	E_{ref}	-	100	Considered paper thickness as 0 mm
Set-up angle of tilt	E_{tilt}	-	14	Assumed sample as 3° tilt
Voltage measurement	$E_{hardware}$	-	76	± 0.076 V accuracy for LabView DAQ system and 1V per 1 mm
Mechanical vibration	E_{vib}	-	1.7	Assumed sample speed as 11.01 mm/s
Temperature fluctuation	E_{temp}	24	4.8	Assumed sample as 100 mm long and 20 mm thick aluminium bar with 10°C temperature difference
Absolute error	E_a	24	196.5	
Percentage error	E_r	0.02 %	0.98 %	

Chapter 6

Conclusion

This chapter draws the comparison between the two laser scanning systems used in present work – surface profile measurement system and thickness measurement system and then outlines the conclusion and recommendations for further works for the latter system.

6.1 Comparison between the two laser scanning systems

Below is a discussion on comparison of the two laser scanning systems used in present work. In the following discussion the surface profile measurement system and the thickness measurement system will be denoted as system1 and system2 respectively for the convenience and readiness.

Reference (stand-off) distance – The reference (stand-off) distance of system1 (58 mm) is about two times greater than that of system2 (30 mm). This may help system1 more suitable and convenient over system2 for many applications.

Measuring range – The measuring range of system2 (± 5 mm) is double over the measuring range of system1 (± 2.5 mm). Moreover, as a result of set-up advantage system2 can measure samples of maximum 20 mm thick where system1 is capable of measuring samples of maximum 5 mm thick.

Data storage capability – System1 can acquire and save a limited amount of data (8000 as per current set-up) but system2 has capability of acquiring and storing unlimited data over the scanning time depending on the capacity of the storage device.

Scanning frequency of sensor head – Though the current set-up limits the scanning frequency of sensor head of system1 to 1 KHz, but the maximum frequency obtainable is 10 KHz what is much higher than system2 (about 2 KHz).

Resolution – The resolution of system1 (0.25 μm) is much higher than that of system2 (1 μm). This is one of the advantages of system1.

Non-Linearity – The non-linearity co-efficient of system1 ($\pm 1.5 \mu\text{m}$ (0.03% FSO)) is comparatively less than that of system2 ($\pm 0.1\%$ of FSO) what makes system1 more accurate in measurement.

Sample travel speed – Though current experiment set-up shows samples to be measured can travel faster in system1 (20 mm/s) than system2 (15.55 mm/s), but it is possible to turn this speed very high in system2 by making some modification in its kinetic system. This will be explained later in this chapter.

Convenience – In system2, there is a controller, Keyence LK-2001, with each of the sensor head, Keyence LK-031, which offers many features for more control and convenience over the measurement task such as setting alarm hold function, key-lock function, data averaging function, etc. Such a useful facility is not present in system1.

Limitation to sample design – Though both of the systems can measure the thickness of a moving sample, but system1 is able to measure thickness only when the bottom surface of the sample is flat and uniform. On the contrary, system2 can measure the thickness of any moving sample regardless of its shape and position (as long as it stays within its measuring range).

Flexibility – In system2, there is an analogue sensor output display unit, Keyence RD-50 RW, which provides many features over the measurement data including the facility of displaying data, setting the display format, doing some simple calculation on data, etc. Moreover, this unit also facilitates system2 an option to work even without the help of a computer system though some important tasks like data saving is not possible in this event. However, such an advantage is not available in system1.

Scanning performances – After all due to the better experiment set-up of kinetic system (sample holding, sample travelling, etc), the scanning performances achieved in system2 is higher than system1.

In order to draw the comparison Table 6-1 summarises the basic technical differences between the two laser scanning systems.

Table 6-1: Comparison between the two laser scanning systems

Area of difference		Surface profile measurement system (System1)	Thickness measurement system (System2)	
Specification				
(A) Scanning system				
Laser scanner		Micro-Epsilon optoNCDT 2000	Keyence LK-031	
Stand-off distance		58 mm	30 mm	
Measuring range		± 2.5 mm	± 5 mm	
Non-linearity		± 1.5 µm (0.03% FSO)	± 0.1% of FSO	
Resolution		0.25 µm (0.005% FSO)	1 µm*	
Sampling rate / cycle		10 kHz	512 µs (≈ 2 kHz)	
Smallest light spot size	SMR	50 µm	30 µm (approximately) at reference distance	
	EMR	130 µm		
(B) Kinetic system				
Apparatus		X-Y Plotter (Roland DXY 1300)	Motorised lead screw table	
Sample travel speed		20 mm/s (maximum)	15.55 mm/s	
(C) DAQ system				
Interface hardware		Micro-Epsilon IFPS 2001	Serial port	NI AT-MIO-16E
Data acquisition rate		1000 /s (maximum)	87 /s	105 /s

Note:

SMR = Start of Measuring Range

EMR = End of Measuring Range

FSO = Full Scale Output

* Resolution was obtained using KEYENCE's analogue sensor controller, RD-50, with the number of averaging measurements set of 64.

6.2 Recommendation for further work

The thickness measurement system consists of three individual systems. Recommendation for further work for each system is discussed separately below.

6.2.1 Laser scanning system

Extension of stand-off distance – Currently the stand-off distance or reference distance i.e. the distance between the sensor and the sample is 30 mm and the measuring range is ± 10 mm. To measure the thickness the sample must be placed within $30 \text{ mm} \pm 10 \text{ mm}$. This distance might not be enough for some applications, for example, where the samples produce significant amount of heat or vapour. Therefore, it might need to extend the stand-off distance by some sort of means to meet the need of the applications. One of the possible choices to do so could be extending the laser beam path by using optical components like lens or prisms.

6.2.2 Kinetic system

(1) Increasing the sample travel speed – The sample travel speed what is currently being achieved from the kinetic system is 15.55 mm/s maximum. This is undoubtedly too slow for any fast, high precision scanning system. The increase in sample travel speed could be gained by utilising a combination of gear-boxes with the stepper motor.

(2) Two or three-dimensional scanning – Presently the sample to be measured can be travelled and scanned in only one direction. It would be a significant improvement if the sample could be travelled and scanned in two or three directions, i.e. X, Y, and Z directions. At least two X-Y stages would be required to perform this task.

(3) Use of proximity sensors and automation in sample movement – It would be a perfect idea if proximity sensors can be used with the kinetic system to change direction or stop automatically, especially, when high sample travel speed is involved.

6.2.3 Data acquisition and analysis (DAQ) system

(1) Development of computer interface – It could be possible to develop hardware and software interfaces with the computer for acquiring analogue signals from the stepper motor and the proximity sensors and then controlling them for better operation of the scanning system.

(2) End-user software development – Investigation of signal capturing as well as data analysis in a stand-alone software program is a key idea to perform end-user software development.

6.3 Conclusion

At present in-line inspection of products is becoming more widely used and of vital importance in manufacturing process industries. Micrometer level inspection of surfaces with optical systems based on discrete triangulation is very possible with good reliability and accuracy.

In present work a real-time laser scanning measurement system based on active laser-optical triangulation measurement with vertically incident mode has been successfully developed for the measurement of veneer thickness and profile, especially, in a defect-scanning system.

In this system a semiconductor laser is used as the light source, a built-in CCD array is used as the light-receiving unit to detect the position of light spot in image plane. A specially manufactured signal processing unit is used to acquire scanning signals and to calculate the thickness. As a result, the system is able to perform a real-time measurement task in a speed of 1953 point per second while its resolution is 1 μm .

Experiments are conducted using a laboratory prototype. Results are found to be reliable, and promising for practical applications. Although these are not quite accurate but they show the tendency of the achieved results. Efforts are made here to avoid the shortcomings and offer an applicable way of fast automatic inspection.

The approach is very much applicable to the measurement of other moving or extruded materials, and for quality control tolerance tests of finished products. The technique involves a digital ranging measurement to the sample face. Since the material is in general not constrained to a bottom plane, and hence may flop about in a random manner, the measurement is made on both sides simultaneously, from which the actual thickness is deduced.

In the conclusion it can be said that the proposed configuration, despite of its inherent limitations, presents advantages over other methods, especially because of its versatility and applicability to the inspection of rough, non optical, surfaces.

REFERENCES

1. L. S. Tanwar, B. Gupta, and S. C. Bansal, Sensitivity enhancement of an electro-optic sensor for displacement measurement, SPIE, J: Optical Engineering, Vol. 33, No. 6, June, 1994, pp 1950-1952
2. P. Cielo, On-line optical sensors for industrial material inspection, SPIE, Vol. 1266, Conf: In-Process Optical Measurements and Industrial Methods, 1990, pp 22-38
3. C. B. Hitz, Understanding Laser Technology, PennWell Books, 2nd Edition, 1991
4. J. Hecht, Understanding Lasers: An entry level guide, IEEE Press, 1992
5. H. Koebner, Industrial Applications of Lasers, John Wiley and Sons, 1984
6. Laser Electro-Optics Technology Series: Applications in Manufacturing, CORD Communications, 1991
7. M. F. M. Costa, and J. B. Almeida, System of Optical non-Contact Micro Topography, J: Applied Optics, Vol. 32, No. 25, Sept, 1993, pp 4860-4863
8. R. J. Collier, C. B. Burckhardt, and L. H. Lin, Optical Holography, Academic Press Inc., 1971
9. P. Hariharan, Optical Holography, Principles, Techniques, and Applications, Cambridge University Press, 1984
10. British Standard Radiation Safety of Laser Products and Systems, British Standards Institution, BS 4803: 1983
11. J. Keat, V. Balendran, K. Sivayoganathan, and A. Sackfield, 3-D data collection for object recognition, Conf: Advances in Manufacturing Technology VIII, 1994, pp 648-652
12. L. S. Wang, D. L. Lee, M. Y. Nie, and Z. W. Zheng, A study of the precision factors of large-scale object surface profile laser scanning measurement, Elsevier, J: Journal of Materials Processing Technology, Vol. 129, 2002, pp 584-587
13. V. Lombardo, T. Marzulli, C. Pappalettere, and P. Sforza, A time-of-scan laser triangulation technique for distance measurements, Elsevier, J: Optics and Lasers in Engineering, Vol. 39, 2003, pp 247-254

14. K. Pietzsch, U. Bauereib, and Ch. Feige, No defect goes undetected - continuous 100% materials testing using a laser scanner, *J: Kunststoffe German Plastics*, Vol. 78, No. 8, 1988, pp 692-696
15. Laser Scanner Inspection System, *J: Optical Information Systems*, Sept-Oct, 1988, pp 226-229
16. O. Kafri, I. Glatt, *The Physics of Moire Metrology*, John Wiley and Sons, 1990
17. M. Francon, *Laser Speckle and Applications in Optics*, Academic Press, 1979
18. R. W. McCullough, P. D. Bondurant, and J. L. Doyle, Laser-optical triangulation systems provide new capabilities for remote inspection of interior surfaces, *J: Materials Evaluation*, Dec, 1995, pp 1338-1345
19. K. R. Wu, A. Yan, J. Y. Liu, D. Zhang, and W. Yao, Reconstruction and analysis of 3-D profile of fracture surface of concrete, *J: Cement and Concrete Research*, Vol. 30, 2000, pp 981-987
20. R. G. Dorsch, G. Hausler, and J. M. Herrmann, Laser triangulation: fundamental uncertainty in distance measurement, *J: Applied Optics*, Vol. 33, No. 7, 1994, pp 1306-1314
21. H. Miao, and X. Wu, Active trigonometry and its application to thickness measurement on reflective surface, *SPIE*, Vol. 3558, 1998, pp 155-160
22. Manuel F. M. Costa, Surface inspection by an optical triangulation method, *SPIE, J: Optical Engineering*, Vol. 35, No. 9, Sept., 1996, pp 2743-2747
23. V. Bodlaj, Non-contact measurement of thickness and distance by laser beam deflection, *J: Siemens Forsch.-u. Entwickl.-Ber.* Vol. 4, No. 6, 1975, pp 336-344
24. A. Abuazza, and M. A. El-Baradie, Laser Scanning Inspection System – An Overview, *Conf: Advances in Materials and Processing Technologies (AMPT)*, Vol. III, 1999, pp 1939-1945
25. L. Guiying, C. Dianren, D. Zhenlin, and S. Zhengxun, Study on a displacement quantity test and measurement system with the laser light triangle method, *SPIE*, Vol. 3558, 1998, pp 165-167
26. L. Zeng, H. Matsumoto, and K. Kawachi, Two-directional scanning method for reducing the shadow effects in laser triangulation, *J: Measurement Science Technology*, Vol. 8, 1997, pp 262-266
27. M. Samson, and M. L. Dufour, A new stereo laser triangulation device for specular surface inspection, *SPIE*, Vol. 1332, *Optical Testing and Metrology III*, *Conf: Recent Advances in Industrial Optical Inspection*, 1990, pp 314-322

28. T. Koezuka, Y. Kakinoki, S. Hashinami, and M. Nakashima, Visual inspection system using multi-directional 3-D imager, SPIE, Vol. 1332, Optical Testing and Metrology III, Conf: Recent Advances in Industrial Optical Inspection, 1990, pp 323-331
29. W. J. H. Okkerse, S. P. P. Ottengraf, B. and Osinga-Kuipers, Bio-film thickness variability investigated with a laser triangulation sensor, J: Biotechnol Bioeng, Vol. 70, 2000, pp 619-629
30. T. A. Clarks, K. T. V. Grattan, N. E. Lindsey, Laser-based triangulation techniques in optical inspection of industrial structures, SPIE, Vol. 1332, Optical Testing and Metrology III, Conf: Recent Advancement in Industrial Optical Inspection, 1990, pp 474-486
31. L. J. Zeng, F. Yuan, D. Q. Song, and R. Zhang, A two beam laser triangulation for measuring the position of a moving object, Elsevier, J: Optics and Lasers in Engineering, Vol. 31, 1999, pp 445-453
32. Z. Xinming, S. Yongxin, and Y. Jiandong, Non-linearity of optical triangulation, SPIE, Vol. 3558, 1998, pp 262-265
33. Z. Ji, and M. C. Leu, Design of optical triangulation devices, J: Optics & Laser Technology, Vol. 21, No. 5, 1989, pp 335-338
34. J. R. Kerr, A Laser-Thickness Monitor, IEEE, J: Journal of Quantum Electronics, June, 1969, pp 338-339
35. N. Hutchins, and K. S. Choi, Accurate measurements of local skin friction coefficient using hot-wire anemometry, J: Progress in Aerospace Sciences, Vol. 38, No. 4-5, May-July, 2002, pp 421-446
36. <http://www.micro-epsilon.de/> [Accessed on: 11-01-2002]
37. <http://www.gamlasers.com/serv01.htm> [Accessed on: 29-08-2003]
38. M. Abe, S. Ohta, and M. Sawabe, Surface inspection using optical fibre sensor, SPIE, Vol. 1332, Optical Testing and Metrology III, Conf: Recent Advances in Industrial Optical Inspection, 1990, pp 366-376
39. P. L. Wong, and K. Y. Li, In-process roughness measurement on moving surfaces, J: Optics and Laser Technology, Vol. 31, No. 8, 1999, pp 543-548
40. W. Xiangjun, and K. Xinyu, Study on non-contact optical sensor for inside diameter measurements, SPIE, Vol. 3558, 1998, pp 288-292

41. Z. Yilbas and M. S. J. Hashmi, Surface roughness measurement using an optical system, Elsevier, J: Journal of Material Processing Technology, Vol. 88, 1999, pp 10-22
42. <http://www.keyence.co.uk/> [Accessed on: 18-07-2001]
43. S. Beary, Development of a laser scanning system for the inspection of surface defects, M. Eng. Thesis, Dublin City University, Ireland, Nov, 1996
44. <http://www.ni.com> [Accessed on: 07-02-2002]
45. R. H. Bishop, Learning with LabVIEW, Addison-Wesley, 1999
46. H. M. Wadsworth, Handbook of Statistical Methods for Engineers and Scientists, McGraw-Hill, 2nd Edition, 1998
47. <http://www.ergotest.com/> [Accessed on: 15-06-2003]
48. <http://www.picotech.com/> [Accessed on: 15-06-2003]
49. C. M. Harris, Shock and Vibration Handbook, McGraw-Hill, 4th Edition, 1996
50. A. Beiser, Physics, Addison-Wesley, 5th Edition, 1991
51. E. O. Doebelin, Measurement Systems, Application and Design, McGraw-Hill, 4th Edition, 1990

Appendix A

Related information regarding laser safety class

A.1 Accessible emission limit (AEL)

This is the maximum accessible emission level permitted for a particular class of laser products. Table A-1 displays the amount of accessible emission limit for laser products of different laser class.

Table A-1: Accessible emission limit (AEL) for wavelength ≥ 400 nm to ≤ 700 nm [10]

Laser class	Class 2	Class 3A	Class 3B	Class 4
Emission duration				
> 0.25 s	10^{-3} W	5×10^{-3} W and 25 W m^{-2}	0.5 W	0.5 W

A.2 Maximum permissible exposure (MPE)

Maximum permissible exposure refers to that level of laser radiation to which, in normal circumstances, persons may be exposed without suffering adverse effects. MPE level represents the maximum level to which the eye or skin can be exposed without consequential injury. It is related to the wavelength of the radiation, the pulse duration or exposure time, the tissue at risk and, for radiation in the wavelength range 400 nm to 1400 nm, the size of the retinal image.

A.3 Laser products classification

A laser product shall be classified on the basis of that combination of output and wavelength of the accessible laser radiation over the full range of operational

capability at any time after manufacture that results in its allocation to the highest appropriate class [10].

The time basis for the classification of all continuous wave lasers and repetitively pulsed laser products shall be 30000 s, except that for all laser products with a wavelength in the visible or infra-red region the design and use of which are such that there is no need to look into a laser beam or to be exposed to laser radiation, the time basis shall be reduced to 300 s.

All of the laser products can be classified into any of the laser class stated below. Table A-2 is the summary of manufacturing requirements for laser products of different class.

A.3.1 Class 1 laser products

Class 1 laser products shall be those that are inherently safe either because of its low power or because their engineering design is such that in any event the MPE level cannot be exceeded.

A.3.2 Class 2 laser products

Class 2 laser products shall be those that are low-power devices emitting visible radiation, i.e. in the wavelength range 400 nm to 700 nm, and no more than the AEL of Class 1 for other spectral regions. For continuous wave lasers the output power in this class shall be limited to 1 mW averaged over 0.25 s. These laser products are not inherently safe, but where eye protection is normally afforded by the aversion responses, including the blink reflex. Precautions should be taken to prevent continuous intentional viewing of the direct beam; a momentary (0.25 s) exposure as would occur in accidental viewing is not considered hazardous. Where reasonably practicable the beam should be terminated at the end of its useful path and the laser should not aimed at personnel, particularly at head height.

A.3.3 Class 3A laser products

Class 3A laser products shall be those that are emitting visible radiation, i.e. in the wavelength range 400 nm to 700 nm, with an output power up to 5 mW for continuous wave lasers and no more than the AEL of Class 1 for other spectral

regions. The irradiance at any accessible point of the beam shall not exceed 25 W m^{-2} . Protection for the unaided eye is normally afforded by aversion responses, including the blink reflex, but direct intra-beam viewing with optical aids may be hazardous.

Table A-2: Summary of manufacturing requirements for laser products [10]

Laser class Subject	Class 1	Class 2	Class 3A	Class 3B	Class 4
Protective housing	Required to prevent radiation in excess of AEL				
Remote control	Not required			Required	
Key control	Not required		Key to be removed when laser product not in use		
Emission indicator	Not required		Required when laser is energised		
Location of controls	Not required		Controls to be so located that adjustment does not require access to AEL above class 1 or 2		
Viewing optics	Emission from all viewing systems to be below class 1 AEL as appropriate				
Scanning laser products	Scan failure not to cause product to exceed its classification				
Class label	Required				
Aperture label	Not required			Required	
Servicing label	Required as appropriate to the class of laser				
Override interlock label	Required under certain conditions as appropriate to the class of laser				
Remote interlock	Not required			Connect to room or door circuits	
Warning signs	Not required	Summarise precautions on warning signs			
Beam termination	Not required	Terminate beam at end of useful length			
Specular reflection	No special precautions	Care to be taken	Prevent unintentional reflection		

A.3.4 Class 3B laser products

Class 3B laser products shall be those that may emit in excess of the AEL for Class 3A (for visible radiation), and/or Class 1 (for invisible radiation). Emission shall not

exceed 0.5 W for continuous wave lasers (emission duration longer than 0.25 s) and 10^5 J m^{-2} for pulsed lasers. Direct intra-beam viewing of these devices may be hazardous but under certain conditions they may be safely viewed via a diffuse reflector. These conditions are: (a) a minimum viewing distance of 50 mm between screen and cornea; and (b) a maximum viewing time of 10 s; and (c) a minimum diffuse image diameter of 5.5 mm. If any of these conditions are not satisfied, careful evaluation of the hazard is necessary.

A.3.5 Class 4 laser products

Class 4 laser products shall be those that are high output devices, with outputs exceeding the AELs for Class 3B as specified in Table A-2. These are capable of producing hazardous diffuse reflections. These may cause skin injuries and could also constitute a fire hazard. Their use requires extreme caution.

Appendix B

Related information regarding products used in Surface Profile Measurement System

B.1 Laser displacement sensor, Micro-Epsilon optoNCDT 2000

Table B-1: Specifications of Micro-Epsilon optoNCDT 2000 [36]

Measuring range	± 2.5 mm	
Stand-off distance	58 mm	
Non-Linearity 0.03 % FSO (typical)	± 1.5 µm	
Resolution 0.005 % FSO	0.25 µm	
Temperature stability ⁽¹⁾	± 0.1 µm / k	
Zero sensitivity		
Long-term stability ⁽²⁾	± 1 µm / month	
± 0.02 % FSO/month		
Light source	Red semiconductor laser	
	Wavelength	670 nm
	Class	Laser class 2
Smallest light spot size	SMR	50 µm
	EMR	130 µm
Sampling rate	10 K Hz	
Angle error at ± 30°	Typically ± 0.5 %	
Tilting at the X or Y axis		
Angle error at ± 15°	Typically ± 0.13 %	
Tilting at the X or Y axis		
Permissible incident light for direct radiation of a diffusely reflecting sample	30,000 lux	
Protection	IP 64 (with connected cable)	
Operating temperature	0 °C to + 40 °C (with free air circulation)	
Storage temperature	- 20 °C to + 70 °C	
Output	Analogue	± 5 V / R > 1 KΩ
	Digital	RS485 / 687.5 KBaud
Power supply through Interface card IFPS 2001	4 supply voltages required + 5 Vdc / 500 mA, + 12 Vdc / 250 mA - 12 Vdc / 120 mA, + 24 Vdc / 30 mA	

The specified data apply for a diffusely reflecting matt white ceramic sample.

⁽¹⁾ applies for fixing by the top dovetail guide.

⁽²⁾ at 20° C constant, sensor permanently in operation.

Notes: The notations SMR, EMR, FSO refer to Start of Measuring Range, End of Measuring Range, and Full Scale Output respectively.

B.2 Data interface card, Micro-Epsilon IFPS 2001

B.2.1 Description

This card provides an RS485 / 687.5 Kbaud interface to a PC-AT (80286...80486). It requires 16-bit AT bus slot and occupies two slots because of the components height on the card. It has an integrated power supply for operating a laser sensor, Micro-Epsilon optoNCDT 2000, that is, the laser sensor gets power through the data interface card and no external power supply unit is needed. The laser sensor is connected with this card by a special sensor cable, C2001-3. The sensor is switched on or off and the data transfer is carried out by the sensor operating software, *Micro-Epsilon ILD2000 Demo Version 3.1*.

B.2.2 Specifications

Table B-2: Specifications of Micro-Epsilon IFPS 2001 [36]

Model	IFPS 2001
Interface	1 x RS485 / 687.5 Kbaud
Current requirement	5 Vdc / 0.5 A +12 Vdc / 1.5 A
Output voltages*	+5 Vdc, +12 Vdc, -12 Vdc, +24 Vdc
Reset	Possible by software
Connector	1 x HD sub-miniature 15-pin connector
Dimension	337 x 114 x 33 mm ³ (equivalent to the depth of 2 PC slots)

* In the standard version, the output voltages are set for 3 m C2001-3 sensor cable.

B.3 Measured value output

After putting the sensor in operation, the averaged value is available in the range of 0...65535 (16-bits) at the output of the serial interface. These output values are interpreted in the following manner (Table B-3).

Table B-3: Output value interpretation [36]

Output value	Interpretation
0 ... 1637	Measuring value out of the range (*)
1638 ... 63896	Measuring value in the range (*)
63897 ... 65534	Measuring value out of the range
65535 >>	Poor Target << no range

(*) Both measured values no longer correspond to the sensor specification. They are used for adjustment in order to slightly exceed or drop below the measured value.

The hardware of the interface corresponds to the standard for RS 485. The interface has been tested for an output cable length of 13 m (3 m sensor power supply unit + 10 m PS-PC card) at a data rate of 687.5 kBaud.

There are three LED indicators on the sensor marked as “*Out of Range*” (means exceed of upper or lower range values of the sensor), “*Poor Target*” (means laser light is projected onto a non-measurable target i.e. reflection too low), and “*ON/OFF*” (means whether laser on work). Table B-4 describes different states of LED indicators with its corresponding serial interface output.

Table B-4: LED indicators with its corresponding serial interface output [36]

LED on the sensor	Description	Serial interface
green >>LASER ON/OFF<<	Laser in operation.	
red >> POOR TARGET <<	Target does not reflect sufficiently. Penetration depth of the laser point is too deep – corona formation is too great.	Output 65535
red >> OUT OF RANGE <<	Target is still in detection range but slightly beyond of measuring range.	Output 0...1637 or 63897...65534
red >> POOR TARGET << red >> OUT OF RANGE <<	No target available.	Output 65535

B.4 Sensor operating software, Micro-Epsilon ILD2000 Demo Version 3.1

Figure B-1 is the starting window of the sensor operating software, *Micro-Epsilon ILD2000 Demo Version 3.1*. Like other customised software, it has many menu-driven options for performing necessary tasks. The laser displacement sensor, Micro-Epsilon optoNCDT 2000, is fully operated and controlled by this software. The features of this program include opening and saving a measurement file, selecting of sensor type, turning sensor power on and off, taking single shot or continuous measurement, setting various options for measurement, etc.



Figure B-1: Starting window of Micro-Epsilon ILD2000 Demo Version 3.1

B.5 Experiment considerations

In order to achieve an accurate measurement from the sensor system, a set of experiment criteria must be fulfilled. These are discussed below.

The stand-off distance is 58 mm

This refers to the distance between the sensor head and the sample.

The measuring range is ± 2.5 mm

The sensor can detect any point on sample surface only when the sample is placed within ± 2.5 mm of the reference plane of the sensor.

The maximum values to be stored is 8,000

The system can store at best 8,000 values at a time into its memory what can be saved onto a storage device for later use.

The maximum sampling rate is 1 kHz

This indicates the frequency of scan limit of the sensor.

The warm-up time is 20 minutes

A warm-up time of at least 20 minutes is necessary before taking data in order to achieve a uniform temperature distribution into the sensor.

Appendix C

Related information regarding products used in Thickness Measurement System

C.1 Figures of products

C.1.1 Laser scanning system



Figure C-1: Keyence LK-031 [42]



Figure C-2: Keyence RD-50RW [42]



Figure C-3: Keyence LK-2001 [42]

C.1.2 Kinetic system

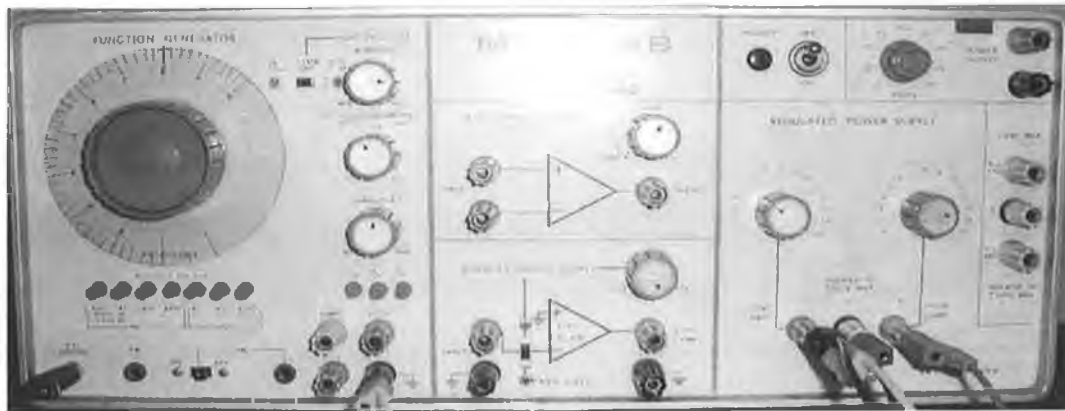


Figure C-4: MINI-LAB 603B

C.1.3 Data acquisition and analysing system



Figure C-5: Data acquisition card [44]



Figure C-6: Break-out box [44]

C.2 Specifications

C.2.1 Keyence LK series

Table C-1: Specifications of Keyence LK series [42]

Model	Sensor head	LK-031
	Controller	LK-2001
Reference distance		30 mm
Measuring range		± 5 mm
Light source		Red semiconductor laser
	Wavelength	670 nm
	Class IEC	Class 2
	FDA	Class II
Spot diameter		Approximately 30 μm (at reference distance)
Resolution		1 $\mu\text{m}^{(1)}$
Linearity		$\pm 0.1\%$ F.S ⁽²⁾
Sampling cycle		512 μs
Analog output	Voltage output	± 5 V (1 $\mu\text{m}/\text{mV}$) ⁽³⁾
	Impedance	100 Ω
	Current output	4 to 20 mA (applicable load: 350 Ω max.)
Alarm output		NPN: 100 mA max. (40 V max.) (N.C) Residual voltage 1 V max.
Power supply		24 VDC $\pm 10\%$
Current consumption		400 mA max.
Temperature fluctuation	Sensor head	$\pm 0.1\%$ F.S/ $^{\circ}\text{C}$
	Controller	$\pm 0.1\%$ F.S/ $^{\circ}\text{C}$
Ambient light		Incandescent or fluorescent lamp: 10,000 lux max.
Ambient temperature		0 $^{\circ}\text{C}$ to +50 $^{\circ}\text{C}$
Housing	Sensor head	Aluminium die-cast
	Controller	Poly-carbonate
Weight (including cable)	Sensor head	Approximately 260 g
	Controller	Approximately 515 g

⁽¹⁾ Resolution was obtained using Keyence's analog sensor controller (RD-50) with the number of averaging measurements set to 64.

Notes: The ripple of the analog output may be 1 mV or more due to common mode noise when observed with an oscilloscope or a high-speed A/D conversion board.

⁽²⁾ Linearity was obtained using Keyence's standard target (Zirconia block gauge).

⁽³⁾ When measurement is impossible, 12 V is output.

C.2.2 Analog sensor controller

An analog sensor controller, Keyence RD-50RW, mainly takes different input signal from external devices, performs different functions and finally displays the value of those tasks. It also can communicate with an external computer via the RS-232C interface connector port. Remote operations such as data transmission and setting changes can be performed at this stage.

Special features [42]:

- ***MDL function*** – Non-linear analogue input from external equipment can be linearised using the Multi-point Digital Lineariser (MDL) function.
- ***Built-in high-pass and low-pass filters*** – This facilitates to detect only the desired frequency range of the analogue signal.

High-Pass Filter (HPF) function enables to obtain only abrupt fluctuations in analogue signal. Low-Pass Filter (LPF) function enables to ignore abrupt fluctuations in analogue signal.

- ***High-speed sampling*** – The high-speed sampling rate of 2,000 times/sec enables detection of any sudden changes in the input signal. The high-speed comparator circuit performs differentiation at a high speed of 1ms.

- **Easy-to-see display** – The RD-50RW uses a three-colour LED display. When the measured value is within the tolerance limits, the value is displayed in green. If the measured value is out of the tolerance limits, it is displayed in orange or red.

Specifications:

Table C-2: Specifications of Keyence RD-50RW [42]

Measurement function		DC voltage measurement
		DC current measurement
A/D converting system		Successive comparison
Measuring range		± 5 VDC, ± 10 VDC
		4 to 20 mA DC (selectable)
Display range		-19999 to +39999
Measuring accuracy		$\pm 0.03\%$ F.S (at ± 5 VDC range)
		$\pm 0.03\%$ F.S (at ± 10 VDC range)
		$\pm 0.05\%$ F.S (at 4 to 20 mA DC range)
Input Impedance		1 M Ω (for voltage input)
		350 Ω (for current input)
		System
	Number of inputs	2
Sampling rate		2000/s
Display rate		20/s
Display character		7-segment, 3-colour LED (character height: 15.24 mm)
Range-over alarm		FFFF is displayed
Analog	Voltage	± 10 VDC
Voltage	Impedance	100 Ω
Output	Response time ⁽¹⁾	1 ms (when average number 1)
Interface		Data output and control input through RS-232C
Rating	Power supply	24 VDC $\pm 10\%$
	Current consumption	240 mA max.
Ambient temperature		0 to +50 °C
Weight		Approx. 700 g (excluding fittings)

(1) Requires 1.5 ms every second during self-compensation sequence to prevent temperature fluctuation.

C.2.3 Power supply unit

Keyence KV-U6W is a dedicated power supply unit that is designed to serve appropriate power to other Keyence products used in the system with more precisely and safely.

Specifications:

Table C-3: Specifications of Keyence KV-U6W [42]

Operation system	Switching type
Input supply voltage	100 to 240 VAC (50/60 Hz) \pm 10%
Output voltage	24 VDC \pm 10%
Output current	0.8 A
Ripple/noise	240 mV p-p max.
Relative humidity	35 to 85%
Ambient temperature	0 to +50 °C
Withstand voltage	1500 VAC applied between all external terminals and housing (1 min)
Vibration	10 to 55 Hz, 1.5 mm double amplitude in X, Y and Z directions respectively
Insulation resistance	50 M Ω min. between external terminal and housing (measured by 500 VDC megohmmetre)
Weight	Approx. 210 g (excluding fittings)

C.3 General information for use

C.3.1 Laser safety note

Products of Keyence LK series are categorised into class A (EN55011: EMI standard). In a domestic environment it may cause radio interference. If signal

interface is deleted from the device, proper cable shielding would be required. However, no such interference was found in the current set-up.

The sensor head is classified as a class 2 laser (Model: IEC 825-1 11.1993 and FDA). Operation of the laser should be indicated by an audible or visual warning signal as a precaution. The Keyence LK-031 sensor uses a semiconductor laser with wavelength 670 nm (visible / red). The maximum optical output power is 1 mW. Despite the low laser power, to look directly into the laser beam should be avoided. It is therefore recommended to wear protective laser goggles or laser safety spectacles while using the LK series.

C.3.2 Experiment set-up

The experiment should be carried out in a dry and clean room that is free from dust, a strong source of illumination and strong wind. Air vents in the main housing must be free. The target should always be placed at right angle to the sensor in order to achieve highest accuracy. A warm-up time of at least 30 minutes is necessary before taking data in order to achieve a uniform temperature distribution in the sensor units. While taking measurement any kind of mechanical vibration of either the target or the sensor must be avoided. The measured signal is available in a voltage range of ± 5 V or in a current range of 4 to 20 mA at the analogue output of the controller unit.

Appendix D

Experiment to determine mechanical vibration in Thickness Measurement System

D.1 Experiment set-up

The equipments used in this experiment were (1) an accelerometer, ET-ACC-02, manufactured by Ergotest [47], (2) an analogue to digital converter, ADC-12, supplied by Pico Technology Ltd. [48], and (3) a 5 V power supply unit.

The necessary data acquisition software was downloaded from the web site of Pico Technology Ltd. and installed into the computer. The software products were *PicoLog Player*, *PicoLog Recorder*, and *PicoScope*.

D.2 Experiment procedure

The accelerometer was fixed firmly with double-sided sticky tape on the top of the lead screw table. The sensitivity axis of the accelerometer was placed perpendicular to the surface of the lead screw table.

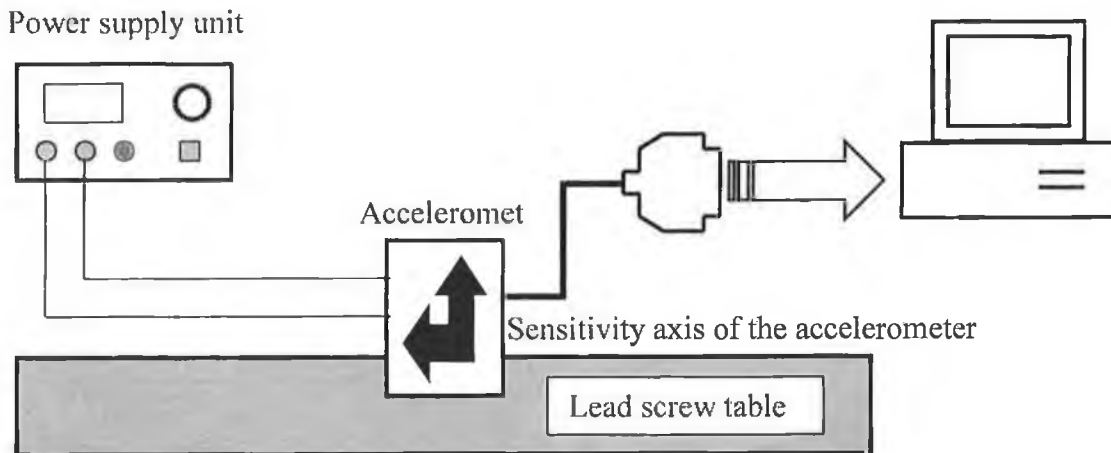


Figure D-1: Set-up diagram of the experiment to determine mechanical vibration

The output signals of the accelerometer were sent to the computer via the ADC-12 which was plugged into the parallel port of the computer. Then the accelerometer was powered on and the kinetic system was turned on to run the lead screw table. The programs *PicoLog Recorder* and *PicoScope* were executed in turns in order to measure the maximum vibration acceleration and the vibration frequency respectively to calculate the actual vibration displacement.

D.3 Calibration

The accelerometer was used to measure the gravitational acceleration in both directions (one with the accelerometer sensitivity axis placed in the direction of gravity and one with the sensitivity axis placed opposite to the gravitational field). The absolute values of the voltage readings were then added and divided by twice the gravitational field ($2 \times 9.81 \text{ m/s}^2$) to obtain the sensor sensitivity which was found to be 10 mV/m/s^2 as follows:

g (in line with gravitational field) = 2.630 V and

$-g$ (opposite to gravitational field) = 2.434 V. Thus,

$2.630 \text{ V} - 2.434 \text{ V} = 2 \times g = 2 \times 9.81 \text{ m/s}^2$ and the sensitivity is 10 mV/m/s^2 .

D.4 Data acquisition

D.4.1 Measurement of maximum vibration acceleration

When the program *Picolog Recorder* was executed it automatically collected the acceleration signals in a period of 500 ms and at a sampling frequency of 2000 Hz. Then the maximum acceleration was taken from the graph. This process was repeated several times at different motor frequency (i.e. sample speed).

Calculation of maximum vibration acceleration: Maximum vibration acceleration was calculated from the peak to peak acceleration what equalled to the minimum acceleration deducted from the maximum acceleration. Following is a sample calculation of maximum vibration acceleration at motor frequency of 700 Hz, see Figure D-2.

Peak to peak acceleration

= Maximum acceleration (at point A) - Minimum acceleration (at point B)

= $(2.470 - 2.386) * 1000 / 10 \text{ m/s}^2$ (as the sensitivity is 10 mV/m/s^2)

= 8.4 m/s^2

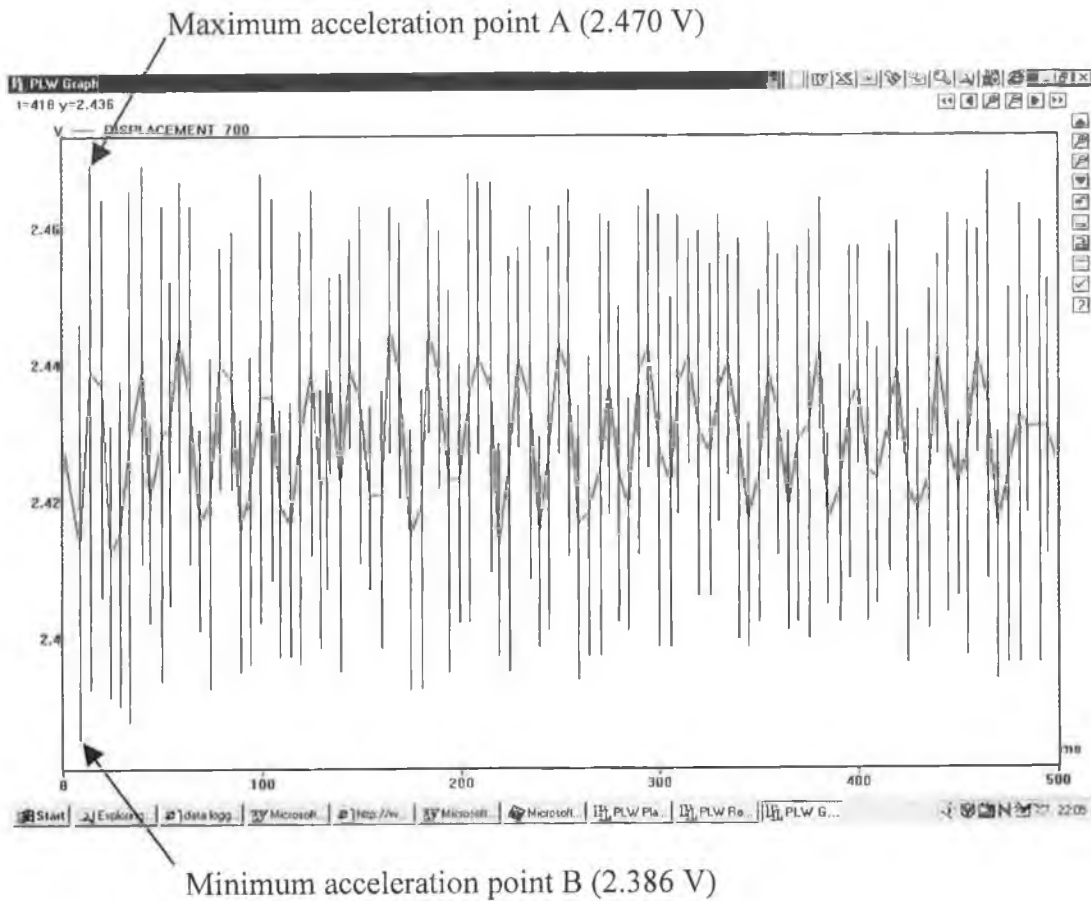


Figure D-2: Acceleration signals at motor frequency of 700 Hz

Table D-1 displays the maximum vibration acceleration at different motor frequency calculated from the above process.

Table D-1: Measurement of maximum vibration acceleration

Motor Frequency (Hz)	Sample Speed (mm/s)	Maximum Acceleration (m/s^2)
600	9.53	10.7
700	11.01	8.4
800	12.52	5.9
900	13.81	2.45

D.4.2 Measurement of vibration frequency

When the program *PicoScope* was executed, it produced the power spectrum density for the vibration at a certain motor frequency. After analysing the graph, the vibration frequency with the maximum power density was selected. Again this process was repeated several times at different motor frequency (i.e. sample speed). Figure D-3 is an example of selection of vibration frequency.

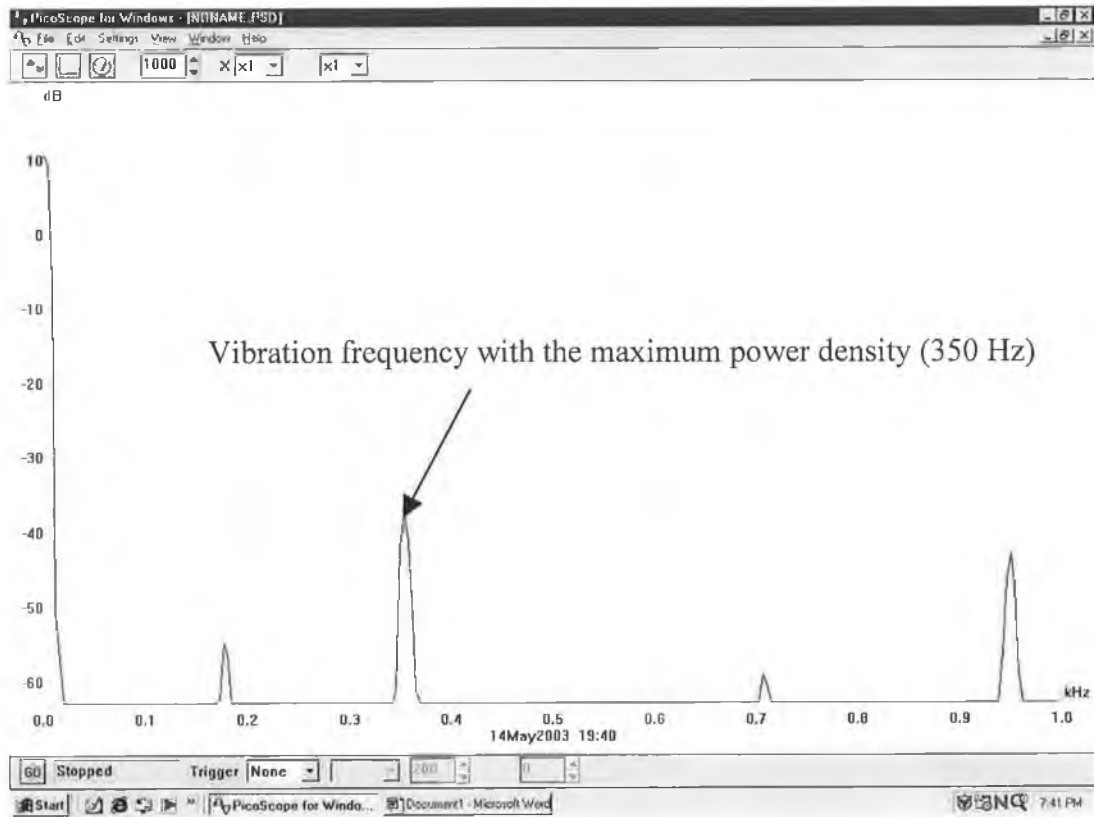


Figure D-3: Vibration frequency at motor frequency of 700 Hz

Table D-2 displays the vibration frequency at different motor frequency found from the above process.

Table D-2: Measurement of vibration frequency

Motor Frequency (Hz)	Sample Speed (mm/s)	Vibration Frequency (Hz)
600	9.53	300
700	11.01	350
800	12.52	400
900	13.81	450

D.5 Calculation of displacement caused by mechanical vibration

Following is a sample calculation of displacement caused by mechanical vibration at motor frequency of 700 Hz.

The required equation for calculation is,

$$\text{Acceleration} = (2 \pi f)^2 \times \text{Displacement} \quad [\text{D.1}]$$

After putting values into the above equation for vibration acceleration and vibration frequency (f) at motor frequency of 700 Hz, see Table D-1 and Table D-2, we get,

$$8.40 = (2 \times 3.141 \times 350)^2 \times \text{Displacement}$$

$$\Rightarrow \text{Displacement} = 0.0017 \text{ mm}$$

Table D-3 tabulates the displacement values caused by mechanical vibration at different motor frequency found from the above calculation.

Table D-3: Measurement of displacement caused by mechanical vibration

Motor Frequency (Hz)	Sample Speed (mm/s)	Displacement (mm)
600	9.53	0.0030
700	11.01	0.0017
800	12.52	0.0009
900	13.81	0.0003

Appendix E

Drawings of the Thickness Measurement Rig assembly

The next few pages are the drawings of the thickness measurement rig assembly in AutoCAD 2000. Following is a list of the figures drawn.

FIGURE E-1: Laser displacement sensor

FIGURE E-2: Spacers for sensor heads

FIGURE E-3: Bracket and spacers

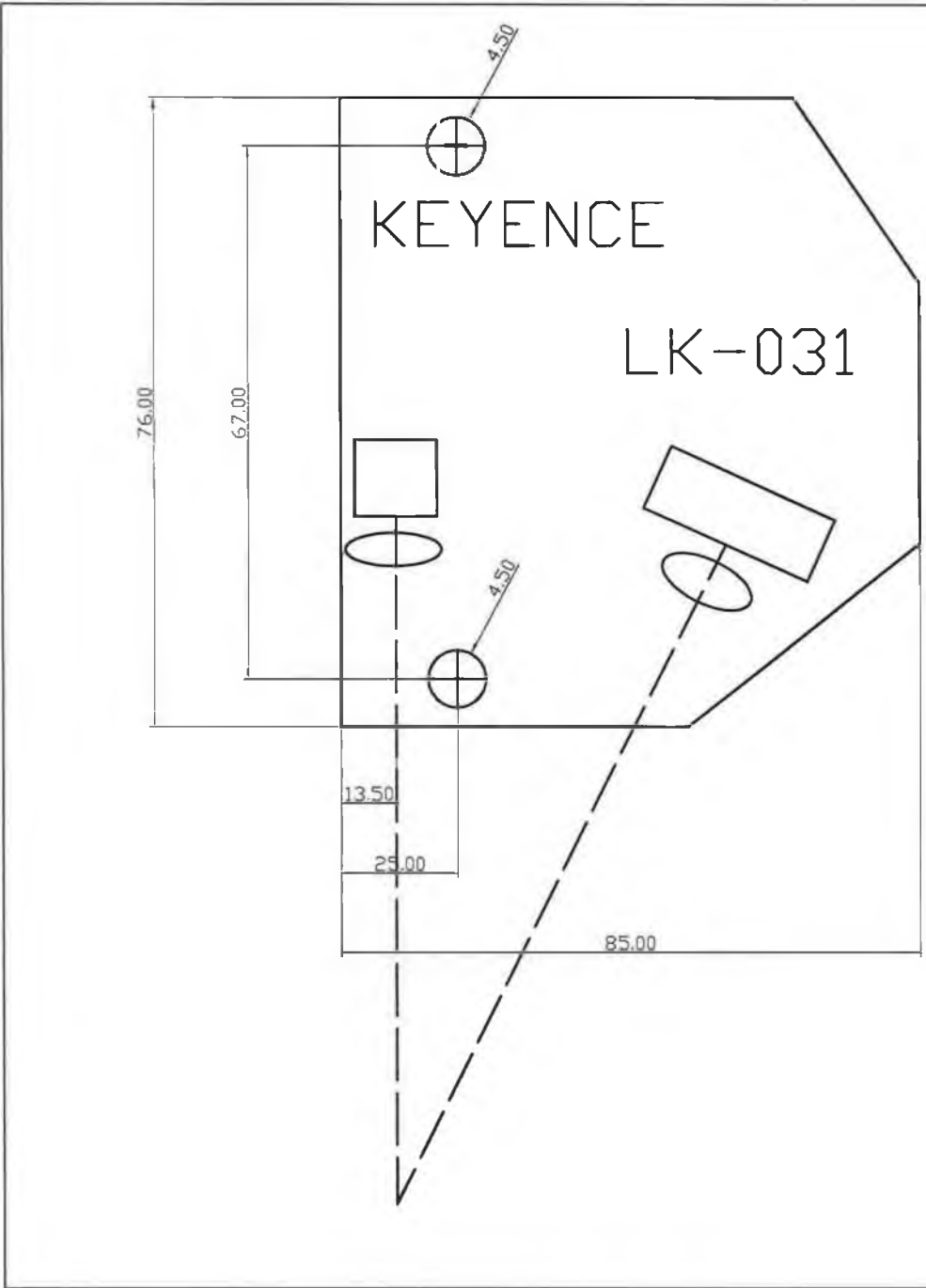
FIGURE E-4: Sample holders

FIGURE E-5: Micrometer stage

FIGURE E-6: Lead screw slide

FIGURE E-7: Lead screw table

FIGURE E-8: Stepper motor



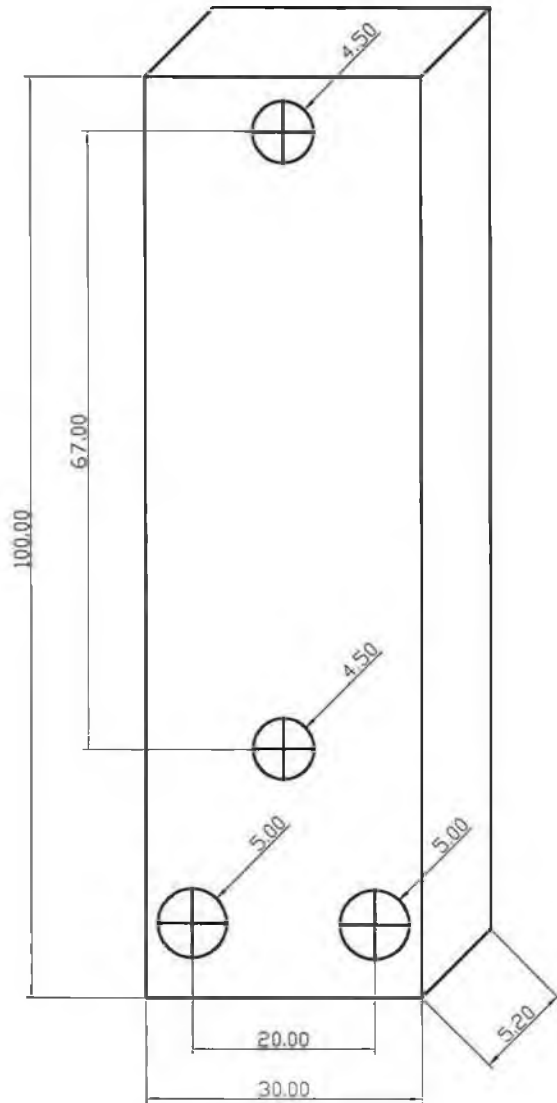
(All dimensions are in mm)

FIGURE E-1

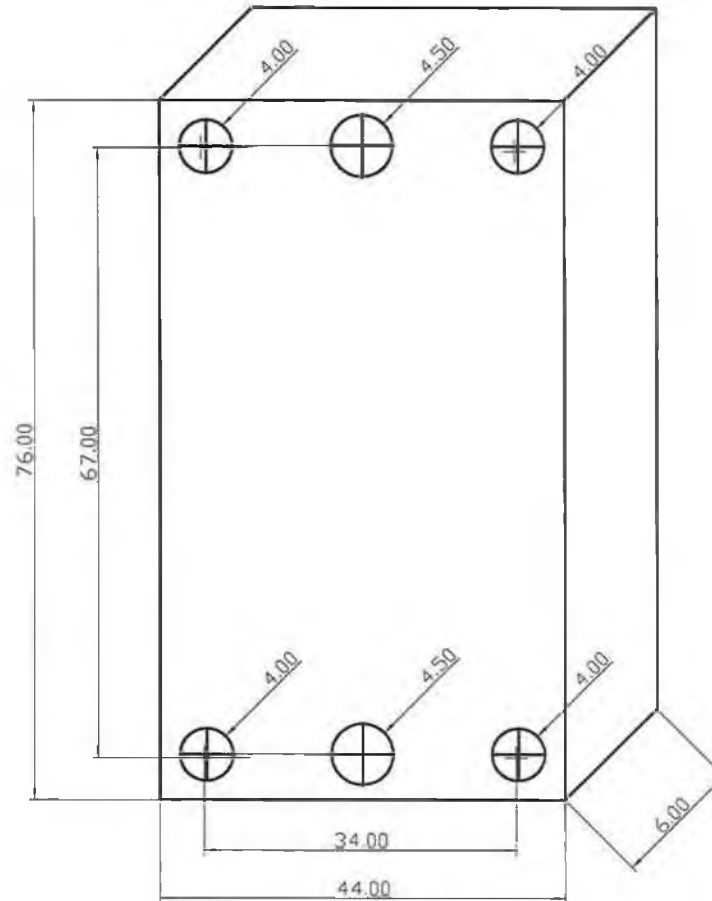
Name: Laser Displacement Sensor

Model: optoNCDT 2000

Manufacturer: Micro-Epsilon Messtechnik
GmbH & Co., Germany



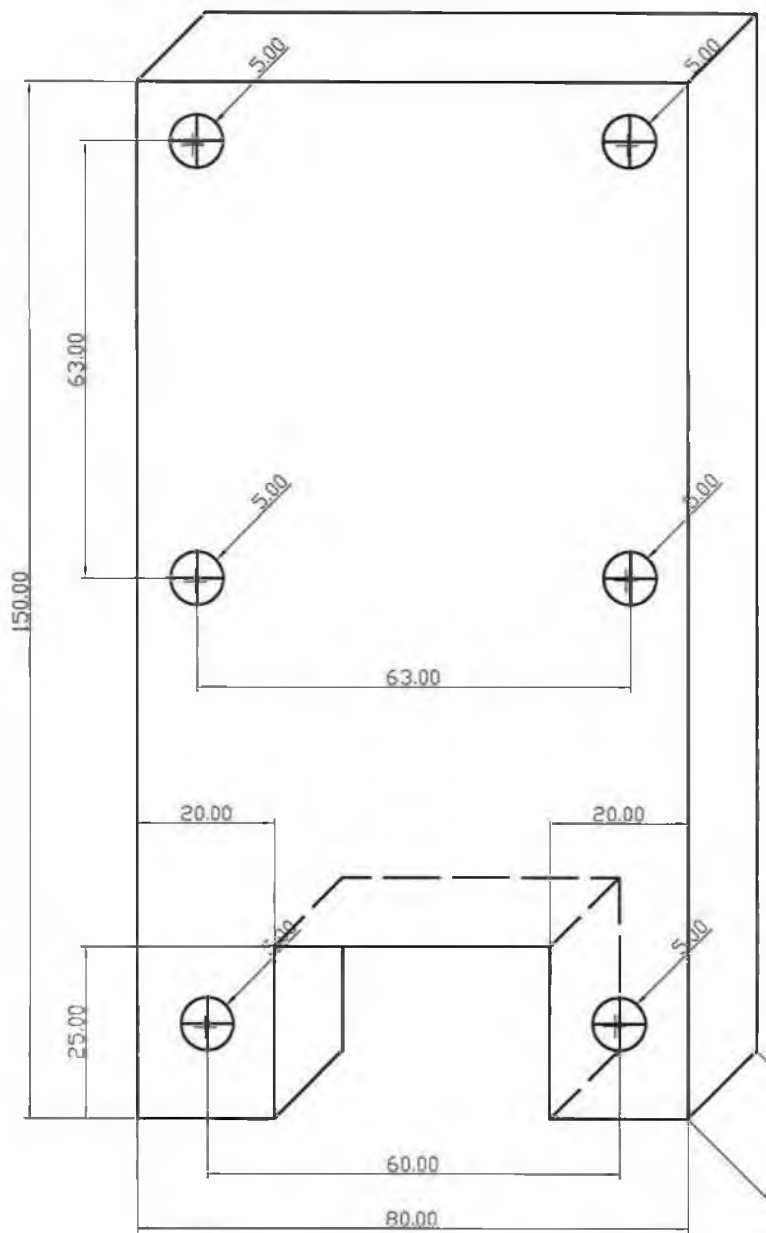
Spacer for Sensor B



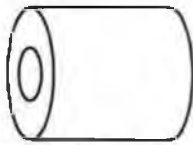
Spacer for Sensor A

(All dimensions are in mm)

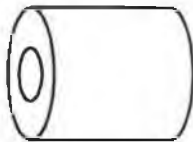
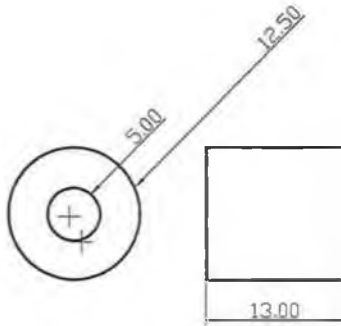
FIGURE E-2
Name: Spacers for Sensor Heads
Date: 22-10-2004



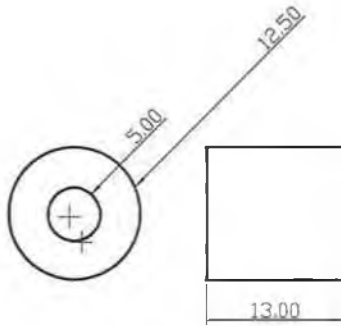
Bracket for Micrometer Stage



Spacer_1



Spacer_2



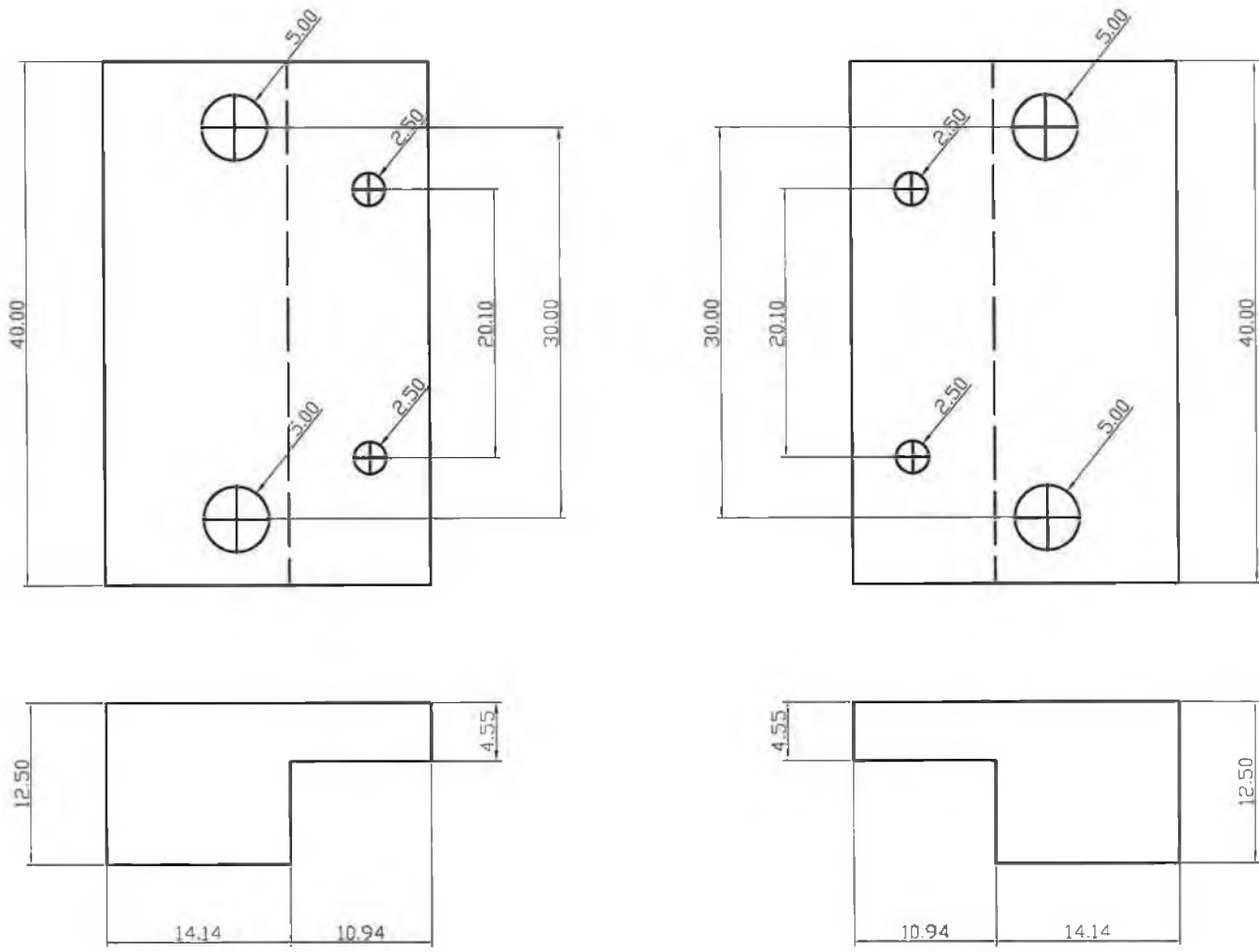
Spacers to adjust the distance of Sensor A with Sensor B

(All dimensions are in mm)

FIGURE E-3

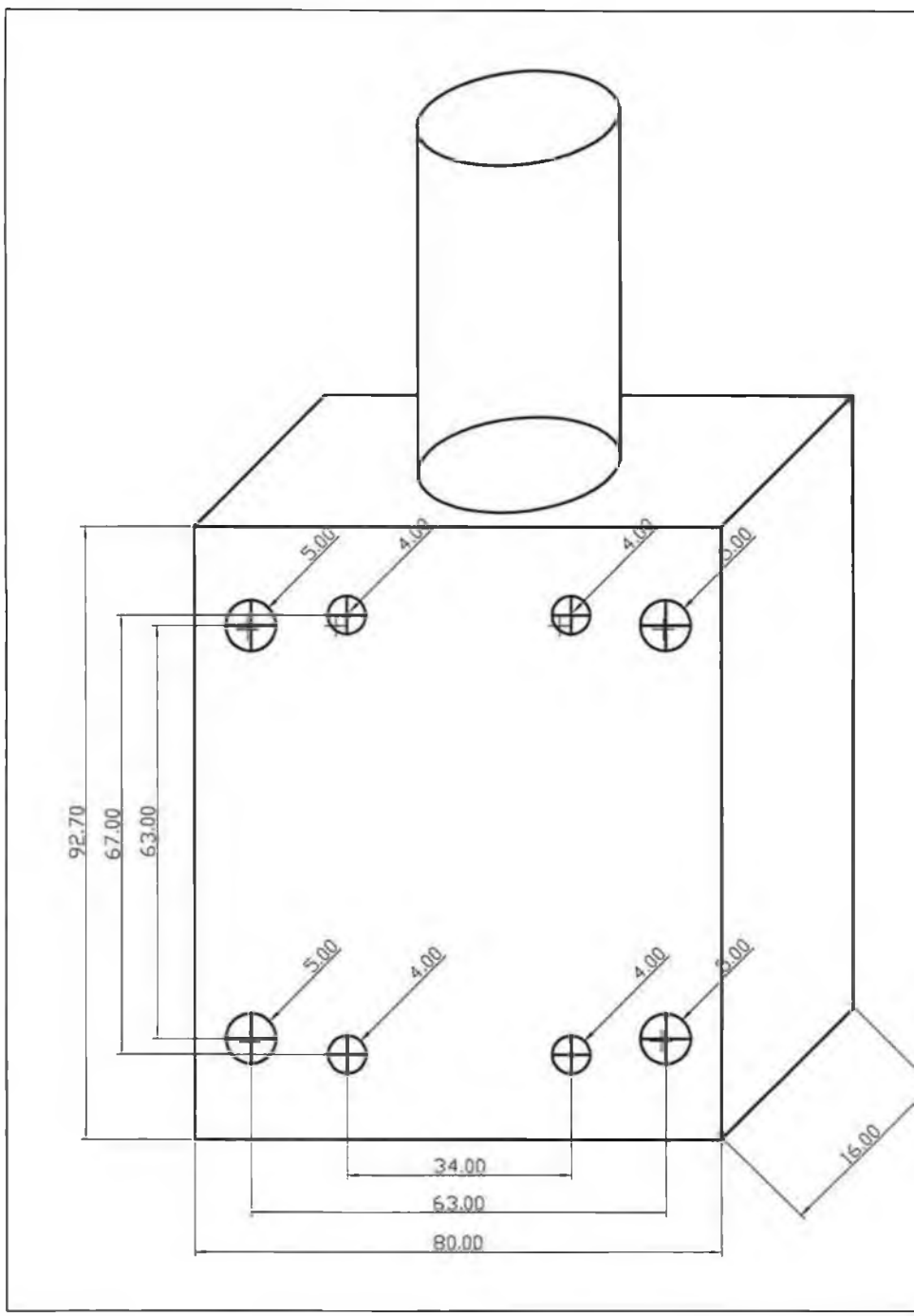
Name: Bracket and Spacers

Date: 23-10-2004



(All dimensions are in mm)

FIGURE E-4
Name: Sample holders
Date: 24-10-2004

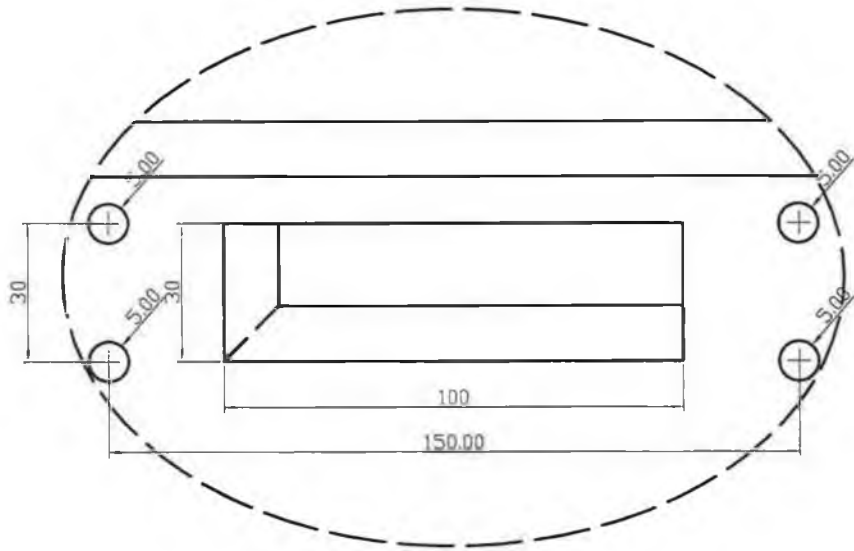
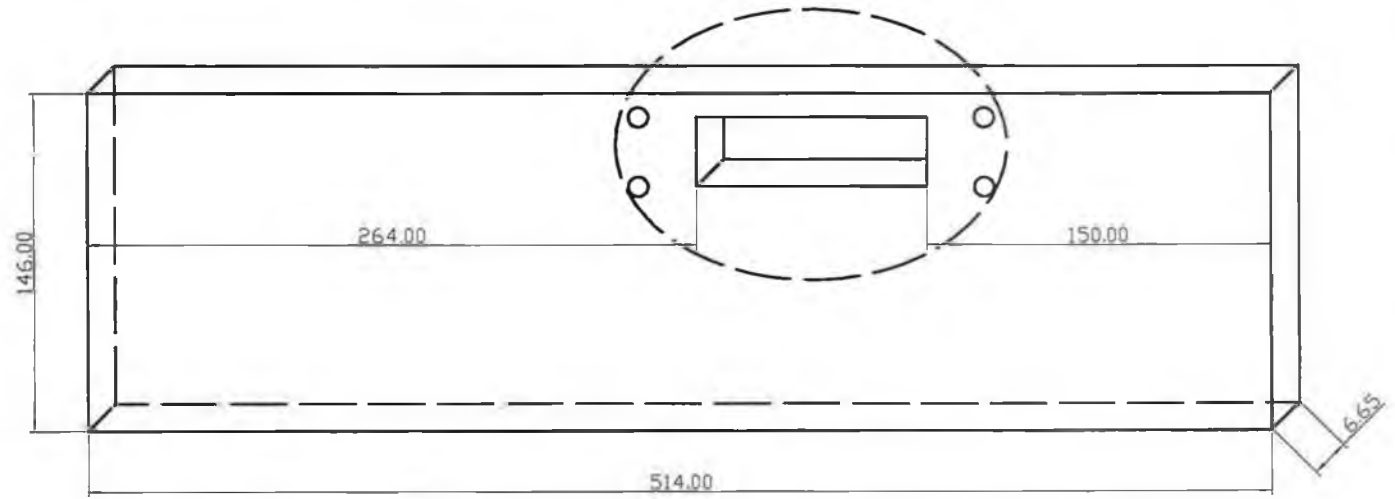


(All dimensions are in mm)

FIGURE E-5

Name: Micrometer Stage

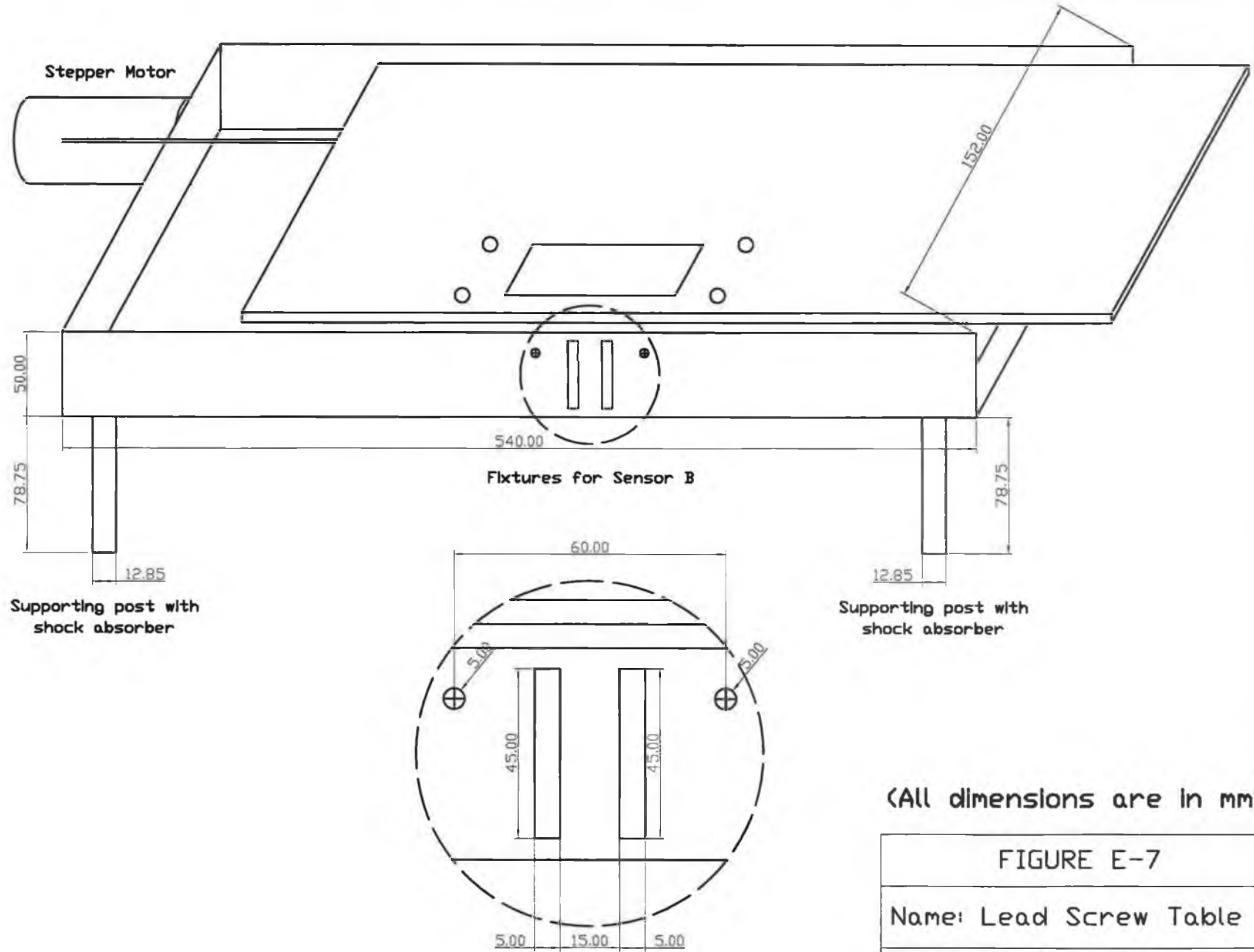
Date: 25-10-2004



Window for scanning facility

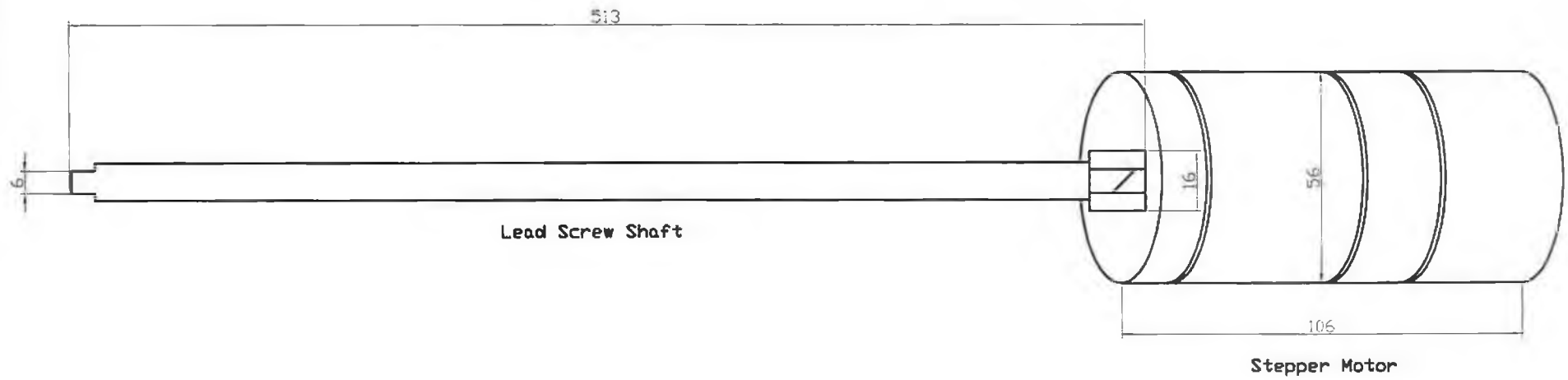
(All dimensions are in mm)

FIGURE E-6
Name: Lead Screw Slide
Date: 26-10-2004



(All dimensions are in mm)

FIGURE E-7
Name: Lead Screw Table
Date: 27-10-2004



(All dimensions are in mm)

FIGURE E-8

Name: Stepper Motor

Date: 28-10-2004

Appendix F

Drawings of the samples

The next few pages are the drawings of the following samples in AutoCAD 2000, which were used in the present work.

FIGURE F-1: Brass plate with 7 through holes

This sample was used in Section 3.6.1 (see Figure 3-4), Section 3.6.2 (see Figure 3-6), and Section 5.4.6 (see Figure 5-18).

FIGURE F-2: Brass plate with 5 blind holes

This sample was used in Section 3.6.3 (see Figure 3-9).

FIGURE F-3: Aluminium taper block

This sample was used in Section 5.4.1 (see Figure 5-5).

FIGURE F-4: Aluminium block with various thickness

This sample was used in Section 5.4.2 (see Figure 5-8).

FIGURE F-5: Kinked thin aluminium plate

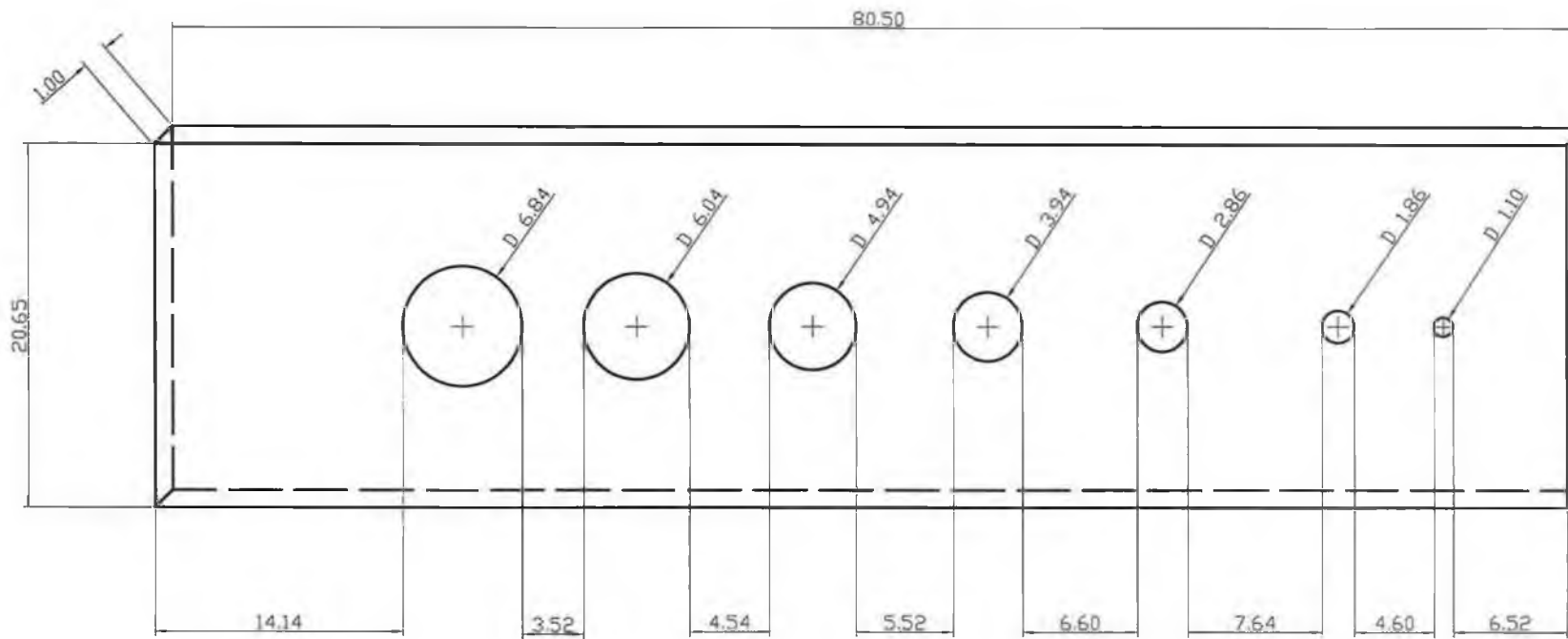
This sample was used in Section 5.4.3 (see Figure 5-11).

FIGURE F-6: Aluminium plate with a rectangular hole inside

This sample was used in Section 5.4.4 (see Figure 5-13).

FIGURE F-7: Double taper aluminium block

This sample was used in Section 5.4.5 (see Figure 5-16).



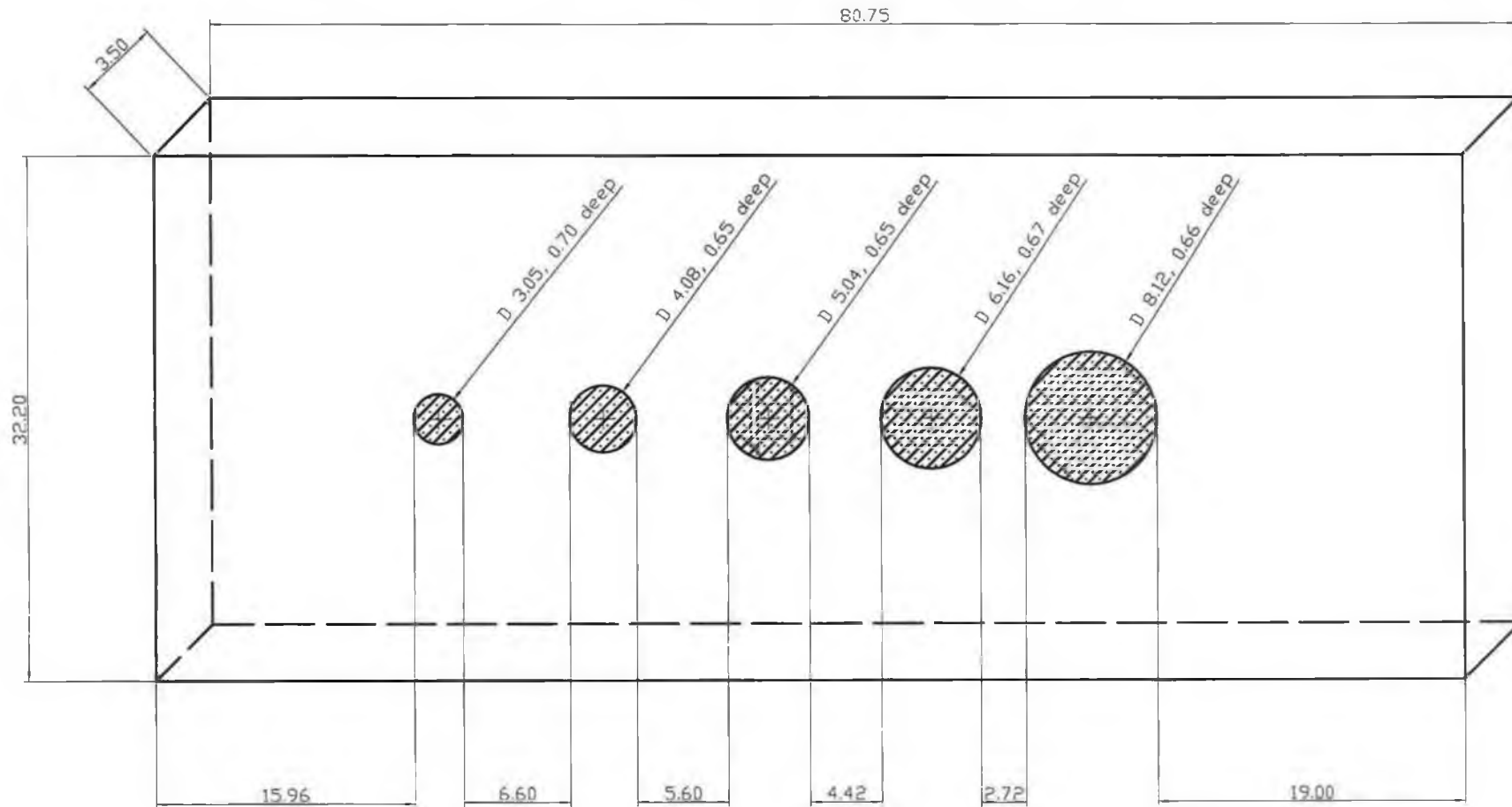
(All dimensions are in mm)

FIGURE F-1

Name: Brass plate with 7 through holes

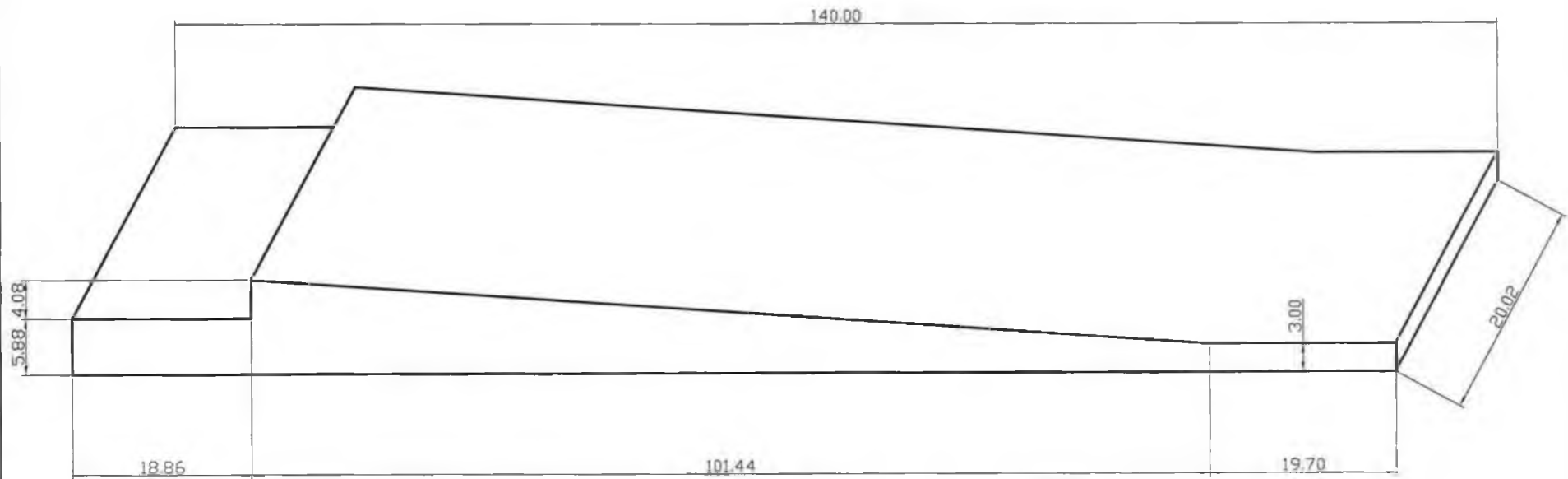
Figure references: 3-4, 3-7, 5-18

Section references: 3.4.1, 3.4.2, 5.4.6



(All dimensions are in mm)

FIGURE F-2
Name: Brass plate with 5 blind holes
Figure reference: 3-9
Section reference: 3.4.3



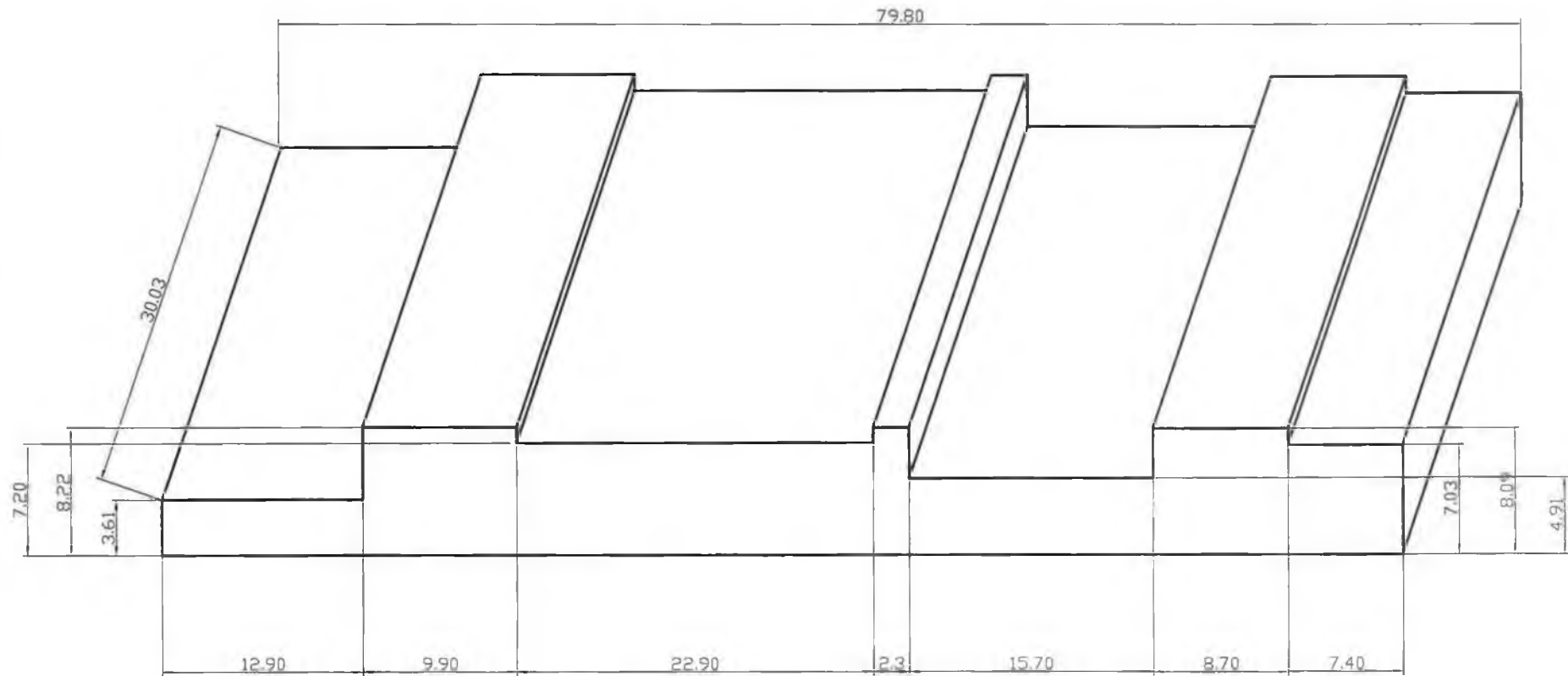
(All dimensions are in mm)

FIGURE F-3

Name: Aluminium taper block

Figure reference: 5-5

Section reference: 5.4.1



(All dimensions are in mm)

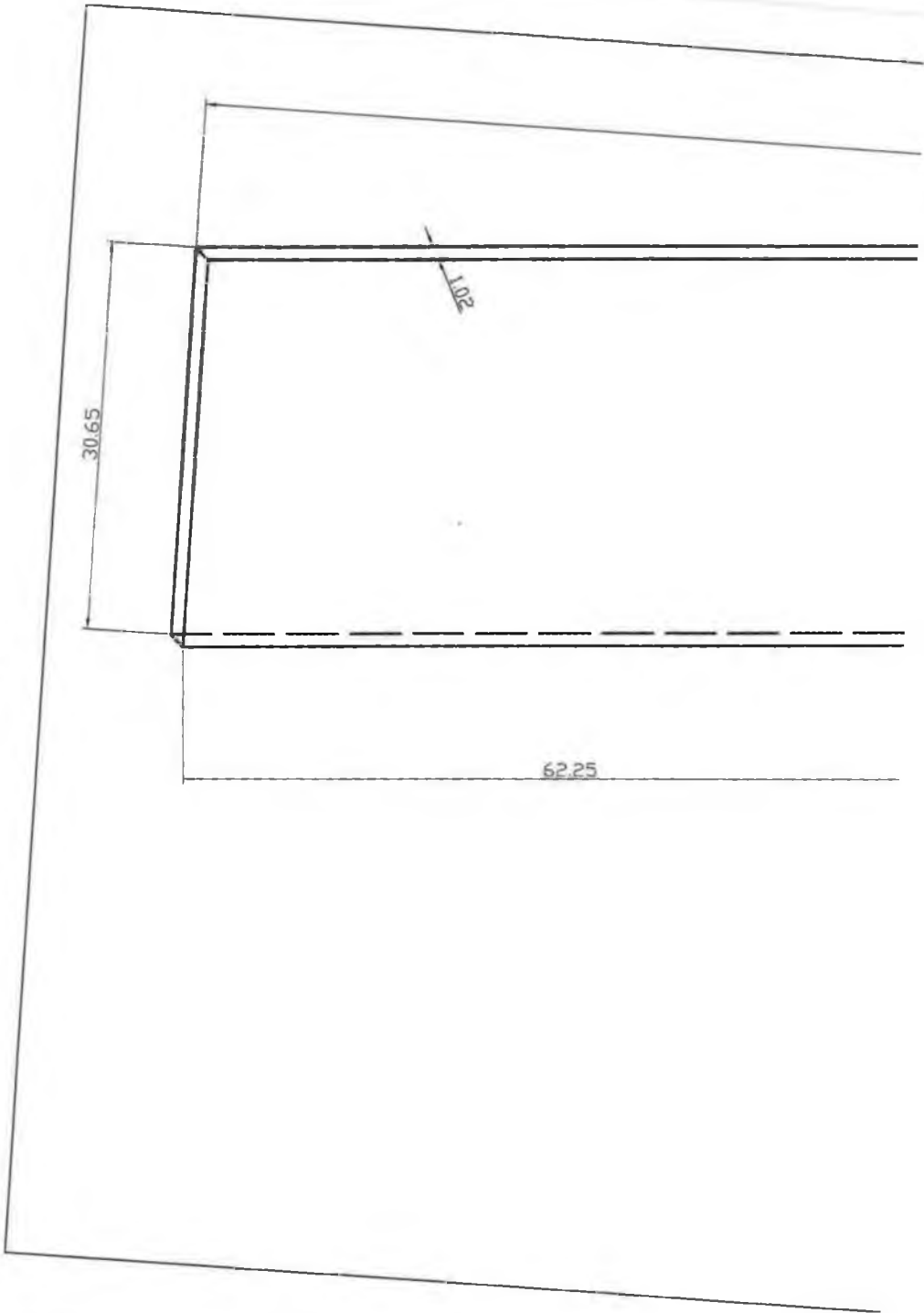
FIGURE F-4

Name: Aluminium block with various thickness

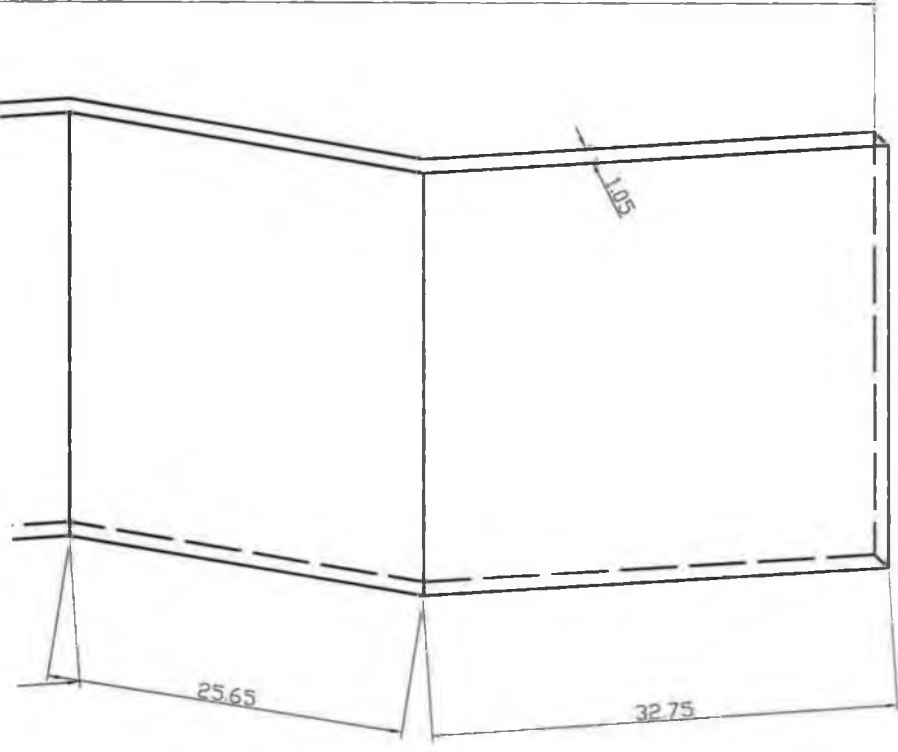
Figure reference: 5-8

Section reference: 5.4.2

151

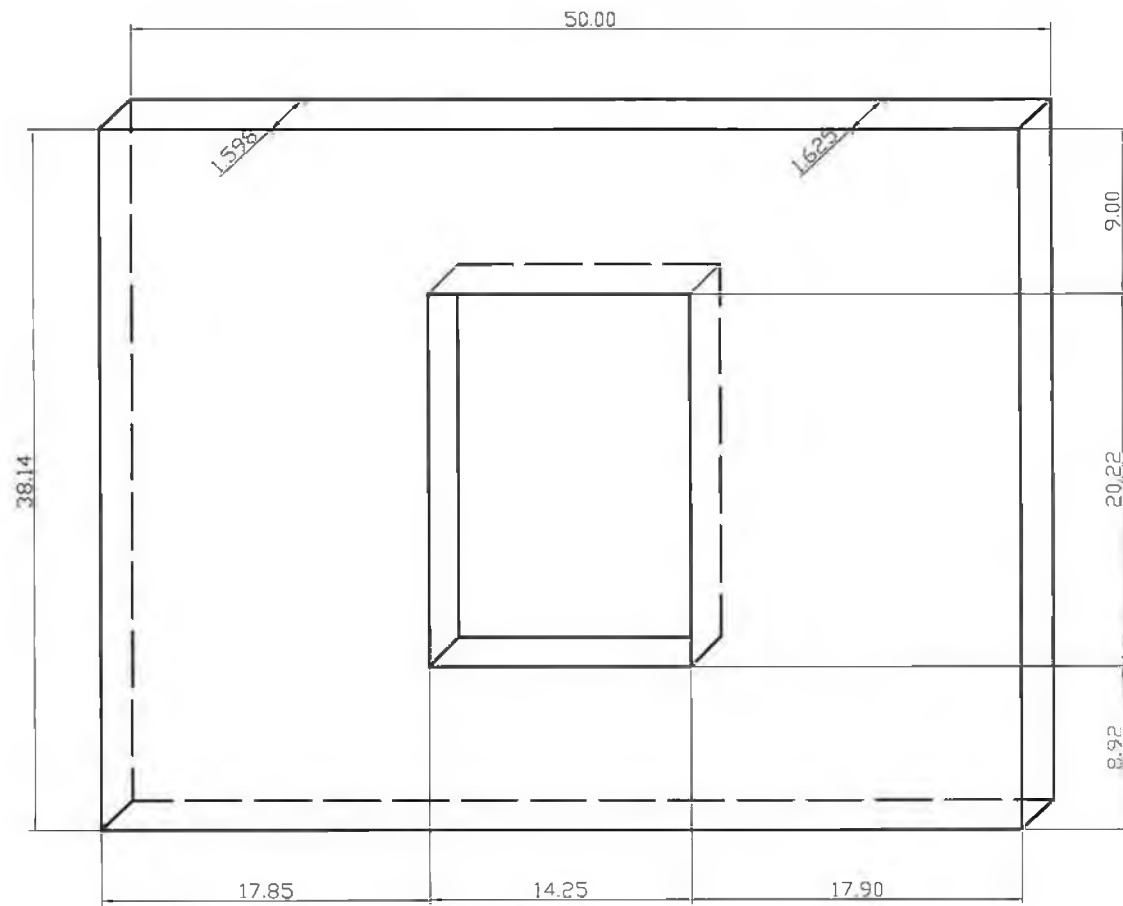


120.65



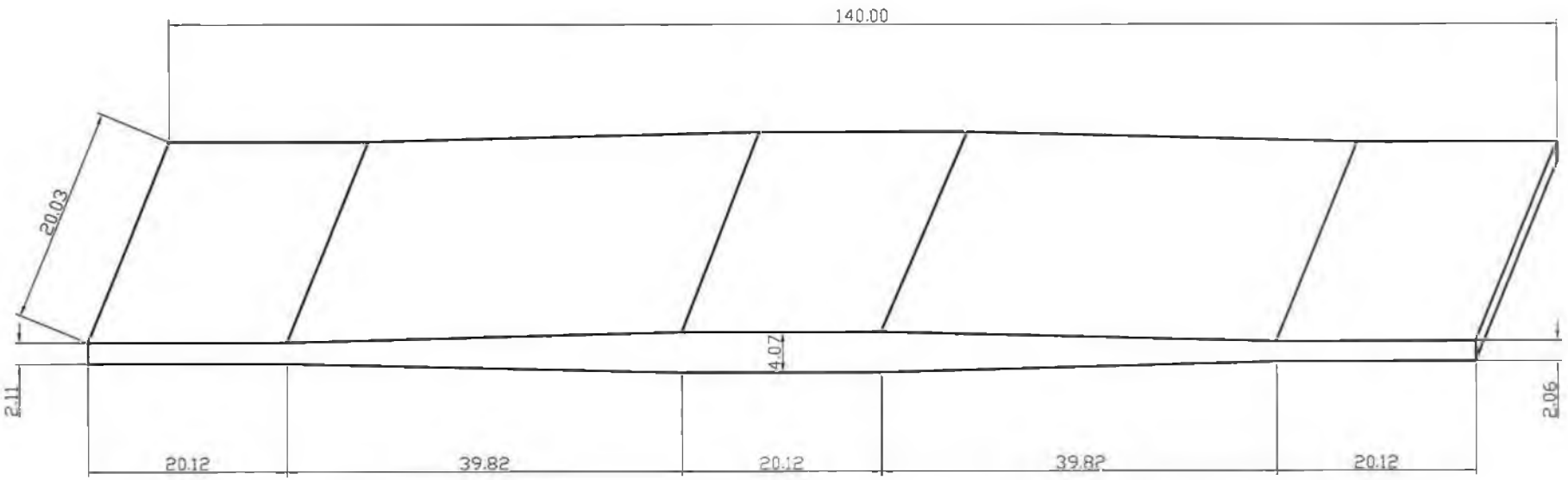
(All dimensions are in mm)

FIGURE F-5
Name: Kinked thin aluminium plate
Figure reference: 5-11
Section reference: 5.4.3



(All dimensions are in mm)

FIGURE F-6
Name: Aluminium plate with a rectangular hole inside
Figure reference: 5-13
Section reference: 5.4.4



(All dimensions are in mm)

FIGURE F-7
Name: Double taper aluminium block
Figure reference: 5-16
Section reference: 5.4.5